

# Accuracy of Marker Actions for the Offline Synchronization of Wearable Devices

DIPLOMARBEIT

zur Erlangung des akademischen Grades

**Diplom-Ingenieur**

im Rahmen des Studiums

**Media and Human-Centered Computing**

eingereicht von

**Christoff Kügler, BSc.**

Matrikelnummer 11807868

an der Fakultät für Informatik

der Technischen Universität Wien

Betreuung: Dipl.-Inf. Dr.sc.techn. Florian Michahelles

Mitwirkung: Dr.-Ing. Florian Wolling, MSc

Wien, 23. Jänner 2026

---

Christoff Kügler

---

Florian Michahelles



Die approbierte gedruckte Originalversion dieser Diplomarbeit ist an der TU Wien Bibliothek verfügbar  
The approved original version of this thesis is available in print at TU Wien Bibliothek.

# Accuracy of Marker Actions for the Offline Synchronization of Wearable Devices

DIPLOMA THESIS

submitted in partial fulfillment of the requirements for the degree of

**Diplom-Ingenieur**

in

**Media and Human-Centered Computing**

by

**Christoff Kügler, BSc.**

Registration Number 11807868

to the Faculty of Informatics

at the TU Wien

Advisor: Dipl.-Inf. Dr.sc.techn. Florian Michahelles

Assistance: Dr.-Ing. Florian Wolling, MSc

Vienna, January 23, 2026

---

Christoff Kügler

---

Florian Michahelles



Die approbierte gedruckte Originalversion dieser Diplomarbeit ist an der TU Wien Bibliothek verfügbar  
The approved original version of this thesis is available in print at TU Wien Bibliothek.

# Erklärung zur Verfassung der Arbeit

Christoff Kügler, BSc.

Hiermit erkläre ich, dass ich diese Arbeit selbständig verfasst habe, dass ich die verwendeten Quellen und Hilfsmittel vollständig angegeben habe und dass ich die Stellen der Arbeit – einschließlich Tabellen, Karten und Abbildungen –, die anderen Werken oder dem Internet im Wortlaut oder dem Sinn nach entnommen sind, auf jeden Fall unter Angabe der Quelle als Entlehnung kenntlich gemacht habe.

Ich erkläre weiters, dass ich mich generativer KI-Tools lediglich als Hilfsmittel bedient habe und in der vorliegenden Arbeit mein gestalterischer Einfluss überwiegt. Im Anhang „Übersicht verwendeter Hilfsmittel“ habe ich alle generativen KI-Tools gelistet, die verwendet wurden, und angegeben, wo und wie sie verwendet wurden. Für Textpassagen, die ohne substantielle Änderungen übernommen wurden, haben ich jeweils die von mir formulierten Eingaben (Prompts) und die verwendete IT- Anwendung mit ihrem Produktnamen und Versionsnummer/Datum angegeben.

Wien, 23. Jänner 2026

---

Christoff Kügler



Die approbierte gedruckte Originalversion dieser Diplomarbeit ist an der TU Wien Bibliothek verfügbar  
The approved original version of this thesis is available in print at TU Wien Bibliothek.

# Kurzfassung

Tragbare Bewegungssensoren ermöglichen die Erfassung menschlicher Aktivitäten und bilden die Grundlage der Human Activity Recognition. Der Einsatz mehrerer Inertial Measurement Units (IMUs) erlaubt eine genauere Analyse, da Bewegungen an verschiedenen Körperstellen parallel aufgezeichnet werden können. Damit einher geht jedoch die Anforderung einer zeitlichen Synchronisation dieser Sensoren, um sicherzustellen, dass Ereignisse, die in der realen Welt gleichzeitig auftreten, auch in den Sensorsignalen zeitlich ausgerichtet sind. Ohne eine gemeinsame Zeitbasis ist diese Synchronisation aufgrund von Uhrendrift, Übertragungsverzögerungen und insbesondere ungenauen Startzeitpunkten der Aufzeichnungen schwierig zu realisieren. Diese Arbeit verfolgt einen datengetriebenen Synchronisationsansatz, bei dem bewusst ausgeführte Bewegungen, sogenannte Markierungen (MAs), zur zeitlichen Ausrichtung von IMU-Signalen an unterschiedlichen Körperpositionen genutzt werden. Untersucht wird, welche Signalcharakteristika zu robusten Synchronisationsereignissen beitragen und wie sich die Synchronisationsleistung über verschiedene Sensorpositionen hinweg unterscheidet.

In einer kontrollierten Nutzer\_innenstudie führen Teilnehmende acht vordefinierte MAs aus, während sie einen Motion-Capturing-Anzug mit 17 über den Körper verteilten, hardware-synchronisierten IMUs tragen. Die MAs erzeugen charakteristische Signalverläufe, die genutzt werden, um korrespondierende Ereignisse in den Sensorsignalen verschiedener Körperpositionen einander zuzuordnen. Dadurch entstehen zeitliche Verschiebungen zwischen den Sensorströmen, die mittels fensterbasierter Kreuzkorrelation auf Basis des Pearson-Korrelationskoeffizienten auf diese ereigniszentrierten Signalabschnitte geschätzt werden. Die Qualität dieser nachträglichen Synchronisation wird über die MAs und Sensorpositionen hinweg anhand statistischer Kennwerte sowie Körperkarten-Visualisierungen analysiert. Auf Grundlage der aufgezeichneten Daten konnte gezeigt werden, dass kurze, impulsartige Bewegungen mit hoher Signaldynamik zu konsistenterer und stabilerer zeitlicher Ausrichtung führen als langsame oder gleichmäßige Übergänge. Periodische oder bewegungsarme Aktionen weisen hingegen eine erhöhte Mehrdeutigkeit und Variabilität der bestimmten zeitlichen Verschiebungen auf. Während Gehen eine Genauigkeit von 4,8 ms für eine Ganzkörpersynchronisation erreichte, zeigen Aktionen wie Klatschen eine eher lokale Wirkung und resultieren in einer Genauigkeit von 17,0 ms, die sich auf den Oberkörper beschränkt. Diese Ergebnisse unterstreichen die Bedeutung der Auswahl geeigneter MAs und Sensorpositionen für eine robuste datengetriebene Sensorsynchronisation in Anwendungen der Aktivitätserkennung.



Die approbierte gedruckte Originalversion dieser Diplomarbeit ist an der TU Wien Bibliothek verfügbar  
The approved original version of this thesis is available in print at TU Wien Bibliothek.

# Abstract

Wearable motion sensors enable the capture of human activities and form the basis of human activity recognition. The use of multiple inertial measurement units (IMUs) worn simultaneously allows for more fine-grained analysis because motions can be recorded at multiple body locations simultaneously. With this comes the requirement of reliable temporal synchronization of these sensors to ensure that events that occur at the same time in the real-world are also temporally aligned within the sensor signals. Without a common time base, this synchronization is difficult to achieve due to clock drift, transmission delays, and, in particular, inaccurate start times of recordings. This thesis uses a data-driven synchronization approach in which deliberately performed movements, referred to as marker actions, are used to temporally align IMU signals recorded at different body locations. The work investigates which signal characteristics contribute to robust synchronization events and systematically evaluates how synchronization performance varies across different sensor placements.

In a controlled user study, participants perform eight predefined MAs while wearing a motion-capturing suit equipped with 17 hardware-synchronized IMUs distributed across the entire body. The MAs produce distinctive, time-localized signal patterns that are used to match corresponding events across sensor streams from different body locations. This introduces temporal offsets between the sensor streams, which are estimated by applying windowed cross-correlation based on the Pearson correlation coefficient to these event-centered signal segments. The quality of this post-hoc synchronization is analyzed across different MAs and sensor positions using statistical measures and body-map visualizations. Based on the recorded data, it was shown that short, impulsive movements with high signal dynamics lead to more consistent and stable temporal alignment than slow or smooth transitions. In contrast, periodic or low-dynamic movements exhibit increased ambiguity and variability in the determined temporal offsets. While walking achieved 4.8 ms accuracy for full-body synchronization, actions such as clapping have a rather local effect and result in 17.0 ms accuracy for only the upper body. These results highlight the importance of marker action selection and sensor placement for robust data-driven sensor synchronization in activity recognition applications.



Die approbierte gedruckte Originalversion dieser Diplomarbeit ist an der TU Wien Bibliothek verfügbar  
The approved original version of this thesis is available in print at TU Wien Bibliothek.

# Contents

<b>Kurzfassung</b>	<b>vii</b>
<b>Abstract</b>	<b>ix</b>
<b>Contents</b>	<b>xi</b>
<b>1 Introduction</b>	<b>1</b>
<b>2 Fundamental Background</b>	<b>5</b>
2.1 Inertial Measurement Units . . . . .	5
2.2 Synchronization of Time Series . . . . .	7
2.3 Mathematical Frameworks . . . . .	11
<b>3 Related Work</b>	<b>17</b>
3.1 Clock-Based Synchronization . . . . .	17
3.2 Signal-Based Synchronization . . . . .	19
3.3 Event-Driven Synchronization . . . . .	20
3.4 Effects of Sensor Placement and Location . . . . .	21
3.5 Human Motion Synchronization . . . . .	22
3.6 Data-Based Synchronization Frameworks . . . . .	23
<b>4 Methodology</b>	<b>25</b>
4.1 Research Concept . . . . .	25
4.2 Data Requirements . . . . .	27
4.3 Experimental Design . . . . .	28
4.4 Synchronization Approach . . . . .	35
<b>5 Implementation</b>	<b>37</b>
5.1 User Study . . . . .	37
5.2 Pearson Correlation . . . . .	42
<b>6 Evaluation</b>	<b>45</b>
6.1 Data Processing . . . . .	45
6.2 Results . . . . .	51
	xi

<b>7 Results and Discussion</b>	<b>63</b>
7.1 Limitations . . . . .	68
7.2 Guidelines . . . . .	70
<b>8 Conclusion</b>	<b>73</b>
<b>Overview of Generative AI Tools Used</b>	<b>77</b>
<b>List of Figures</b>	<b>79</b>
<b>List of Tables</b>	<b>81</b>
<b>Bibliography</b>	<b>83</b>
<b>A Appendices</b>	<b>1</b>
A.1 User Study Forms . . . . .	1
A.2 User Study Questionnaires . . . . .	5
A.3 Body Maps . . . . .	14

# CHAPTER 1

## Introduction

Wearable sensing systems have become an essential technological foundation for research [ARS20] and applications [Sta18] concerned with human activity recognition (HAR). On the consumer market, the use of wearables for day-to-day activity tracking is on the rise. Within this domain, Inertial Measurement Units (IMUs) are often used as a primary data source to capture movement [Sta25].

A defining feature of many IMU-based motion analysis setups is the use of multiple sensors attached to various body positions [BAL09, SBM<sup>+</sup>22, LHB04, LJS<sup>+</sup>02]. By placing IMUs on different body segments, it becomes possible to capture more complex, full-body motion and to analyze coordination patterns that are not observable from a single IMU. This multi-sensor perspective is particularly valuable in applications that depend on inter-limb relationships or temporal dependencies between body parts, such as the comparison of left–right limb motion or the assessment of movement symmetry. As a result, the analytical focus shifts from isolated sensor streams to the joint interpretation of multiple time series that collectively describe a single movement episode [BAL09, SBM<sup>+</sup>22]. The increasing reliance on multi-IMU configurations has direct methodological implications for how motion data are collected and processed. In contrast to single-sensor setups, multi-sensor recordings are only interpretable if the individual data streams share a common temporal reference [SY04, RN10, XGMW17], this is especially important in the context of ML as time discrepancies have shown to decrease HAR performance [WKTM25, DRE<sup>+</sup>21]. Temporal alignment is, therefore, not an optional refinement, but a foundational requirement for any analysis that compares or combines signals across body locations. Without reliable and accurate alignment, relationships between sensors may reflect artifacts of acquisition timing rather than genuine aspects of human movement, thereby undermining the validity of subsequent analysis steps [XGMW17].

These temporal misalignments stem from the fact that wearables are typically embedded in autonomously operating distributed systems, and their data are subject to

system-level effects such as unsynchronized start times, internal buffering, or device-specific timing behavior [XGM17]. Even when sensors are part of an integrated system, the recorded signals may exhibit small but consequential offsets at the sample level. These deviations are often negligible when analyzing a single sensor in isolation, but they become critical when the goal is to analyze coordinated motion across multiple body segments. Against this backdrop, data-driven approaches to synchronization have gained prominence as a pragmatic solution for aligning multi-IMU recordings [BC, WSL<sup>+</sup>19, PGH<sup>+</sup>09, BMBK20, Alt11, SZL<sup>+</sup>13]. Rather than relying on external synchronization techniques, these approaches infer temporal alignment from the recorded signals themselves and can therefore be applied retrospectively during data analysis. This makes them particularly attractive in settings where real-time synchronization cannot be guaranteed and, if necessary, needs to be corrected after data collection. From a methodological standpoint, data-driven synchronization enables researchers to treat alignment as an explicit and inspectable step in the analysis process, rather than as an implicit assumption about the recording system. Within data-driven synchronization, event-driven strategies are of particular practical relevance. Event-driven systems use deliberately performed movements during data collection as temporal reference points that can be identified across sensor streams [WSL<sup>+</sup>19, BAL09, SBM<sup>+</sup>22]. Such marker actions (MAs) are easy to integrate into experimental protocols and do not require additional hardware or calibration procedures. Their use reflects an intuitive assumption: if a participant performs a distinct, well-defined movement, this movement should leave a recognizable signature in the sensor signals that can be used to align recordings. However, the apparent simplicity of event-driven synchronization masks a set of subtle methodological considerations. Different movements may produce fundamentally different signal characteristics depending on their dynamics, duration, and how motion propagates through the body. Moreover, the same event can manifest differently across body locations, leading to variation in how clearly the event is reflected in individual IMU signals. These factors suggest that the effectiveness of event-driven synchronization is not solely determined by the synchronization algorithm, but also by the properties of the chosen MA and its interaction with sensor placement.

The motivation for this thesis arises from this intersection of practical necessity and methodological uncertainty. As multi-IMU systems continue to be used in increasingly complex and data-intensive studies even beyond HAR [LAK19, EOBW18], there is a growing need for empirically grounded guidance on how synchronization should be approached at the level of experimental design. Specifically, understanding how different MAs influence the quality and robustness of data-based synchronization is essential for designing studies that produce reliable, interpretable motion data. By situating synchronization within the broader context of wearable motion capture and experimental methodology, this thesis aims to contribute to more principled and transparent practices in multi-IMU data collection and analysis.

---

## Problem Statement

Temporal synchronization in multi-IMU systems refer to the problem of aligning multiple time series such that events within the signal correspond with the measured event in the real world. In the context of human motion analysis, this alignment is essential because motion patterns are inherently coordinated across body segments. Any temporal mismatch between sensor streams therefore compromises the ability to interpret inter-sensor relationships in a meaningful way. A range of synchronization strategies exists in the literature, broadly spanning hardware-based, network-based [EGE02, CGDSVdP24], and data-driven [SBM<sup>+</sup>22, BAL09] approaches. Hardware-level synchronization mechanisms, such as master clocks or wired triggers, can provide high accuracy but are impractical in real-world scenarios [OSK<sup>+</sup>21]. Network-based solutions, while suitable for wireless operation, are sensitive to communication delays and their effectiveness varies across devices and recording conditions.

IMU setups sometimes rely on offline, data-driven synchronization, where temporal alignment is inferred retrospectively from the recorded sensor signals instead of needing to communicate with a master clock or negotiating time with other sensor nodes. These approaches treat synchronization as an optimization problem and estimate relative time shifts by maximizing signal similarity measures, such as correlation. While this paradigm avoids additional hardware requirements, periods of low activity or repetitive data characteristics can lead to ambiguous or unstable alignment results. The central problem addressed in this thesis is that, despite the use of data-based synchronization in previously mentioned work, there is limited understanding of how the choice of performed motion influences synchronization quality. Without clear guidance on which movements produce reliable temporal anchors, synchronization performance remains inconsistent and difficult to predict. This uncertainty motivates a systematic investigation of synchronization-relevant motion events and their impact on alignment accuracy and stability in multi-IMU data.

A recurring limitation in prior work is the lack of systematic investigation onto the role of sensor placement in synchronization performance, as synchronization methods are commonly evaluated using sensor placements confined to similar body regions and rarely span both the upper and lower body. Consequently, it remains unclear how synchronization accuracy varies when sensors are distributed across different body segments, particularly in multi-IMU setups where motion dynamics and signal properties differ substantially between locations. In addition, many studies are conducted under restricted sampling conditions. While some work offers recording frequencies of up to 200 Hz [BGJ15a, BGJ15b], evaluations sometimes use sampling frequencies of 100 Hz [BAL09, SBM<sup>+</sup>22], and sometimes even as low as 25 Hz [GDHW22, GLD<sup>+</sup>24], which may be insufficient to fully capture fast or highly transient movements. As a result, synchronization performance for rapid MAs or high-jerk motion patterns remains under-explored. This limitation is particularly relevant for wearable systems intended to capture short-duration or high-dynamic events. Another common limitation concerns sample size. A substantial portion of prior work validates synchronization methods using very small

participant cohorts [BAL09, SBM<sup>+</sup>22, BAL09, SBM<sup>+</sup>22], sometimes comprising fewer than five subjects [BAL09]. While such studies provide valuable proof-of-concept results, small sample sizes limit the statistical robustness of the findings and reduce confidence in their generalizability across users with differing movement patterns, body morphologies, or sensor placements. A further open issue concerns the characteristics of the signals themselves that enable reliable event-driven synchronization. While many event-driven approaches demonstrate that synchronization is possible using specific MAs or detected landmarks, the work referenced above provides little systematic insight into why certain events perform well and others do not. As a result, event selection in prior studies is often heuristic or application-specific, and the transferability of synchronization events across different body locations or sensor configurations is not well understood.

Taken together, these gaps indicate that, despite substantial progress in synchronization methodologies, there is insufficient empirical understanding of how synchronization performance depends on the interaction between sensor placement, event selection, and participant variability in realistic multi-IMU scenarios. Addressing these limitations is essential for assessing the practical applicability and reliability of synchronization strategies in wearable sensing systems.

# Fundamental Background

This chapter provides the fundamental background necessary for understanding the methods and analyses presented in this thesis. It first introduces IMUs as the primary sensing modality, outlining their basic principles and the characteristics of the signals they produce. The chapter then discusses the general problem of time-series synchronization, illustrating often used methodologies. Finally, key mathematical frameworks for quantifying similarity and alignment between time series are presented, including correlation-based measures such as the Pearson correlation coefficient. Together, these foundations establish the technical and conceptual basis for the synchronization approaches examined in subsequent chapters.

## 2.1 Inertial Measurement Units

This section introduces the core principles, sensor components, and data characteristics of IMUs that are relevant for HAR as they form the sensing foundation of many wearable systems. A clear understanding of the fundamentals is necessary to motivate subsequent discussions on multi-sensor synchronization and time-series alignment.

IMUs are composed of multiple complementary sensor components, each contributing distinct but interrelated motion information [AGKK13] as illustrated in Figure 2.1. The accelerometer measures linear acceleration along each spatial axis and captures both dynamic motion and the static influence of gravity, making it particularly useful for detecting translational movements and estimating orientation under stationary conditions. Gyroscopes address this limitation by measuring angular velocity around each axis, enabling precise tracking of rotational motion and rapid changes in orientation even under non-stationary conditions. Their primary drawback is the accumulation of drift over time, which leads to increasing orientation errors when angular velocities are integrated [ZW12]. To mitigate this effect, some IMUs additionally incorporate magnetometers that measure the Earth's magnetic field to provide an absolute reference

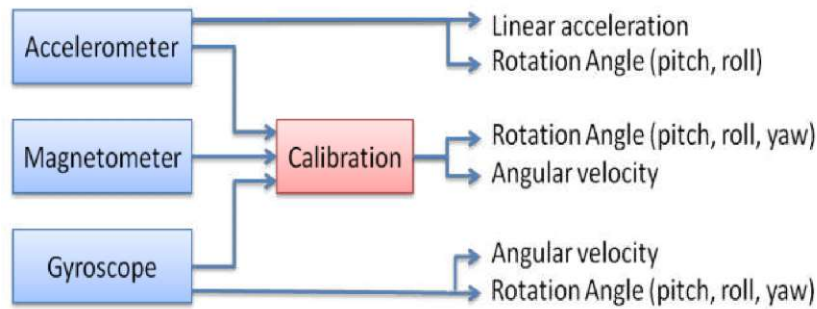


Figure 2.1: Schematic illustration of an IMU based on three types of sensors and their sensing abilities. [AGKK13]

for heading. While magnetometers can improve long-term orientation stability, their readings are vulnerable to magnetic interference from surrounding materials and infrastructure, particularly in indoor environments [ZZ04]. The combination of these sensor components allows IMUs to capture rich motion dynamics, but it also necessitates careful consideration of sensor-specific error characteristics and downstream processing strategies such as calibration and fusion, depending on the application context [ZW12].

IMU configurations are commonly distinguished by the combination of sensor components they include and the resulting number of measurable degrees of freedom (DOF) [AGKK13]. A basic configuration integrates tri-axial accelerometers and tri-axial gyroscopes, yielding six degrees of freedom that describe linear acceleration and angular velocity along and around the three spatial axes. This configuration is sufficient for capturing short-term motion dynamics and is widely used in applications where magnetic interference is a concern. More advanced configurations extend this setup by incorporating a tri-axial magnetometer, increasing the system to nine degrees of freedom and enabling the estimation of absolute heading in addition to relative orientation changes. The choice between six- and nine-DOF IMUs therefore reflects a trade-off between robustness to external interference and the need for absolute orientation information. In practice, the effective usefulness of higher DOF depends not only on the available sensors but also on how their measurements are combined and interpreted, as well as on application-specific accuracy requirements and tolerance to error accumulation.

The signals produced by the individual IMU sensor components represent continuous physical quantities and must therefore be transformed into a digital representation before they can be processed computationally. This conversion is performed by an analog-to-digital converter (ADC), which samples the continuous sensor signals and maps them onto a finite set of discrete values. During this quantization process, the measurement range of each sensor is divided into a fixed number of discrete levels. A higher number of quantization levels increases the effective resolution of the measurements and reduces quantization noise, but also results in increased data volume and storage requirements. In addition to quantization, the sampling frequency determines the temporal resolution of the

recorded data by specifying how many samples are captured per second. In the context of human activity recognition and motion analysis, typical sampling frequencies range from approximately 25 to 200 Hz [GLD<sup>+</sup>24, GDHW22, BAL09, SBM<sup>+</sup>22]. Higher sampling rates enable more accurate capture of rapid movements and short-lived motion events, at the cost of increased data throughput and higher power consumption, which must be balanced against application-specific constraints and hardware capabilities [AGKK13].

## 2.2 Synchronization of Time Series

When data is collected from multiple devices, a range of challenges arises that are not present in single-sensor settings. In such multi-device setups, synchronization becomes a fundamental prerequisite for meaningful analysis [SS16, LHY<sup>+</sup>20]. This section illustrates why synchronization is necessary and shows existing methods used to achieve temporal alignment.

In multi-IMU environments, synchronization ensures that measurements captured by different sensors are temporally aligned, such that samples across devices refer to the same physical instant. Without this alignment, temporal relationships between signals cannot be interpreted reliably, rendering joint analysis across body locations unreliable or infeasible [ONNK06]. This issue is particularly critical in the context of HAR, where many algorithms explicitly depend on temporal patterns [BC, SZL<sup>+</sup>13], phase relationships [BGJ15a, SBM<sup>+</sup>22, BAL09], or cross-correlation [BMBK20] between signals. Multi-sensor approaches commonly fuse data from several devices to derive composite features [SWR<sup>+</sup>09]. In machine-learning-based approaches [WKT25, DRE<sup>+</sup>21], even small temporal deviations can negatively affect classification performance. While Bannach et al. [BAL09] claim that sub-second accuracy is sufficient for HAR, Wolling and Kostolani et al. [WKT25] show that time shifts of 300 ms “already significantly degrade the HAR performance” and sub-150 ms alignment is advisable.

### 2.2.1 Timestamp Method

A widely adopted approach [LC10, SBK05] for synchronizing time series data in multi-IMU systems is the timestamp-based method. In this approach, each IMU assigns a timestamp to every recorded sample using its local clock. Once the data streams are transmitted to a central system, temporal alignment is achieved by comparing and matching these timestamps across sensors. This method is particularly attractive for mobile and wearable applications, as it does not require additional synchronization hardware or explicit communication between devices during data acquisition. As long as each sensor provides timestamped measurements, the approach scales well to larger sensor networks and heterogeneous device setups.

Despite its conceptual simplicity, timestamp-based synchronization introduces several challenges in practice. Xu et al. [XGM17] have identified four major sources of temporal discrepancy that can undermine synchronization accuracy: timestamp scale inconsistency,

timestamp frequency inconsistency, timestamp drift, and timestamp absence. Timestamp scale inconsistency arises when different devices represent time with varying resolutions or units. For example, one sensor may report timestamps with second-level precision, while another provides millisecond-level precision. In such cases, it becomes unclear how precisely measurements from different body locations correspond to the same instant, which complicates any analysis that relies on fine-grained temporal relationships. Timestamp frequency inconsistency refers to differences in how often timestamps are generated or transmitted by individual devices, for example, when sensors with fixed reporting intervals are combined with sensors that operate at variable or adaptive frequencies. As a result, matching samples from different devices to the same point in time becomes ambiguous, since corresponding measurements may not exist or may be irregularly spaced across data streams. This problem complicates interpolation and resampling strategies, and can lead to temporal gaps or mismatches in the aligned signals. Another critical limitation is timestamp drift, which is caused by imperfections in a device's internal clock. Factors such as temperature variation, hardware aging, or manufacturing tolerances can cause clocks to drift over time [XGM17]. Even if multiple sensors are synchronized at the beginning of a recording session, their clocks may gradually diverge, leading to increasing temporal misalignment as the recording progresses. This effect is particularly problematic for long-duration recordings, where small clock inaccuracies can accumulate into substantial offsets. Timestamp absence represents a further challenge in systems where devices do not provide absolute timestamps but instead report time relative to their individual start times. In such cases, the absolute timing of measurements is unknown, and alignment must rely on timestamps assigned upon data reception. However, this strategy is inherently unreliable due to variable transmission delays, buffering effects, and processing latencies, which introduce additional uncertainty into the timing information. Together, these limitations illustrate that while timestamp-based synchronization is flexible and widely applicable, its effectiveness depends strongly on device characteristics and operating conditions, motivating the exploration of alternative or complementary synchronization strategies in multi-IMU systems.

### 2.2.2 Hardware-Based Synchronization

The most precise approach for synchronizing multiple sensors is based on hardware-level synchronization+[WLF<sup>+</sup>24, BRR13, PDST20]. In this setup, all sensors are physically connected and share a common reference signal, such as a global or master clock or a dedicated synchronization pulse, as shown in . This physical connection is typically achieved by wiring sensors together. As a result, hardware-based synchronization can achieve nanosecond-level precision [PDST20], making it the gold standard for applications that require strict temporal consistency across multiple data streams.

A key advantage of hardware-level synchronization is its independence from software-based alignment procedures and signal-specific characteristics. Because synchronization is enforced at the acquisition stage, no post hoc synchronization algorithms are required, and

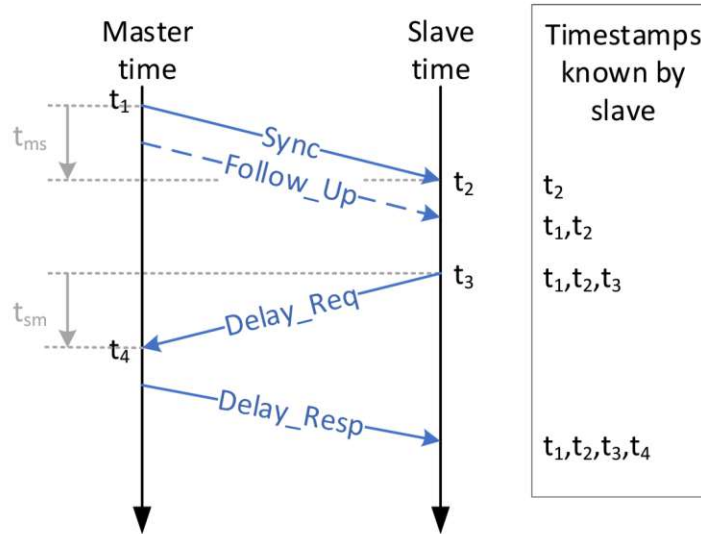


Figure 2.2: Schematic illustration of message exchange and delay estimation using round-trip time between master and slave. The slave estimates the delay as  $[(t_2 - t_1) + (t_4 - t_3)]/2$ , assuming a symmetric delay. [PDST20]

the quality of alignment does not depend on the structure, periodicity, or distinctiveness of the recorded motion signals [WLF<sup>+</sup>24]. In addition, this approach is inherently robust to common sources of temporal discrepancy such as clock drift, timestamp inconsistencies, or variable transmission delays, as all sensors operate under the same timing reference throughout the recording process [XGMW17]. Despite these advantages, hardware-based synchronization has practical limitations. The requirement for wired connections between sensors increases system complexity, cost, and setup effort, and restricts the mobility of the wearer. These constraints make hardware-level synchronization impractical for many real-world scenarios, particularly in wearable and mobile contexts where freedom of movement, ease of deployment, and scalability to larger sensor networks are critical considerations. Consequently, while hardware-based approaches offer superior temporal accuracy, their applicability is often limited to controlled laboratory environments or specialized setups, motivating the widespread use of alternative synchronization methods in practical multi-IMU systems.

### 2.2.3 Event-Driven Synchronization

This synchronization method is a data-driven approach that aligns multiple time series based on the detection of notable events that are observable across sensors [BGJ15a, SBM<sup>+</sup>22]. In this context, an event is defined as a characteristic and temporally localized feature within a signal that can be identified reliably in multiple IMU data streams. Rather than relying on explicit timing information, this method seeks to align signals by maximizing the temporal overlap of corresponding events, thereby inferring synchro-

nization directly from the recorded motion patterns [BAL09]. This makes event-driven synchronization particularly attractive in scenarios where timestamp information is unreliable, unavailable, or affected by drift.

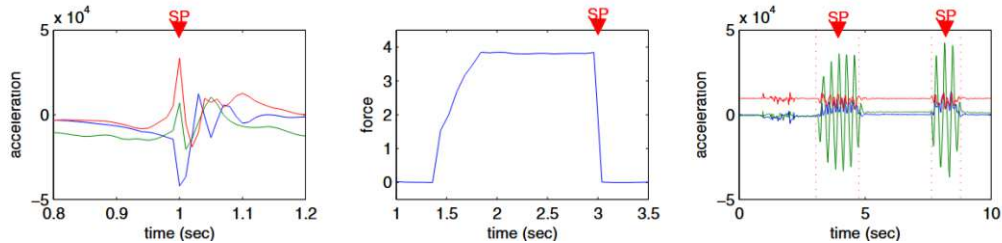


Figure 2.3: Identification of synchronization points (SP) for Event-Driven Synchronization in acceleration data and force data time series. [BAL09]

Multiple methods can be employed to detect events within the signal. Peak detection methods are used to capturing fast and impulsive movements, like shaking a sensor, where sudden changes in acceleration or angular velocity produce distinctive signal features [BAL09]. For other events, such as pushing a button or clapping with wrist-mounted sensors, trailing edge detection is used [BAL09]. Gait detection can be achieved by applying a threshold to the vector-magnitude of acceleration data [SBM<sup>+</sup>22]. For smaller datasets, or to establish a base line, manual annotation of notable events can be a useful tool [SBM<sup>+</sup>22]. Despite its advantages, event-driven synchronization has inherent limitations as this approach relies on the reliable detection of events, which can be difficult in real-world settings [BAL09].

#### 2.2.4 Template Matching

Another approach for synchronizing time series that relies on comparing recorded signals against a predefined reference pattern, is called Template Matching [BGJ17]. In this context, a template represents a characteristic signal segment that corresponds to a specific motion or activity and is assumed to occur in all relevant data streams. Synchronization is achieved by identifying the temporal position at which this template best matches each signal, thereby inferring the relative alignment between sensors. Template matching can be understood as a generalization of event-based methods, where the defining event is represented not by a single point in time but by a structured temporal pattern that is then compared to different signals. Depending on the implementation, this comparison may be based on simple metrics such as correlation or on more elaborate distance measures that capture shape similarity [Oka19, SPB09, BH01, NSR12, FMPP13]. By leveraging a richer representation of motion than single-point events, template matching can be more robust to noise and minor temporal variations within the signal. However, the effectiveness of template matching depends on the quality and representativeness of the chosen template [SPB09]. A template that captures only a narrow range of motion variability may fail to generalize across different users, execution styles, or sensor placements [NSR12]. Additionally, constructing suitable templates often requires

prior knowledge, manual annotation, or an initial training phase, which may limit scalability and flexibility. From a computational perspective, template matching can also be computationally expensive [NSR12], as each template must be compared against potentially long time series. Despite these limitations, template matching provides a useful synchronization strategy [NSR12, Oka19] when characteristic motion patterns are known in advance and consistently present across sensors, offering a middle ground between rigid timestamp-based methods and fully data-driven alignment techniques.

## 2.3 Mathematical Frameworks

For signal-based synchronization, mathematical characteristics can be used to align multiple time series. Three approaches that use such characteristics to calculate the similarity between two or more signals are described in the following.

### 2.3.1 Dynamic Time Warping

This approach allows for comparing and aligning time series that may differ in length or temporal progression. Unlike methods that assume a fixed correlation between time indices (see 2.3.2 and 2.3.3), Dynamic Time Warping (DTW) allows non-linear comparison of time axis, enabling similar patterns to be matched even when they occur at different speeds [BK59]. Originally developed for speech recognition [MRR80], DTW has since been applied to a variety of time-series analysis problems, including gesture [Cor01] and motion [NR07, GJ06] data analysis. Given two time series

$$X = (x, x_1, x_2, \dots, x_N), \quad Y = (y, y_1, y_2, \dots, y_M).$$

DTW begins by computing a local cost matrix [Sen09], where each entry represents the dissimilarity between individual samples of the two sequences  $c_{i,j} = d(x_i, y_j)$  with  $d(x, y)$  denoting a distance measure between samples. This matrix captures all pairwise local distances between  $X$  and  $Y$ . An alignment between the two sequences is represented by a warping path, which defines how samples of  $X$  are matched to samples of  $Y$  while preserving temporal order. The optimal warping path and the corresponding DTW distance are computed efficiently using dynamic programming. To this end, an accumulated cost matrix is constructed recursively as

$$D(i, j) = c_{i,j} + \min\{D(i-1, j-1), D(i-1, j), D(i, j-1)\} \quad (2.1)$$

The final DTW distance is obtained from the last matrix entry, and the optimal alignment can be recovered by backtracking [Sen09]. By permitting local stretching and compression of time, DTW can align sequences with similar overall structure but differing local timing. However, as noted by Senin [Sen09], unconstrained DTW may produce unintuitive alignments for noisy or highly repetitive signals, motivating the use of additional constraints to limit excessive warping.

### 2.3.2 Cross-Correlation

This is a widely used analytical tool for quantifying the similarity between two time-dependent signals as a function of their relative temporal displacement [ON01]. Given two discrete-time sequences  $x[n]$  and  $y[n]$ , cross-correlation evaluates how well one signal matches a time-shifted version of the other over a range of temporal offsets, commonly referred to as lags. By systematically varying the lag, cross-correlation reveals temporal relationships between signals, such as recurring patterns, lead-lag dependencies, or structural similarity over time. Formally, the cross-correlation between two discrete-time signals is defined as

$$R_{xy}[k] = \sum_n x[n] y[n + k] \quad (2.2)$$

where  $k$  denotes the lag and the summation is taken over the indices for which both  $x[n]$  and  $y[n + k]$  are defined. Conceptually, this expression can be interpreted as an inner product between the signal  $x$  and a time-shifted version of  $y$ . Large values of  $R_{xy}[k]$  indicate that the two signals exhibit similar structure over the overlapping region at lag  $k$ . For real-valued signals, cross-correlation is closely related to convolution, differing primarily in the time reversal of one of the arguments. A defining characteristic of the cross-correlation is that its magnitude depends on the absolute scale and energy of the involved signals. Multiplying one signal by a constant factor scales the cross-correlation values proportionally, and changes in the number of overlapping samples across lags can also affect the magnitude. This sensitivity can be advantageous when signal amplitude or energy is meaningful, as it preserves information about the strength of co-varying activity. However, it complicates comparisons across signals with different amplitudes, sensor gains, or measurement units.

To mitigate these effects, the energy-normalized cross-correlation can be employed. It is defined as

$$\rho_{xy}[k] = \frac{\sum_n x[n] y[n + k]}{\sqrt{\sum_n x[n]^2} \sqrt{\sum_n y[n + k]^2}} \quad (2.3)$$

where normalization is performed over the overlapping region at each lag. This formulation yields a dimensionless similarity measure that is invariant to multiplicative scaling of either signal and bounded within a fixed range for real-valued data. Normalized cross-correlation is therefore well suited for applications in which the relative shape of the signals is of interest, rather than their absolute magnitude. Nonetheless, this variant does not account for constant offsets in the signals, so large mean values can dominate the correlation even when the dynamic components are weak. A stricter normalization removes this limitation by subtracting the mean from each signal segment prior to normalization. This yields a lag-dependent form equivalent to the Pearson correlation coefficient computed over overlapping segments, defined as

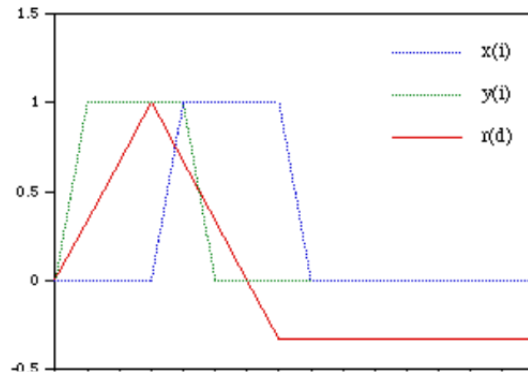


Figure 2.4: Illustration of the cross-correlation  $r(d)$  between two signals  $x(i)$  and  $y(i)$ . [Bou96]

$$r_{xy}[k] = \frac{\sum_n (x[n] - \bar{x})(y[n+k] - \bar{y}_k)}{\sqrt{\sum_n (x[n] - \bar{x})^2} \sqrt{\sum_n (y[n+k] - \bar{y}_k)^2}} \quad (2.4)$$

where  $\bar{x}$  and  $\bar{y}_k$  denote the means of the respective signal segments over the overlap region [Bou96]. This formulation is invariant to both additive offsets and multiplicative scaling, emphasizing co-fluctuations around the local mean rather than absolute levels. As a result, it is particularly useful when baseline differences or slow-varying components are present in the data. The choice between non-normalized, energy-normalized, and mean-removed cross-correlation depends on the analytical objective. Non-normalized cross-correlation is appropriate when absolute signal magnitude and energy carry semantic meaning. Energy-normalized cross-correlation enables comparisons across signals of different scales while retaining sensitivity to constant offsets. Mean-removed normalization further isolates dynamic similarity and is often preferred when comparing signals from heterogeneous sources or measurement conditions.

Finally, it is important to note that cross-correlation inherently reflects the structure of the signals under analysis. In the presence of periodic or quasi-periodic components, such as oscillatory or cyclic behavior, cross-correlation may exhibit multiple local maxima at different lags, each corresponding to a distinct repetition of the underlying pattern. In such cases, cross-correlation reliably indicates the existence of strong repeating structure but may not uniquely identify a single dominant temporal relationship without additional constraints or contextual information. This limitation arises from the signal properties themselves rather than from the cross-correlation formulation.

### 2.3.3 Pearson Correlation Coefficient

Correlation describes the degree to which two variables change together. If large values of one variable tend to occur alongside large values of another, the two variables are said

to be positively correlated. Conversely, if one variable increases while the other decreases, they are negatively correlated. In quantitative terms, correlation captures the strength and direction of a linear relationship between two variables. The Pearson Correlation Coefficient (PCC) is a statistical measure that describes how strongly two variables are linearly related [BCHC09, Sed12]. Let  $X = (x_1, x_2, \dots, x_n)$  and  $Y = (y_1, y_2, \dots, y_n)$  be two sets of sampled measurements of equal length  $n$ . The PCC quantifies the degree of linear association between  $X$  and  $Y$  and is defined as

$$r = \frac{\sum_{i=1}^n (x_i - \bar{x})(y_i - \bar{y})}{\sqrt{\sum_{i=1}^n (x_i - \bar{x})^2} \sqrt{\sum_{i=1}^n (y_i - \bar{y})^2}} \quad (2.5)$$

where  $\bar{x} = \frac{1}{n} \sum_{i=1}^n x_i$  and  $\bar{y} = \frac{1}{n} \sum_{i=1}^n y_i$  denote the arithmetic means of  $X$  and  $Y$  respectively [Cha24].

The numerator of Equation 2.5 represents the covariance between the two variables and describes how  $X$  and  $Y$  vary together around their respective means  $\bar{X}$  and  $\bar{Y}$ . The denominator normalizes this covariance by the product of the standard deviations of  $X$  and  $Y$ . This normalization removes the influence of the scale and units of measurement, ensuring that  $r$  is dimensionless and constrained to the interval  $[-1, 1]$ . A value of  $r = 1$  indicates a perfect positive relationship,  $r = -1$  a perfect negative relationship. The closer the absolute value of  $r$ , the stronger the indicated linear relationship. A value of  $r = 0$  describes the absence of linear correlation, though non-linear relationships may exist [Eme15, Arm19].

An important property of the Pearson coefficient is its scale invariance. Multiplying one variable by a nonzero constant or adding an offset does not change the correlation, as both the covariance and the standard deviation are scaled proportionally. This feature is particularly relevant in HAR, where identical movements can produce signals of different magnitudes across sensors due to placement, orientation, or calibration differences. The PCC focuses on the shape of the signals rather than their absolute amplitudes.

Furthermore, the coefficient is symmetric, meaning that

$$\text{corr}(X, Y) = \text{corr}(Y, X) \quad (2.6)$$

Thus, the correlation reflects a mutual relationship between the two signals and is independent of their order [Cha24].

### 2.3.4 Windowed Pearson Correlation

As described in Section 2.3.3, the Pearson correlation coefficient  $r$  quantifies the linear relationship between two signals  $X$  and  $Y$  when computed over their full length. In many practical settings, however, time series are non-stationary, meaning their statistical properties and mutual relationships can vary over time. For motion signals recorded by IMUs, phases of strong similarity may alternate with phases where the signals diverge due

to changes in movement execution, sensor placement effects, or transient artifacts. A single global correlation value computed over an entire recording may therefore obscure such temporal structure by averaging over intervals with substantially different relationships.

The windowed Pearson correlation addresses this limitation by computing the Pearson correlation coefficient locally on short segments (windows) of the signals, yielding a time-resolved similarity measure. Let the window length be denoted by  $\omega$ , representing the number of consecutive samples included in each local computation. For a window starting at index  $k$ , the corresponding sub-sequences are

$$X_k = (x_k, x_{k+1}, \dots, x_{k+\omega-1}), \quad Y_k = (y_k, y_{k+1}, \dots, y_{k+\omega-1}).$$

The windowed correlation value is then obtained as

$$r_k = \text{corr}(X_k, Y_k),$$

using the Pearson correlation definition from Equation 2.5. Repeating this computation while shifting the window along the time axis produces a sequence  $\{r_k\}$ , where each coefficient is associated with the corresponding time interval covered by the window. Plotting  $r_k$  over time yields a temporal correlation profile, highlighting intervals of stronger or weaker linear similarity between the signals. The selection of window parameters introduces an explicit trade-off between temporal resolution and estimate stability. If  $\omega$  is chosen too small, each  $r_k$  is computed from few samples and becomes more sensitive to noise and small perturbations, potentially resulting in high variance and unstable correlation estimates. Conversely, if  $\omega$  is too large, temporal variations are smoothed out and short-lived relationships may be averaged away, reducing the benefit of local analysis. In addition to the window length, the step size (or hop size) determines by how many samples the window start index  $k$  is advanced from one computation to the next. A smaller step size leads to overlapping windows, which typically yields a smoother correlation profile and finer temporal sampling of correlation changes, at the cost of additional computation and stronger dependence between consecutive  $r_k$  values.

It is useful to relate windowed Pearson correlation to classical operations from signal processing. Conceptually, the procedure resembles cross-correlation in that it repeatedly computes a similarity measure over sliding overlaps. More generally, this sliding-window computation is structurally similar to convolution and cross-correlation, both of which produce an output by shifting one signal relative to another and aggregating overlapping samples via a sum of products. In particular, the numerator of the Pearson correlation within a window corresponds to an inner-product-like term between the locally mean-centered segments. This similarity in structure explains why windowed correlation can be viewed as convolution-like in an operational sense. Crucially, however, windowed Pearson correlation is not a convolution in the strict mathematical sense: due to mean removal and normalization by the local standard deviations, the mapping from input signals to  $r_k$  is non-linear and time-variant. Unlike convolution with a fixed kernel, the effective normalization depends on the local signal statistics in each window, which changes as the window moves.

## 2. FUNDAMENTAL BACKGROUND

---

In summary, windowed Pearson correlation extends the global PCC by providing a local, time-resolved measure of linear similarity. At the same time, it can be interpreted as a sliding, normalized inner-product computation that is operationally related to cross-correlation and convolution, while differing fundamentally through its local centering and normalization. These properties make windowed correlation suitable for analyzing time-varying relationships in real-world signals, while requiring careful choice of window length and step size to balance robustness and temporal sensitivity.

## Related Work

This chapter reviews prior work on temporal synchronization and signal alignment in wearable and multi-sensor systems, with a particular focus on approaches relevant to HAR and multi-IMU setups. Existing literature spans a broad range of methods, including clock-based synchronization, signal-based alignment, event-driven techniques, and data-driven frameworks that infer temporal relationships directly from recorded data. In addition, work addressing the influence of sensor placement and on-body location is considered, as these factors strongly affect signal characteristics and comparability across sensors. Together, the presented research provides the conceptual and methodological context for the synchronization problem addressed in this thesis.

### 3.1 Clock-Based Synchronization

Clock-based synchronization methods aim to align the internal clocks of distributed sensors by means of explicit timing information or hardware-level coordination. In contrast to signal-based or event-driven approaches, these methods focus on achieving a shared notion of time directly at the clock level. This is often accomplished through specialized hardware components or dedicated communication protocols. As a result, clock-based synchronization can achieve microsecond-level synchronization [EGE02, WLF<sup>+</sup>24], but frequently at the cost of increased system complexity, additional hardware requirements, or reduced flexibility.

A prominent example of this class of methods is the Reference-Broadcast Synchronization (RBS) system [EGE02]. In RBS, nodes periodically transmit reference beacons to neighbouring nodes, which record the reception time of these broadcasts and use it as a common reference point for clock comparison. By eliminating uncertainties associated with sender-side transmission delays, this approach enables highly accurate synchronization between receivers. The authors report a clock agreement of approximately  $1.85 \mu\text{s}$ . However, the method requires specialized hardware support, which limits its applicability in lightweight

or low-cost wearable systems. Similarly, a unified clock-reference hardware solution that enables synchronization across multiple sensors with microsecond-level precision was developed [WLF<sup>+</sup>24]. This approach relies on dedicated hardware to distribute a shared clock reference, thereby reducing drift and offset between individual sensor clocks. While highly accurate, such solutions typically assume tight hardware integration and may not generalize well to heterogeneous or off-the-shelf IMU setups. Another hardware-oriented approach was explored, which presented a synchronization circuit that exploits ambient magnetic fields emitted by power lines as a timing reference [BRR13]. By leveraging this external signal, this system performs clock drift computation on a dedicated circuit rather than on the main CPU, resulting in improved energy efficiency. This design highlights how offloading synchronization tasks to external hardware can reduce computational overhead on sensor nodes, although it assumes the availability of a stable ambient reference signal.

In the context of wireless multi-IMU systems, a low-power, wirelessly synchronized platform in which multiple IMUs transmit data to a central capture unit was developed [CGDSVdP24]. Synchronization is achieved through coordinated wireless communication, with reported accuracy ranging from 1  $\mu$ s to 200  $\mu$ s depending on energy consumption settings. This work highlights the trade-off between synchronization accuracy and power efficiency that is characteristic on many clock-based approaches in wearable sensing. A similar system presented a monitoring system for patients with neuromuscular disorders, where up to eight wireless IMUs communicate with a base station [LCC<sup>+</sup>09]. In this system, synchronization is closely tied to node-level energy optimization, emphasizing prolonged battery life over maximal temporal precision. Further, an algorithm for synchronizing a multi-IMU network consisting of a single master unit and several slave units, relying on a centralized time reference to coordinate sensor clocks was proposed [CA20].

Beyond IMU-specific systems, several general-purpose synchronization protocols have been proposed for wireless sensor networks. For instance, the Time-Diffusion Synchronization Protocol [SA05], which enables a network to converge toward a common notion of time and maintain synchronization within a bounded deviation. In a related vein, the Timing-sync Protocol for Sensor Networks (TSPN) was introduced [GKS03]. It employs a hierarchical network structure and pairwise synchronization to establish a global time reference. TSPN achieves network-wide synchronization of less than 20  $\mu$ s under the reported conditions.

In summary, clock-based synchronization methods offer high temporal accuracy by explicitly aligning sensor clocks, often achieving microsecond-level precision. However, they typically rely on specialized hardware, centralized architectures, or strict communication assumptions. These constraints can limit their applicability in flexible, heterogeneous scenarios, motivating the exploration of alternative data-driven approaches in multi-IMU systems.

## 3.2 Signal-Based Synchronization

Signal-based synchronization methods aim to align sensor data streams only by exploiting temporal relationships inherent in the recorded signals themselves. In contrast to clock-based approaches, these methods do not rely on explicit clock coordination or hardware-level timing mechanisms. Instead, synchronization is achieved post-hoc by analyzing similarities, recurring patterns, or characteristic events within the sensor signals. This makes signal-based methods particularly attractive for heterogenous sensor setups and scenarios in which hardware synchronization is unavailable or impractical.

A prominent class of signal-based synchronization techniques are based on DTW. It aligns two time series by non-linearly warping the time axis to minimize a distance measure between them. Prior work [BC, SZL<sup>+</sup>13] describes the use of DTW for identifying similar patterns in time series data, demonstrating its general applicability to time-alignment problems. These works show that DTW can compensate for local variations in speed or temporal distortions between signals.

Beyond time-warping approaches, cross-correlation-based methods have been widely employed to estimate temporal offsets between motion signals. These methods quantify similarity as a function of relative time lag and identify the lag that maximizes correlation. Altmann et al. [Alt11] examined the use of windowed cross-lagged correlation for comparing human motion time series. Their study highlights that while windowed approaches can capture time-varying relationships between signals, auto-correlation within the signals can introduce biased correlation estimates. This observation is particularly relevant for motion data, which often exhibits strong temporal dependencies. The influence of parameter selection in windowed cross-correlation was analyzed in further research [BMBK20]. Their results indicate that window size plays a critical role in determining synchronization quality, with smaller windows generally yielding better results. In contrast, the choice of maximum lag length was found to have a comparatively smaller effect. These findings underline the importance of careful parameter tuning when applying windowed correlation methods of time-series data. Preprocessing has been identified as a crucial factor in correlation-based synchronization. It was shown [PGH<sup>+</sup>09], that periodic trends in time series can severely distort cross-correlation analysis, potentially leading to misleading synchronization results. They showed that detrending is therefore necessary, especially for long recordings where slow-varying trends may dominate the correlation structure. This highlights the need for appropriate preprocessing steps prior to applying correlation-based alignment methods.

In summary, signal-based synchronization methods provide a flexible alternative to clock-based approaches by relying on patterns and correlations in the sensor data itself. While these methods can operate without specialized hardware and are well-suited for post-hoc analysis, their performance depends strongly on signal characteristics, preprocessing, and parameter choices. These trade-offs motivate a careful methodological design when applying signal-based synchronization in multi-IMU and wearable sensing scenarios.

### 3.3 Event-Driven Synchronization

Event-driven synchronization methods align multiple sensor data streams by detecting and matching distinctive events within the recorded signals. These events serve as temporal anchors that can be identified independently in each data stream and subsequently used to estimate relative time offsets between sensors. Unlike clock-based approaches, event-driven methods do not require explicit clock coordination, and unlike pure signal-correlation-based methods, they rely on salient, discrete features rather than continuous similarity. As a result, event-driven synchronization is particularly well suited for post-hoc alignment of wearable sensor data.

In the context of IoT and wearable systems, signal-based synchronization has also been approached through the exploitation of interaction events between sensors. Bennett et al. [BGJ15b] proposed a method for synchronizing data streams in multi-IMU environments by leveraging events observed during sensor interactions. Their approach improved average clock drift by approximately 60 %, demonstrating that naturally occurring events during the interaction between two study participants can serve as effective synchronization cues. Building on this idea, they investigated which interactions between wearable and environmental sensors are most suitable for synchronization [BGJ17]. They validated their approach experimentally with four participants and reported a median drift error reduction between 66 % and 98 %. Bennett et al. [BGJ15a] further developed a system that identifies events within time series and uses these events as alignment cues, enabling synchronization to be carried out offline after data collection. The reported synchronization accuracy ranges between 277 ppm and 445 ppm, demonstrating that event-based alignment can substantially reduce clock drift without requiring hardware-level synchronization.

Several works employ external or physical events to generate explicit synchronization markers that are observable across multiple sensors. Two approaches [GDHW22, GLD<sup>+</sup>24] utilized magnetometers embedded in IMUs to detect externally generated electromagnetic pulses as shared events. Using this approach, they achieved a sub-sample synchronization error of approximately 8 ms at a sampling frequency of 25 Hz. The authors argue that the method is context-independent, as it does not rely on user-specific motion patterns. Similarly, further work [SM23] proposed an event-driven synchronization method using magnetometer data that achieves sub-sample accuracy, reporting a synchronization error of 2.6 ms at 100 Hz.

Other approaches exploit motion-specific events inherent to human activity. Shabani et al. [SBM<sup>+</sup>22] presented a method for synchronizing IMUs attached to the foot and shank by detecting manually annotated heel-strike and toe-off landmarks. Their approach achieved mean lag time of 25.56 ms. In contrast, other work [BAL09] proposed automatic detection of synchronization actions within sensor data streams. Using data collected from five users, they achieved a synchronization error of less than 300 ms for 80 % of the recordings. These works highlight both the potential and the limitations of relying on motion-derived events, as detection accuracy and consistency can vary across

users and activities. A further example of marker-based synchronization was presented by using a single, intentionally performed MA to align sensors [WSL<sup>+</sup>19]. In their setup, participants struck a table with their fist to induce a prominent acceleration peak in wrist-mounted IMUs while other sensors were resting on the table surface. This controlled event produced a distinctive signal that could be reliably detected and used as a synchronization reference. A more general post-hoc framework was introduced [SZ19], which proposed an event-driven synchronization approach based on motion events detected in pairs of IMUs. Their method reported a drift improvement of up to 98 % and achieved a mean absolute synchronization error of approximately 6 ms at a sampling frequency of 100 Hz. This work demonstrates that event-driven synchronization can achieve high accuracy even in the absence of explicit timing signals.

Beyond motion-specific events, TouchSync [YTLH19] was introduced, a software-based synchronization protocol for wearable devices. TouchSync exploits naturally synchronous skin electric potentials induced by powerline radiation as shared events observable across devices. By integrating these physiological signals into a Network Time Protocol-like framework, the method achieves millisecond-level synchronization accuracy. This approach illustrates that event-driven synchronization can also leverage shared physical phenomena rather than explicit communication or deliberate user action. Related concepts can also be found in communication and signal processing literature. It was demonstrated that synchronization based on a known reference preamble, combined with cross-correlation, leads to highly accurate alignment [FWD<sup>+</sup>03]. While not specific to wearable sensors, this work validates the general principle of event-driven synchronization, where distinctive reference signals are used to establish temporal correspondence between data streams. Finally, prior work [VJH<sup>+</sup>25] also examined human motion datasets in the context of social interaction studies, where synchronization between behavioral data streams presents similar challenges. Several of the reviewed datasets employed event-driven synchronization techniques, suggesting that findings from event-driven wearable synchronization may generalize beyond HAR to other domains involving multimodal and multi-agent temporal alignment.

### 3.4 Effects of Sensor Placement and Location

The placement of sensors on the human body plays a crucial role. Different body locations are subject to varying motion dynamics, impact forces, and constraints, which directly influence the characteristics of recorded sensor signals. As a result, the choice of sensor placement affects not only recognition performance, but also the extent to which data from different devices or studies can be meaningfully compared.

Early work in this area introduced a multi-IMU system for context-aware wearable computing [LJS<sup>+</sup>02]. A central focus of their work was the systematic investigation of suitable on-body locations for sensor placement. By analyzing sensor data collected from multiple body positions, the authors highlighted how placement decisions impact the ability to capture relevant motion patterns. Their study established that certain

locations are more informative than others depending on the target application, thereby emphasizing sensor placement as a key design decision in wearable systems. The influence of sensor placement was further examined by investigating walking data recorded by accelerometers to determine whether two sensors were worn by the same person [LHB04]. Their results demonstrate that reliable identification is achievable when both devices are carried at the same body position. However, performance degrades when sensors are placed on different body locations. This finding underscores the strong dependence of signal characteristics on sensor placement and illustrates the challenges that arise when comparing or fusing data from heterogenous on-body locations.

Complementing these empirical studies, Zeagler et al. [Zea17] compiled and synthesized existing literature on wearable sensor placement and provided updated guidelines for on-body positioning. Their work outlines the rationale behind selecting particular body locations, taking into account the intended application of the wearable system and the affordances associated with each position. By summarizing common placement strategies and their respective advantages and limitations, this review highlights that sensor placement is a trade-off between data quality, user comfort, and application requirements.

A further concern is the fact that human body motion involves substantial soft-tissue deformation, meaning that surface motion does not rigidly follow skeletal kinematics. The SMPL body model introduced by Loper et al. [LMR<sup>+</sup>15] captures pose-dependent and dynamic surface deformations, showing that body surface vertices can undergo systematic, non-rigid displacements relative to joint motion, particularly in regions with high amounts of soft tissue such as the thighs, abdomen, and upper arms [LMR<sup>+</sup>15]. Building on this deformable surface representation, Ray et al. [RZL25] proposed the W2W framework, which uses SMPL-based simulations to systematically evaluate IMU sensor placement across the body. Their results reveal clear, task-dependent trends in spatial utility: forearms and hands perform best for object-manipulation tasks, thighs, shanks, and lower back for locomotion and posture-related activities, upper arms and hips for asymmetric actions, and pelvis, chest, and ankles for full-body rotational movements. Balance-intensive tasks favor lower back, thighs, and ankles, while expressive gestures are best captured at the forearms, shoulders, and head [RZL25]. Although SMPL does not model wearable attachment and W2W assumes rigid coupling between sensors and the body surface, these findings highlight that surface deformation and sensor location strongly influence the information content of on-body measurements, which is critical when comparing signals across body positions.

### 3.5 Human Motion Synchronization

Conducted research [CTVNVdB19] offers a valuable insight into human rhythmic coordination. Using cross-correlation and coherence analysis of 3D motion capture data, the study quantified inter- and intra-person synchronization under different stimuli. It found that external cues such as a metronome enhance timing precision parallels the role of

distinct MAs in multi-IMU synchronization.

Further work [LD09] analyzed motor-control timing in human rhythmic behaviors. Their proposed detrended windowed autocorrelation method reliably identifies the underlying timing structure. This framework was taken as conceptual inspiration for the windowed correlation methods employed in this thesis, where discrete MA correspond to the event-based timing referenced in the research.

### 3.6 Data-Based Synchronization Frameworks

Data-based synchronization approaches treat temporal alignment as an optimization problem that can be solved empirically from observed data, rather than through explicit analytical models or predefined timing protocols. In contrast to clock-based synchronization, which relies on direct clock coordination, and signal-based methods that exploit continuous similarity between time series, data-based approaches focus on adapting synchronization parameters based solely on measured input-output behavior. This paradigm is particularly attractive in systems where accurate modelling of individual sensors or communication delays is feasible.

An early illustration of this principle was presented by introducing an autonomous synchronization mechanism for communication networks [TKKN03]. Their work demonstrates how local timing adjustments between neighbouring nodes can propagate through the network to achieve global alignment. Although developed in the context of communication systems, this principle is conceptually relevant for wearable sensing, as it motivates the idea that local synchronization event (such as MAs between adjacent body segments) can be combined to synchronize an entire multi-sensor system. Building on the notion of synchronization without explicit system models, a distributed output-feedback learning algorithm that achieves robust optimal synchronization among heterogeneous agents using only input-output data was proposed [CLX<sup>+</sup>23]. In their framework, each agent adapts its behavior based on locally observed signals, without requiring knowledge of global system dynamics. This perspective closely parallels multi-IMU event-driven synchronization, where each sensor operates as an independent unit and temporal alignment must be inferred from recorded measurements.

A related data-based viewpoint was adopted by formulating synchronization as an optimization problem under uncertainty within a leader-follower framework [ZLG22]. In this setup, synchronization error is minimized directly from observed data, rather than derived from analytical timing equations. This formulation supports the methodological decision in the present work to evaluate synchronization quality empirically and to focus on model-free alignment strategies.

Data-based synchronization has also been applied to domains beyond wearable sensing. Research [LDCE09] investigated the synchronization of seismic sensor data using microseisms as naturally occurring reference signals. Their approach achieved synchronization accuracy between 0.05 s and 0.2 s, demonstrating that alignment can be recovered post-

### 3. RELATED WORK

---

hoc even in large-scale and noisy sensing environments. This work highlights the general applicability of data-based synchronization in settings where explicit timing references are unavailable. Further extending data-based concepts, it was demonstrated that independent sensors can achieve phase synchronization through shared environmental fluctuations, such as temperature and humidity, without any direct communication [HYH12]. This phenomenon, referred to as noise-induced phase synchronization, shows again that temporal alignment can emerge from correlated external inputs rather than explicit coordination mechanisms. This observation provides a theoretical foundation for signal-based and event-driven synchronization approaches, where shared motion patterns or environmental stimuli act as implicit or explicit synchronization cues.

# Methodology

Across the reviewed literature, a broad spectrum of synchronization approaches has been proposed, ranging from clock-based and signal-based methods to event-driven and data-driven techniques. Clock-based solutions achieve high temporal precision but often rely on specialized hardware or centralized architectures, limiting their application in flexible wearable systems. Signal-based methods enable post-hoc alignment approaches but are sensitive to preprocessing choices and parametrization, while event-driven approaches depend strongly on the detectability and consistency of suitable synchronization markers. Data-driven framework demonstrate that synchronization can emerge empirically from observed data, yet they often abstract away from practical constraints such as sensor placement and motion variability. Taken together, existing work highlights that there remains a lack of systematic investigating into how synchronization performance is determined by the interaction between sensor placement, signal characteristic, and MA selection. This gap motivates the research questions addressed in this thesis.

- RQ1: What characteristics make for a good synchronization event?
- RQ2: How can the same event be detected at different body positions?
- RQ3: Which actions result in the best synchronization accuracy across different body positions?

## 4.1 Research Concept

The aim of this thesis is to determine which MA yield the most reliable cross-position temporal alignment in multi-IMU recordings. Further, the goal is to see which features within a signal can be used to predict the quality of a MA in terms of synchronization so that concrete recommendations for MA can be made.

The methodological foundation of this work relies on the precise definition of the constructs central to the investigation of MA in multi-IMU recordings. The central construct of interest is synchronization quality, defined as the degree of temporal correspondence between motion signals recorded at distinct body positions. Synchronization quality is treated as a relational property between two sensor locations and represents how consistently prominent motion events occur at comparable points in time. It encompasses two complementary dimensions: (1) accuracy, referring to the typical temporal alignment observed across repetitions, and (2) precision, denoting the variability of this alignment across multiple executions and participants. Together, these characteristics describe how reliably a given MA produces temporally consistent sensor responses throughout the body.

Cross-position alignment refers to the systematic comparison of signals between different body positions. Within this study, alignment is conceptualized as a pairwise relationship between a designated base position, which serves as a reference, and a set of comparison positions distributed across the body. The introduction of a base position is a necessary consequence of the adopted synchronization approach described in Section 4.4, which estimates temporal offsets exclusively through pairwise sensor comparisons. By defining a fixed reference, all other sensor signals can be aligned consistently relative to the same temporal baseline. This enables a structured evaluation of how motion originating from a specific body location potentially propagates through an individual and becomes detectable in a more distant location.

The concept of a MA is defined as a discrete, voluntary executed human movement designed to create a characteristic acceleration response across the body's IMUs. Depending on the nature of the movement, this activity may be predominantly localized and restricted to specific limbs such as clapping, distributed across multiple segments of the body, or even whole-body movements such as jumping. The methodological rationale of employing such actions lies in their potential to generate prominent, repeatable acceleration patterns that can serve as synchronization references across sensor locations. From a design perspective, the set of MA need to cover a broad spectrum of motion characteristics. This includes variation in dynamic profile, such as impulsive and continuous motions, and in body-region involvement, spanning either specific body regions or the full body. By systematically encompassing this diversity, the study aims to ensure that the evaluation of synchronization quality reflects a comprehensive range of movement scenarios rather than a narrow subset of motion types. Each MA thereby represents a controlled movement, chosen to investigate the dependence of cross-position alignment on the temporal structure of human motion.

The analysis proceeds from a conceptual framework that treats synchronization as a characteristic described by temporal correlation of motion patterns across the multiple body positions. Each MA is examined in terms of its capacity to produce consistent, temporally distinct acceleration signatures that can be observed across the entire body. The first component of the analysis focuses on the assessment of synchronization quality, which is calculated by comparing the temporal correspondence between signals obtained

from a designated base position and the remaining comparison positions. This evaluation is conducted at MA-level aggregation to evaluate general trends across motion types. Comparative analysis across MA enables the identification of those actions that yield the most robust and consistent alignment patterns, thereby addressing the third research question regarding overall synchronization quality.

The second analytical component focuses on the identification of predictive features that characterize effective synchronization events, directly corresponding to the first research question. For this purpose, a set of predefined conceptual constructs is used as a theoretical basis for quantifying event quality. These constructs are evaluated as potential predictors of the synchronization outcomes described above. The overall analytical design thus enables an integrated evaluation of what features define a reliable synchronization event, how these features manifest across different body positions, and which MA are most effective in generating temporally aligned body responses, and ideally full-body responses. All concrete computational procedures, statistical methods, and metric definitions are presented in Section 5.

## 4.2 Data Requirements

The dataset used for the evaluation must provide temporally synchronized inertial measurements across all predefined body positions to enable valid assessment of cross-position alignment. Concretely, for each body position, the recorded data must contain uninterrupted tri-axial acceleration signals with sufficient temporal resolution to preserve the characteristic timing structure of the MAs and their propagation through the body. In this work, only accelerometer data are considered, as the analysis focuses on signal energy and temporal structure. Because of this, gyroscope and magnetometer signals were not found to provide additional information relevant to the synchronization task. To ensure orientation invariance in subsequent evaluation, the signals must allow for the derivation of an orientation-invariant acceleration representation. (e.g., by magnitude), while retaining access to the underlying axes for diagnostic checks. Hardware-level synchronicity during data acquisition is required to ensure that all sensor streams share a common temporal baseline. This avoids introducing artificial temporal offsets caused by transmission latency, or buffering, and ensures that any misalignment observed during analysis can be attributed to the performed MAs and body-position effects rather than to acquisition-related synchronization errors. Multiple repetitions per MA and participant are required to support aggregation at the levels of MA and position. Finally, the dataset must satisfy the following integrity and traceability constraints. It must provide complete coverage of positions per session, consistent session identifiers linking participant, position, MA, and trial, and accompanying procedural metadata (e.g., trial order) sufficient to enforce predefined inclusion and exclusion rules in a reproducible manner.

Therefore, a specifically designed user study is required to generate a dataset that satisfies the methodological requirements of this thesis. Existing public datasets [FZF26, RCSANTPM25] offer low sampling frequency of 50 Hz to 60 Hz and do not specify the

used synchronization method. A dedicated study enables standardized instructions and trial structure to ensure comparability across participants and repetitions and sufficient coverage of localized and whole-body motions.

The data acquisition protocol requires participants who are able to accurately execute a predefined set of MAs with sufficient consistency across repetitions and body positions, while keeping a realistic degree of inter-individual variability. Consequently, the target population is defined as healthy adults without known motor impairments, capable of performing short, repeated whole-body and limb-specific movements without fatigue or external assistance. No specialisation in motion capture, biomechanics, or sensor technology is required, as the objective is to evaluate synchronization robustness under typical user conditions rather than expert-level execution. A moderately homogeneous demographic with respect to age and physical condition is preferred in order to limit confounding effects introduced by extreme anthropometric differences in age-related motor variability, while still allowing natural variation in movement amplitude, timing, and coordination. Familiarity with digital or interactive systems, such as gaming or consumer motion-tracking devices, is not a prerequisite but is acceptable, as it reflects common exposure and does not bias the temporal characteristics of the recorded signals. Overall, the participant requirements are driven by the need to obtain high-quality IMU data that are representative of realistic usage scenarios, while ensuring that observed synchronization performance can be attributed primarily to the properties of the MAs and sensor placement rather than to pathological or demographic-extreme movement patterns.

### 4.3 Experimental Design

The experiment is structured according to a between-subject design, in which each participant performs the complete set of predefined MAs under identical recording conditions. This design choice ensures that all comparisons between MAs and body positions are based on data acquired from multiple individuals. Within this framework, the independent variable is the type of MA being executed, selected from a set of eight MAs, while the dependent variables are derived from the subsequent signal analysis and include measures of signal correlation, estimated temporal lag, and lag variability. By holding all other factors constant, the experimental design isolates the influence of the participant and the executed MA on synchronization performance. To mitigate systematic effects that may arise from repeated execution of movements, such as learning, anticipation, or fatigue, the order of MAs is randomized within each trial. This randomization ensures that no single action consistently benefits from a fixed temporal position within the sequence and that performance differences cannot be attributed to order effects. In addition, all participants complete the same number of trials using identical equipment and under the same experimental conditions, which further strengthens internal validity and supports consistent data acquisition across the dataset. A standardized procedure is applied throughout all sessions, including the use of uniform verbal instructions and

the incorporation of rest breaks between trials to minimize unintended variation in task execution.

In order to complement the quantitative IMU-based measurements, two questionnaires are integrated into the experimental design. A pre-experiment questionnaire captures demographic and background information, a post-experiment questionnaire collects subjective assessments related to the recording session. These subjective ratings provide contextual information that supports a qualitative interpretation of the MA, particularly with respect to their practicality and suitability for repeated use in future data collection scenarios.

The following subsections provide a detailed description of the individual components of the experimental design. This includes a precise definition of the MAs, the questionnaires, and the procedure used for collecting both inertial and questionnaire data. Together, these elements define a controlled and reproducible experimental protocol that forms the methodological basis for the analysis presented in Section 6.

#### 4.3.1 Gesture Definition

To ensure that the user study captures a broad spectrum of human motion while remaining practically feasible, an initial set of ten candidate MAs was qualitatively assessed with respect to their assumed suitability for data-driven synchronization. As summarized in Table 4.1, each MA was rated along three dimensions: (1) assumed synchronization quality (1–10, weighted higher due to its primary relevance), (2) physical comfort (1–5), (3) and ease of movement (1–5). The resulting score represents the unweighted sum of these criteria and serves solely as a coarse comparative indicator rather than a quantitative performance metric. This assessment was used to balance diversity in movement patterns—ranging from cyclic to non-cyclic motions and from low- to high-intensity actions, against practical considerations of repeatability and signal interpretability. Based on this evaluation, quick start was excluded due to its low overall score, reflecting both limited assumed synchronization robustness and less favorable practical characteristics. Relaxed standing was likewise excluded, not primarily because of its numerical score, but due to the anticipated lack of distinctive signal features, as quasi-static postures are unlikely to produce temporally distinctive patterns suitable for reliable cross-sensor alignment. The remaining eight MA were selected to form a balanced dataset spanning different body regions, durations, amplitudes, and kinematic structures, thereby enabling a systematic evaluation of the synchronization approach across heterogeneous motion conditions.

*Clap.* Participants are instructed to clap their hands once. This MA represents a short, impulsive upper-body motion characterized by a single, sharp acceleration peak in the arm sensors. Due to its highly localized nature, strong synchronization is assumed among the upper-limb IMUs (forearms, upper arms), while limited correlation is anticipated in the lower-body sensors. Despite its simplicity, this MA serves as a valuable control

Action	Synchronization	Comfort	Ease of Movement	Score
sit down / stand up	9	5	4	18
stomp on ground	8	4	5	17
clap	7	5	5	17
walking	6	4	4	16
heel raise	5	4	4	13
jumping jack	8	1	1	11
forward fold	5	3	3	11
running in place	7	2	1	10
relaxed standing	1	5	5	11
quick start	3	2	2	7

Table 4.1: Qualitative relationship between signal features and synchronization outcomes. The table summarizes how strong characteristics correlate with higher synchronization accuracy and precision across MA.

movement because of its ease of execution and its well-defined temporal signature, which provides a clear benchmark for alignment quality.

*Stomp.* Participants are asked to stomp on the ground with their right foot once. This MA targets the lower limbs and is primarily characterized by a high-magnitude impact on the right foot IMU, propagating upwards through the leg and pelvis sensors. Minimal synchronization is assumed in upper-body sensors. Similar to Clap, analyzing Stomp allows the evaluation of how effectively temporal events in distal body sensors can be aligned with central trunk sensors, despite their localized activation.

*Jump.* Participants perform four to five jumping jacks at a comfortable pace. This cyclic, full-body MA produces synchronized oscillations across multiple sensors and engages both upper and lower limbs simultaneously. Although not representative of everyday movement, this MA is valuable for investigating periodic synchronization behavior, where recurring motion cycles create consistent correlation patterns between IMUs. The Jump action thus serves as a reference for assessing synchronization under repetitive, high-energy motion.

*Fold.* Participants are instructed to bend forward and attempt to touch the ground with their hands, ideally keeping their legs straight. This MA constitutes a slow, deliberate movement involving a large orientation change in the torso, head, and arms. Unlike the impulsive MA described above, Fold emphasizes continuous, low-frequency motion. It therefore provides insight into how synchronization behaves in slow, low-jerk transitions, where dynamic acceleration peaks are minimal.

*Walk.* Participants are asked to walk naturally for approximately five seconds. This MA produces a rhythmic, periodic gait pattern that is representative of real-world human locomotion. The Walk action activates nearly all IMUs in coordinated, phase-shifted

patterns, reflecting natural inter-limb synchronization. Because of its regularity, this MA serves as a baseline for natural synchronization, allowing comparison with more artificial or controlled motions. It also provides a test case for evaluating whether spontaneous, everyday movements are sufficient for alignment without explicit synchronization markers.

*Heel.* Participants raise their heels and then return to the ground once. This MA represents a small-amplitude, controlled lower-limb motion that still propagates measurable acceleration through the body. It is particularly suitable for assessing the system's sensitivity to fine-grained movements, as it produces subtle yet distinct temporal signals. Synchronization of such micro-movements provides insight into the algorithm's ability to detect weak temporal cues in the data.

*Sit.* Participants sit down on a chair (as seen on the bottom right in Figure 5.2) and stand up again after approximately two seconds. This MA combines two opposite motion phases (sit-down, stand-up) making it inherently more complex than single-phase movements. The Sit action reflects natural everyday motion but poses additional challenges for synchronization because of its non-linear dynamics and variable duration. It allows the analysis of multi-phase events and temporal segmentation, where start and end points may vary subtly between trials.

*Run.* Participants are instructed to run in place for about three seconds. This high-frequency, cyclic MA produces strong periodic acceleration peaks across both upper and lower body segments. The resulting data will presumably exhibit higher amplitude variability and noise due to impact and body oscillation. The Run MA is therefore useful for assessing the robustness of synchronization methods under dynamic, high-energy conditions, where sensor saturation or motion artifacts may occur.

Overall, the eight selected MA together constitute a comprehensive motion set, balancing localized and full-body movements, cyclic and non-cyclic patterns, as well as low- and high-intensity dynamics. The emphasis on movements that can be performed by almost the entire population ensures broad accessibility while maintaining sufficient complexity for algorithmic evaluation. A summarized comparison of key characteristics for each MA is provided in Table 4.2.

### 4.3.2 User Questionnaires

Two structured questionnaires were incorporated into the experimental design to augment the sensor readings with participant-related information that cannot be inferred from IMU signals alone. While the primary outcome measures of this work are derived from quantitative synchronization analyses, the perception of an MA (including its perceived effort, clarity, and ease of execution) constitutes relevant contextual information when interpreting feasibility and applicability across users and recording conditions. The questionnaires therefore serve a complementary role, as they capture subjective assessments of the MAs along dimensions that are practically relevant for the deployment of event-based synchronization in real-world data collection, and they document participant-related factors that may influence action execution, such as familiarity with motion-based interac-

Gesture	Cyclic	Duration (approx.)	Signal Intensity	Primary Movements	Body Seg-	Motion Pattern	Assumed Synchronization Difficulty
<b>Clap</b>	No	< 1 s	High	Arms, upper torso		Single impulse	Low
<b>Stomp</b>	No	< 1 s	Medium	Legs, lower body		Single impulse	Medium
<b>Jump</b>	Yes	4–5 s	High	Full body		Repetitive	Low
<b>Fold</b>	No	3 s	Low	Trunk, upper body		Slow continuous	High
<b>Walk</b>	Yes	5 s	Medium	Full body		Repetitive	Medium
<b>Heel</b>	No	1–2 s	Low	Full body		Double impulse	Medium
<b>Sit</b>	No	3–4 s	Low	Torso, lower limbs		Slow continuous	Very High
<b>Run</b>	Yes	5 s	High	Full body		Repetitive	Low

Table 4.2: Overview of the eight MAs performed by participants. The set includes both cyclic and non-cyclic gestures with varying intensity, motion patterns, and synchronization difficulty across body positions.

tion or general activity habits. Importantly, the questionnaires are not intended to replace sensor readings, but to provide structured evidence that supports the methodological evaluation of MAs as synchronization events, particularly when multiple candidate actions yield similar quantitative outcomes or when specific actions exhibit high between-subject variability.

The questionnaire component is deliberately split onto two parts, motivated by both response-quality considerations and operational constraints of the recording procedure. First, administering an initial questionnaire before the recording session reduces the impact of physical and cognitive fatigue on response behavior. Since the experimental protocol requires participants to execute multiple actions, often repeatedly, post-session responses alone would be prone to shortened answers, satisficing behavior, and conflation of individual actions due to reduced recall fidelity. Collecting baseline information prior to any exertion increases the likelihood of attentive, complete responses and provide a consistent reference point. Second, the instrumentation procedure imposes unavoidable setup time, as the motion capture suit must be physically adjusted to each participant's physiology after arrival. Embedding the initial questionnaire into this phase creates a productive waiting period, reduces idle time, and lowers perceived burden by structuring the session into alternating phases of preparation, assessment, and execution. This design choice improves participant experience without altering the recording conditions. Participants remain engaged while the experimenter performs required configurations, and the overall workflow becomes more efficient and predictable.

The second questionnaire is positioned after the action execution phase to capture immediate reflections on the performed MAs. This timing enables participants to evaluate the actions with fresh experimental memory, which is critical for questions that depend on perceived exertion, coordination demands, comfort while wearing the suit, and perceived distinctiveness of the action as a deliberate "event". In the methodological terms, separating baseline characteristics from post-execution rating allows the study to disentangle stable participant attributes (e.g., prior exposure to motion tracking, or typical activity levels) from action-specific evaluations that are grounded in the actual recording context. Taken together, the two-questionnaire structure operationalizes this component as a controlled measurement instrument. It improves data quality through reduced fatigue-related response degradation, integrates seamlessly with the suit adjustment process to minimize downtime, and yields complementary information that supports a more comprehensive assessment of MAs beyond purely signal-based synchronization metrics. The full questionnaires can be found in Appendix A.2.

### 4.3.3 Procedure

The experimental procedure was designed to ensure methodological consistency, participant comfort, and data integrity, across all sessions. Each session followed a standardized sequence, consisting of introduction and familiarization, a pre-questionnaire, equipment preparation, recording phase, and a post-questionnaire, as illustrated in Figure 4.1.

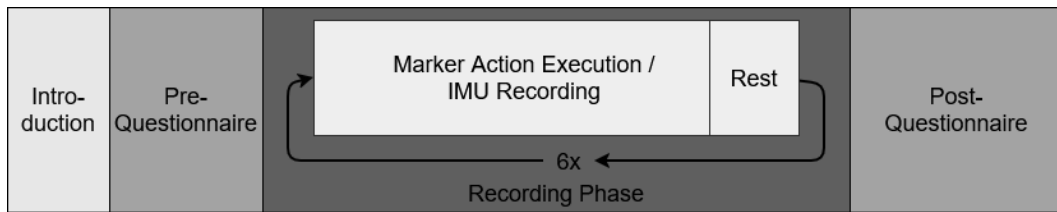


Figure 4.1: Illustration of the temporal order and relative positioning of user study procedure steps showing a briefing phase, a pre- and post-questionnaire phase, and the recording phase as a central element.

After confirming their voluntary participation in the user study through a consent form (see Appendix A.1), participants first complete a pre-experimental questionnaire. This questionnaire collects demographic information on age, gender, height, and weight, as well as prior experience with motion-tracking systems and general physical activity level. These data is necessary to ensure that the participants fulfill the requirements specified in Section 4.2. Additionally, they will later be used to characterize the sample and assess potential demographic influences on sensor synchronization performance.

Participants are then led to a designated preparation room to change into the motion capturing suit. The suit's integrated IMUs are pre-installed but not connected to any power source at this stage to ensure privacy and data protection. Participants are instructed to wear form-fitting clothing underneath the suit to ensure tight contact between the sensors and the body surface. Additionally, adjustable straps are used to secure the sensors at each body segment, minimizing sensor movement relative to the participant's body during motion execution.

Once the suit is fitted, the MA are verbally explained by the instructor and demonstrated once to ensure consistent understanding and execution across participants. Each participant is given the opportunity to practice the MA briefly, allowing them to familiarize themselves with the suit and reduce unnatural movement behavior during the actual recording. Before the recording phase begins, participants are provided with a portable power bank, which they connected to the suit to power the IMUs. A short five-second test recording is conducted to verify the correct connection of all sensors and ensure stable data transmission.

Following the setup, the participant confirms readiness to begin the recording phase. The experimenter then initiates the first of six trials. Each trial contains the full set of eight MA in a randomized order. The sequence of MA is not revealed to the participant beforehand to prevent anticipatory behavior. The experimenter announces each MA in real time during the recording to guide the participant. Prior to each recording, the experimenter informs the participant that the recording is about to begin. Similarly, participants are notified immediately after each recording is stopped. No data is recorded outside of the official recording sessions or without the participant's explicit awareness and consent.

Between trials, participants are encouraged to rest and are provided with refreshments (water, soft drinks) and snacks (cookies, sweets). If a MA is performed incorrectly or a recording error occurs, the trial is immediately aborted and repeated in full to maintain a consistent dataset. As a result, each participant contributes a total of 48 valid MA recordings, six for each of the eight movement types.

After completing all six trials, participants fill out the post-experimental questionnaire. This form collects subjective evaluations of comfort, fatigue, and perceived difficulty for each MA, as well as open-ended feedback on the overall experiment. These responses provide valuable qualitative insight into participant perception and can later be considered in interpreting the synchronization results.

In total, each recording session is designed to last approximately 30–40 minutes, including setup, rest, and questionnaire completion time. This duration target is chosen to balance data quantity and participant comfort while maintaining high recording quality across all sessions.

## 4.4 Synchronization Approach

To analyze temporal alignment between inertial signals recorded at different body positions, this work adopts a correlation-based synchronization approach centered on the PCC. The underlying assumption is that well-defined MAs induce characteristic acceleration patterns that are observable across multiple IMUs with a consistent temporal structure. By quantifying the linear similarity between these signals under varying temporal offsets, the PCC provides a principled means of estimating relative delays between sensors without relying on external time references or explicit event annotations. Temporal offsets are estimated by evaluating the PCC as a function of a temporal lag between two signals within sliding windows. The lag value that maximizes the correlation is interpreted as the optimal temporal alignment for the respective signal pair within a given repetition. Repeating this procedure across multiple executions of the same MA yields a set of lag estimates that jointly characterize the synchronization behavior between two body positions. This windowed formulation is essential to accommodate non-stationary signals and allows the analysis to be adapted to both short, impulsive movements and longer, more periodic actions.

From the collection of pairwise lag estimates, two aggregate measures are derived to summarize synchronization performance. The mean lag represents the systematic temporal offset between two sensors and captures whether events tend to be detected earlier or later at one body position relative to another. In contrast, the lag standard deviation quantifies temporal consistency across repetitions and serves as an indicator of synchronization stability. Together, these measures provide complementary perspectives. While the mean lag reflects the accuracy, the standard deviation reflects the precision of the synchronization. To support interpretation beyond individual signal pairs, these summary metrics are further aggregated spatially across the body. For each MA, lag statistics computed relative to a fixed reference sensor are mapped onto an anatomical

representation of the body. This body-map abstraction enables the spatial distribution of synchronization quality to be assessed at a glance, highlighting which body regions exhibit stable and consistent temporal alignment and which regions show increased variability or systematic delay. By combining correlation-based lag estimation with spatial aggregation, the methodology supports both fine-grained pairwise analysis and holistic, body-level assessment of synchronization characteristics.

Overall, this methodological framework establishes a consistent link between the temporal structure of performed MAs, the resulting inertial signals, and their suitability for event-driven synchronization. It provides a unified basis for comparing different MAs and body positions using interpretable, quantitative measures, while remaining independent of specific implementation choices or visualization techniques described in later sections.

# Implementation

The implementation builds on the experimental design of the user study and translates it into a concrete data acquisition and analysis pipeline. Motion data were recorded using a multi-IMU setup during the execution of predefined MAs and subsequently processed to enable temporal alignment across sensor streams. Signal synchronization was implemented using the Pearson correlation coefficient, allowing relative temporal offsets between sensors to be estimated in a reproducible and systematic manner. This section details how the study procedure, data handling, and alignment computations were operationalized in practice.

## 5.1 User Study

The data acquisition phase marks the beginning of the experimental pipeline, as all subsequent preprocessing, synchronization, and evaluation steps directly depend on the quality and structure of the recorded data. Particular care was, therefore, taken to design and execute a recording procedure that yields consistent, well-defined inertial measurements while remaining feasible within a controlled experimental setting. In addition to the IMU data itself, auxiliary participant-related information was collected to contextualize the recordings and support later interpretation.

### 5.1.1 Participants

Participants were recruited through two channels, through personal invitation by the author and through a computer science course at TU Wien. The participants in the computer science course signed up voluntarily, but were asked to participate in at least one user study to advance their studies. 33 subjects participated in the experiment (23 male, 10 female). The participants were between 16 and 40 years old (mean  $M = 23.0$ , standard deviation  $SD = 4.2$ ), with an average body weight of  $72.5 \pm 16.6$  kg, and an average body height of  $174.0 \pm 8.9$  cm.

All participants were students of computer science, comprising both undergraduate and graduate levels. Prior experience with motion tracking systems varied among participants. 26 individuals reported previous interaction with such systems, mostly in entertainment contexts (e.g., Microsoft Kinect, Nintendo Wii Sports), whereas only one participant had prior experience wearing a full-body motion capture suit. Regarding physical activity, 13 participants reported engaging in exercise more than three times per week, while an additional 13 participants exercised at least once per week. Participants were also asked about their gaming habits to assess their familiarity with interactive motion-based systems. 14 participants played video games at least once a week, while 5 participants reported never playing video games.

Eligibility criteria required participants to be capable of performing 30 minutes of low-intensity physical activity with rest periods. Furthermore, their BMI needed to be in the “normal” range, ensuring proper fitting of the motion capturing suit and avoiding fatigue effects. Participants were excluded if they reported any musculoskeletal disorders or other physical limitations (e.g., scoliosis, chronic joint pain) that could increase the risk of injury. All participants provided written informed consent prior to participation, in accordance with institutional research ethics guidelines<sup>1</sup>. One participant was excluded after data collection because, due to issues with balance during the Heel MA, they were unable to perform all required gestures correctly. The 32 remaining participants successfully completed the recording sessions.

### 5.1.2 Setup and Sensor Placement

The inertial data were acquired using the Rokoko SmartSuit Pro II<sup>2</sup>. This suit was chosen because of its proven use in research [HKB<sup>+</sup>23, HKB<sup>+</sup>25], recording capabilities of up to 200 Hz, and comprehensive set of body positions which records participant movement through a distributed set of 17 body-attached IMUs that are built directly into the suit. These sensors are positioned at predefined anatomical locations covering the major segments of the human body, namely the head, shoulders, upper arm, lower arms, forearms, lower back, hips, thighs, lower legs, and feet. This configuration provides comprehensive spatial coverage of both upper- and lower-body motion, enabling the simultaneous capture of localized and global movement patterns across the full body. The exact placement of the sensors is fixed by the suit design and is illustrated in Figure 5.1, which serves as a reference for the spatial interpretation of the recorded data. For the purposes of data processing and analysis, each sensor is uniquely identifiable within the recorded dataset and can be consistently mapped to its corresponding body segment using a predefined labelling scheme. From a data collection perspective, a sensor placement at the sternum would have been desirable, as this location is commonly used by consumer-grade physiological sensors, such as heart rate monitors, and could have enabled additional analysis or alignment with external wearable devices. Similarly, a sensor positioned at the wrist, instead of just the lower arms would reflect consumer-grade

<sup>1</sup><https://www.tuwien.at/en/research/rti-support/responsible-research-practices>, accessed 01.02.2026

<sup>2</sup><https://www.rokoko.com/products/smartsuit-pro>, accessed 23.01.2026

devices more accurately. However, no sensor repositioning or customization beyond the standard suit configuration was performed. This decision was made to ensure proper fitting of the sensors on the specified positions by the suit, which could be compromised by repositioning the sensors. These limitations are discussed in-depth in Section 7.1.

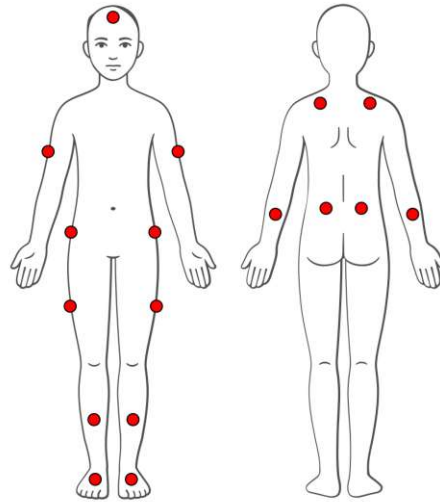


Figure 5.1: Schematic representation of the 17 body positions where IMU data were recorded during the user study.

The user study was conducted in a controlled laboratory environment at TU Wien, as illustrated in Figure 5.2. The laboratory provided a defined experimental space designed to support reproducible recording conditions across participants and sessions. At the center of the room, a dedicated area of approximately 3 m by 4 m was verbally explained to the participants, and reserved exclusively for the execution of the MAs. This area offered sufficient freedom of movement for all actions included in the protocol while maintaining spatial consistency across trials. All objects such as table, chairs, and other furnishings were positioned outside the designated execution area to ensure unobstructed movement and to eliminate potential hazards that could result in physical harm during the performance of the MAs.

The recording workstation, consisting of a laptop connected to the Rokoko motion capturing system, was positioned on the right-hand side of the room and remained stationary throughout the study. To ensure reliable communication between the recording system and the motion capture hardware, both the laptop and the central hub of the Rokoko SmartSuit Pro II were connected via a local wireless area network established specifically for the experiment. This dedicated network configuration minimized interference from external devices and ensured stable connectivity during all recording sessions. On the opposite side of the room, multiple sizes of the Rokoko SmartSuit Pro II were organized

## 5. IMPLEMENTATION

---

and made readily accessible to facilitate efficient fitting and adjustment for each participant. This arrangement allowed suit changes and size adaptations to be performed with minimal interruption to the experimental workflow. A separate room adjacent to the laboratory was provided for the participants to change into the suit in private. In addition, refreshments, including water, soft drinks, and light snacks, were provided in the left corner of the room. These were available to participants during short rest periods between trials and contributed to maintaining comfort over the course of the recording sessions.

Environmental conditions within the laboratory were controlled to ensure consistency across participants. The room was air-conditioned and maintained at a constant temperature of approximately 21 °C, which helped mitigate thermal discomfort associated with wearing an insulating motion capture suit for extended periods. Uniform lighting conditions were maintained throughout the sessions, and the laboratory was acoustically isolated from external disturbances. Together, these measures ensured a stable and distraction-free environment, reducing the likelihood that environmental factors influenced participants' movement execution or overall comfort during the experiment.



Figure 5.2: Setup of the user study in the laboratory showing the execution area in the middle and the technical setup on the right.

### 5.1.3 Recording of Acceleration Data

For each participant, IMU data were acquired across six complete recording sessions (hereafter referred to as trials). Each trial comprised the execution of the full set of eight predefined MA defined in Section 4.3.1, with the order of actions randomized independently for each trial. This randomized presentation was deliberately introduced to mitigate systematic effects arising from repeated exposure, such as learning, anticipation, or motor adaptation, which could otherwise bias the temporal dynamic characteristics of the recorded signals. By varying the action order across trials, the resulting acceleration profiles more reliably reflect the intrinsic properties of each MA rather than execution artifacts induced by fixed sequencing. Following the execution of each individual MA, participants briefly returned to a neutral standing pose before proceeding to the next action. This introduced a clearly distinguishable temporal boundary in the continuous action stream, such as residual momentum, postural transitions, or unintended preparatory movements, thereby limiting cross-action interference in the recorded signals. This design choice ensured that the acceleration patterns associated with each MA could be analyzed in isolation without contamination from preceding actions. Each trial had an approximate duration of 50-60 seconds, with minor variations attributable to individual differences in execution speed and movement precision. Upon completion of a trial, the recorded IMU data were automatically stored as comma-separated value (CSV) files using a predefined and consistent naming convention. This standardized file structure encodes relevant session metadata, including participant identifier, trial order, and recording timestamp. It enables automated association between raw sensor data, trial-level annotations, and subsequent synchronization results during downstream processing.

All inertial data were recorded using the Rokoko SmartSuit Pro II, which continuously streamed IMU measurements at a sampling rate of 200 Hz, corresponding to 200 samples per second for each individual sensor channel. This sampling rate was selected to ensure adequate temporal resolution for capturing short-duration, high-dynamic MA while remaining within the operational constraints of the recording hardware. Each IMU provides 3-axis acceleration ( $a_x, a_y, a_z$ ), 3-axis gyroscope ( $\omega_x, \omega_y, \omega_z$ ), and 3-axis magnetometer ( $m_x, m_y, m_z$ ). Data transmission was performed wirelessly and remained well within the supported tracking range of up to 100 m, such that no signal degradation or interruptions due to range limitations were expected during the recording sessions. Rokoko Studio was deliberately not used for data acquisition, as it exposes only the proprietary Sensor Fusion 2.0 output of the system. In this representation, measurements from the accelerometer, gyroscope, and magnetometer are internally fused by the manufacturer and provided as a single, preprocessed four-dimensional quaternion for each limb segment. While this representation is suitable for real-time animation and motion reconstruction, it obscures the raw inertial measurements and introduces algorithmic processing that cannot be controlled or inspected. Because the synchronization analysis in this work operates directly on raw acceleration signals and relies on their temporal structure, the use of fused quaternion data would have limited both methodological and analytical flexibility. To address this limitation, a custom data acquisition script provided by Rokoko

was employed to extract the raw sensor measurements for each time frame. This script delivers unprocessed accelerometer, gyroscope, and magnetometer reading directly from all sensors, enabling full access to the underlying inertial data required for subsequent signal processing and synchronization analysis. Despite bypassing Rokoko Studio and its higher-level abstractions, the sensor data were still transmitted via the suit's central hub. This design ensures that all sensor streams remain hardware-synchronized at the point of acquisition, providing a common temporal reference across body-mounted units. As a result, any temporal misalignment observed during later analysis can be attributed to signal-level effects and processing decisions rather than to inconsistencies in sensor transmission.

#### 5.1.4 Questionnaire Data

The two questionnaires defined in the experimental design were administered digitally using a dedicated laptop and implemented with Microsoft Forms. This setup ensured a standardized presentation of all question items and response options across participants while allowing direct electronic capture of responses without intermediate transcription. Each participant completed the questionnaires individually on the same device, which reduced variability introduced by differing hardware or input modalities. The use of a dedicated laptop further ensured that questionnaire completion was spatially and temporally integrated into the experimental session and did not rely on participants' personal devices.

The first questionnaire was administered prior to the execution of the recording phase, while the second questionnaire was completed immediately after the recording phase. Responses were recorded automatically by Microsoft Forms and exported in tabular format for further processing. Each response was associated with a unique identifier corresponding to the same identifier used for the IMU recordings, enabling unambiguous, but pseudonymous linkage between subjective questionnaire data and the respective inertial measurements. The questionnaire data were stored separately from the raw IMU signals but referenced within the same session-level metadata structure. No additional processing beyond basic plausibility checks (e.g., completeness of responses) was applied at this stage. Details on questionnaire content, question items, and scales are provided in Section 4.3.2 and in Appendix A.2.

## 5.2 Pearson Correlation

The Pearson correlation coefficient (PCC) is employed in this work as a quantitative measure of linear similarity between two time-dependent signals  $x(t)$  and  $y(t)$ . For each signal pair, the PCC yields a scalar coefficient  $r \in [-1, +1]$  that characterizes the degree to which the temporal patterns of the two signals are linearly related. A value of  $r = 1$  indicated perfect positive correlation, meaning that both signals exhibit identical temporal structure up to a scaling factor. Conversely, a value of  $r = -1$  corresponds to perfect negative correlation, while  $r = 0$  indicates the absence of a linear relationship. In the

contet of temporal alignment, higher values of  $r$  therefore indicate a stronger similarity between the compared signals and, by extension, a better temporal correspondence. A formal mathematical definition of the PCC is provided in Section 2.3.3.

For the correlation-based synchronization, the raw inertial measurements are processed into their Eukclidean norm, as it captures the overall intensity of movement while remaining invariant to rotations of the sensor coordinate frame. Given the three-axis accelerometer readings  $a_x(t)$ ,  $a_y(t)$ , and  $a_z(t)$ , the acceleration magnitude  $a_{mag}(t)$  is computed as

$$a_{mag}(t) = \sqrt{a_x(t)^2 + a_y(t)^2 + a_z(t)^2} \quad (5.1)$$

This transformation yields a one-dimensional signal per sensor that reflects the overall movement dynamics independent of directional space. By reducing the dimensionality of the data in this manner, the subsequent correlation analysis becomes less sensitive to differences in sensor orientation and placement, while preserving the temporal characteristics that are relevant for synchronization.

To estimate the temporal offset between two non-stationary signals, the Pearson correlation coefficient is computed within a sliding-window framework. One signal is selected as the reference signal  $x(t)$ , while the second signal  $y(t)$  is shifted by a temporal lag  $\tau$  over a predefined range. In this work, the lag range is chosen as  $\tau \in [-200, 200]$  samples, which corresponds to a temporal displacement of  $\pm 1$  seconds at a sample rate of 200 Hz. This range is sufficiently wide to capture plausible misalignments between sensors while remaining computationally tractable. For each candidate lag value  $\tau$ , the PCC is computed as

$$r(\tau) = \text{pearsonr}(x(t), y(t + \tau)) \quad (5.2)$$

yielding a correlation function  $r(\tau)$  that describes the similarity between the two signals as a function of temporal displacement. The optimal temporal offset is then determined as the lag value that maximizes this function,

$$\tau_{best} = \text{argmax}(r(\tau)) \quad (5.3)$$

This value represents the estimated relative delay between the two signals within the analyzed window, illustrated in Figure 6.2. In practice, the lag values are evaluated in discrete steps determined by the sampling frequency of the recorded data. With a sampling rate of 200 Hz, the smallest possible lag increment corresponds to a temporal resolution of 5 ms. This resolution directly influences the precision of the estimated temporal offset. Larger step sizes would reduce computational cost but at the expense of temporal accuracy. Because several of the investigated MA involve rapid and transient movements, such as clapping or running in place, preserving the highest possible temporal resolution is essential to accurately capture sharp peaks and sudden changes in the acceleration signals. The length of the sliding window used for correlation is selected based on the temporal characteristics of the analyzed MA. Periodic or cyclic motions, such as walking or other repetitive actions, require larger window sizes to encompass one or more complete motion cycles, thereby providing a stable basis for correlation. In contrast,

## 5. IMPLEMENTATION

---

short and discrete gestures, such as clapping, are analyzed using smaller windows in order to preserve temporal precision and avoid smoothing out of brief but informative signal features. Together, the use of acceleration magnitude preprocessing, windowed Pearson correlation, and fine-grained lag evaluation constitutes the core synchronization mechanism implemented in this work.

# Evaluation

This chapter presents the evaluation of the synchronization framework applied in this thesis. It first describes the preprocessing steps applied to the recorded sensor data and outlines how the Pearson correlation coefficient was used to quantify temporal alignment across the dataset. The chapter then summarizes the performed computations and provides an overview of the resulting synchronization outcomes.

## 6.1 Data Processing

The evaluation is based on a structured data processing pipeline that transforms the raw IMU recordings into analyzable synchronization measures. Continuous sensor streams are first segmented into individual MAs to ensure temporal isolation of each movement. Temporal offsets between sensors are then estimated using windowed cross correlation, enabling robust alignment under local temporal variability. The calculated lag metrics are subsequently aggregated across body positions and represented using body maps, allowing spatial patterns in synchronization behavior to be examined across the full sensor layout.

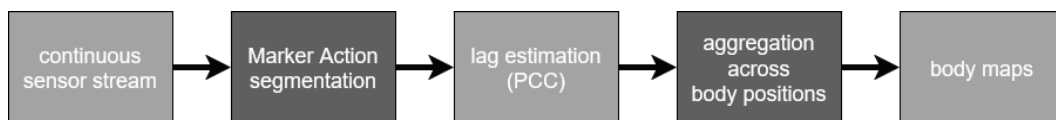


Figure 6.1: Illustration of the data processing pipeline from raw sensor data to aggregated body maps showing estimated lags using PCC.

### 6.1.1 IMU Data

The Rokoko Smartsuit Pro II provides 3-axis acceleration  $(a_x, a_y, a_z)$ , 3-axis gyroscope  $(\omega_x, \omega_y, \omega_z)$ , and 3-axis magnetometer  $(m_x, m_y, m_z)$  data with a sampling frequency of

200 Hz for every IMU. After each day of recording, the recordings were checked visually for plausibility and completeness. Two recordings displayed faulty sensor data, where the values showed constant maximum acceleration. To keep the consistency of six sessions per participant, the two participants with faulty recordings were excluded entirely. One additional participant was excluded for failing to execute the MAs correctly, as this person could not perform the Heel MA due to issues with balance. Additionally, they did not adhere to the rest period between MAs, making segmentation of the events within the data impossible. With this, out of 198 expected recordings per MA, 180 were valid after preprocessing. Consistent execution of the MA across participants was maintained by standardized instructions and demonstrations by the instructor. Furthermore, the order the MA were performed in was randomized as described in Section 4.3.3.

For the analysis of the individual MA, the recordings needed to be segmented. This was done manually by a custom annotation tool. This custom implementation allowed to load the data format provided by the Rokoko Suit, to control how each data series is presented, and to export each MA in the format needed for further processing. For every trial, the tool loads the sensor data of three important body positions (right lower arm, right lower back, right foot). These three positions were chosen because they allowed identification of every MA. The sensor right lower back was chosen because of its central position near the center of mass, which makes it easy to detect full-body MAs. For localized upper body MAs, such as Clap, a lower hand sensor is needed to reliably detect the event within the signal. Finally, the sensor on the right foot was selected with similar reasoning in reference to the Stomp MA. Additionally to the sensor data, the MA sequence for that specific trial is loaded. The program then asks the annotator to move a red vertical line to the beginning or the end of a specific MA, respectively. After confirmation by clicking on the graph, the frame numbers from the start and the end of the MA are saved. Additionally, a separate csv file only containing the signals of the selected MA is also saved in a folder named after the MA. A screenshot of the annotation tool can be seen in Figure 6.2. After successful annotation, the annotator is left with eight folders (one for each MA) each containing 180 csv files with the respective snippets from each valid trial.

### 6.1.2 Windowed Pearson Correlation Coefficient

The pair-wise synchronization between sensors was assessed using Pearson correlation coefficients computed in a sliding-window manner. The analysis was performed separately for each MA. For a given MA, temporal alignment between sensors was estimated by selecting one signal as a reference  $b$  and computing the correlation-lag curve with respect to a target signal  $a$  from another body position. Repeating this procedure across all sensor pairs yielded a complete set of correlation coefficients characterizing the relative temporal alignment for each MA.

Operationally,  $a$  is shifted sample-wise over a symmetric lag interval  $[-L, +L]$  while  $b$  is kept fixed. At every discrete lag  $\tau \in \{-L, \dots, 0, \dots, L\}$  the Pearson correlation coefficient  $r(\tau) = \text{pearsonr}(a + \tau, b)$  is evaluated on the common overlapping window of the two sequences. This produces, for each  $(\text{base}, \text{window})$  pair, a vector of coefficients

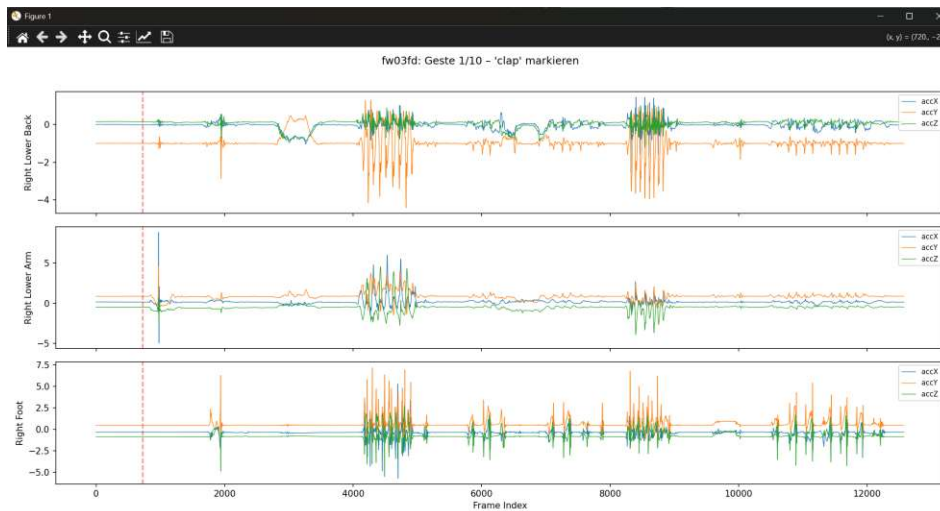


Figure 6.2: Annotation tool for MA segmentation of the recordings showing 3-axis acceleration data of three important body positions and the MA to annotate next.

---

**output:** list of r-values per (base, window) pair

```

1 b ← base_signal;
2 for every other sensor position as window_signal do
3   r ← {};
4   a ← window_signal.shift (-max_lag);
5   for i ← 0 to max_lag * 2 do
6     r ← pearsonr (a,b);
7     coeffs.append (r);
8     a ← a.shift (1);
9   end
10 end

```

---

$\{r(\tau)\}$  that characterizes the similarity of the two signals as a function of relative delay as seen in Figure 6.3. The best lag  $\tau_{best}$  is obtained as the argmax of this vector,  $\tau_{best} = \text{argmax}(r(\tau))$ , and converted to time by  $\Delta t = \frac{\tau_{best}}{f_s}$  with a sampling rate  $f_s = 200$ . The corresponding peak value  $r_{max} = r(\tau_{best})$  serves as a quality indicator of the alignment. Repeating this procedure for all sensor positions with respect to their reference yields a complete set of pair-wise lag estimates and correlation strengths for the MA under analysis.

### 6.1.3 Computing Summary Metrics

From the set of pairwise IMU correlations and their corresponding optimal lag estimates  $\tau_{best}$ , two aggregate summary metrics are derived to characterize the temporal relationship

between sensor signals across repetitions. These metrics provide a compact representation of both the systematic temporal offset and the variability of the synchronization performance between two IMUs, thereby enabling comparisons across MAs and body positions.

The first metric is the mean lag  $\mu_\tau$ , which represents the average temporal offset between two IMU signals over  $N$  repetitions. It is computed as

$$\mu_\tau = \frac{1}{N} \sum_{i=1}^N \tau_i \quad (6.1)$$

where  $\tau_i$  denotes the optimal lag estimated for the  $i$ -th repetition. The mean lag captures systematic delays between signals. A positive value indicates that the characteristic event in the second signal  $y(t)$  is detected later than in the reference signal  $x(t)$ , whereas a negative value indicates that the event in  $y(t)$  occurs earlier. Therefore, the mean lag  $\mu_\tau$  provides a direct measure of relative temporal alignment between two body-mounted sensors. As this does not convey how stable this offset is across repetitions, the lag standard deviation  $\sigma_\tau$  is computed as

$$\sigma_\tau = \sqrt{\frac{1}{N-1} \sum_{i=1}^N (\tau_i - \mu_\tau)^2} \quad (6.2)$$

This metric quantifies the dispersion of the estimated lag values around their mean and therefore reflects the temporal consistency of the synchronization. A low standard deviation indicates that the estimated lag is stable across repetitions, suggesting a reliable and repeatable temporal relationship between the two signals, as seen in Figure 6.12. In contrast, a high standard deviation implies increased variability in the estimated lag, which may be indicative of inconsistent event timing, ambiguous signal features, or reduced suitability of the corresponding MAs for synchronization.

Both metrics are computed over all available repetitions and aggregated across participants for each MA and each considered pair of body positions. The aggregation enables a systematic comparison of synchronization behavior across different movement types and sensor combinations. The resulting summary statistics form the basis for the quantitative evaluation presented in subsequent sections, where differences in mean lag and variability are analyzed with respect to MA characteristics and body segment relationships.

#### 6.1.4 Visualization and Output

To facilitate the interpretation of the synchronization process, the PCC  $r(\tau)$  is visualized as a function of the temporal shift  $\tau$ , as seen in Figure 6.3. This representation provides an intuitive depiction of how strongly two IMU signals are linearly related across different temporal offsets and allows the overall structure of the correlation-lag relationship to be inspected directly. The peak of this curve corresponds to the optimal temporal offset  $\tau_{best}$ , i.e., the lag value that maximizes the correlation between the two signals. For improved

readability and rapid identification of this optimum,  $\tau_{best}$  is explicitly highlighted by a vertical reference line in the plot. This visualization enables a concise assessment of both the sharpness of the correlation peak and the precision of the estimated lag. In addition to the correlation-lag plot, a second visualization is generated in which the base signal  $x(t)$  and the temporally shifted signal  $y(t + \tau_{best})$  are overlaid in the same domain. This direct comparison provides a qualitative confirmation of the synchronization result and supports visual inspection of the aligned motion patterns. By displaying both signals simultaneously, difference in amplitude, residual phase offsets, or local misalignments can be readily identified. This dual-plot representation combines a quantitative correlation-based view with an intuitive signal-level perspective and is used consistently throughout the analysis.

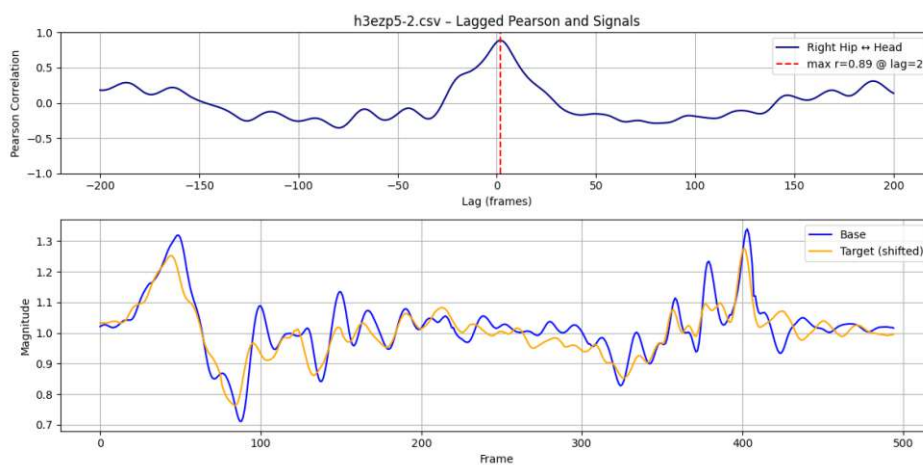


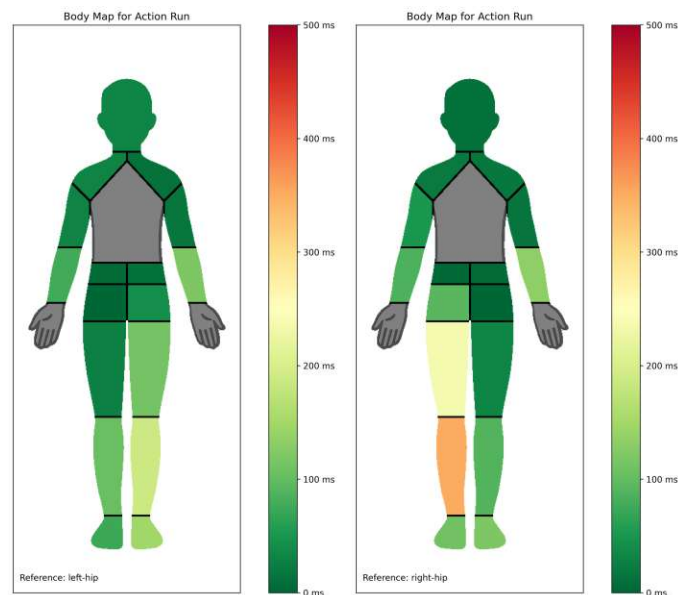
Figure 6.3: Visualization of the correlation coefficient  $r(\tau)$  plotted against the lag  $\tau$ , and the corresponding base signal  $x(t)$  and shifted signal  $y(t + \tau_{best})$  below.

Beyond pairwise signal plots, aggregated visualization techniques are employed to summarize synchronization behavior across multiple body positions. For each MA, body maps are rendered from lag statistics computed per target sensor relative to a fixed reference sensor. These visualizations are generated using a Python-based rendering pipeline implemented with the `matplotlib` and `OpenCV` libraries. The renderer consumes a CSV file containing the lag values  $\tau_i$  resulting from the correlation analysis. Per-sensor summary statistics are then derived by computing either the mean lag  $\mu_\tau$  or its standard deviation  $\sigma_\tau$ , with all values converted from samples to milliseconds prior to visualization. The formula for converting lag estimates  $\tau$  expressed in samples to lag estimates  $\tau_{ms}$  in milliseconds is defined as

$$\tau_{ms} = \frac{\tau * 1000}{f_s} \quad (6.3)$$

with sampling frequency  $f_s = 200$ . The specific statistic to be visualized is selected via a `statistic` flag (`mean` or `std`) when executing the rendering script. The resulting values are mapped onto an anatomical layout defined by a set of polygonal regions,

each corresponding to a sensor location. These polygons are specified by fixed coordinates and overlaid onto a transparent human silhouette to provide a spatially intuitive representation of synchronization performance across the body. Each polygon is filled using a color sampled from a reversed red–yellow–green colormap (RdYlGn\_r) under linear normalization. For mean lag visualizations, values are normalized within the range  $v_\mu \in [0, 200]$ , while standard deviation visualizations use  $v_\sigma \in [0, 200]$ . A warning is emitted by the rendering pipeline if any value exceeds the corresponding normalization range. In the resulting body maps, color encodes relative synchronization quality with respect to the reference sensor. Body positions rendered in green indicate mean lag values close to that of the reference, whereas red regions denote larger deviations and thus poorer synchronization performance. These visual summaries allow rapid comparison of synchronization characteristics across body segments and MAs. The final visualizations are exported at a resolution of 300 dpi and stored in a designated output directory, making them suitable for inclusion in both analysis workflows and publication-quality figures.



(a) Average mean lag for MA Jump in reference to the Left Hip sensor. (b) Average mean lag for MA Jump in reference to the Right Hip sensor.

Figure 6.4: Body maps showing the MA Jump, once with the left hip as the reference, once as the right hip as the reference.

The pair-wise nature of the sensor comparison required the selection of a single reference position for each MA in order to obtain a concise and interpretable representation of the results. Using a fixed reference sensor per MA allows all estimated temporal offsets to be expressed relative to a common baseline, resulting in exactly one body map per action. Without this constraint, each sensor would need to be treated as an individual

reference, yielding a separate body map for every sensor–action combination. Given the 17 sensor positions and 8 MAs considered in this study, this would result in 136 individual body maps, substantially reducing clarity and comparability. The chosen approach therefore enables a compact visualization of synchronization behavior across the body while preserving the relative temporal relationships between sensors. For most MA, the right hip was chosen because its positioning right on the pelvis makes a very stable position with minimal individual movement. Additionally, this is the closest sensor position to the center of gravity of the human body. For Clap and Stomp, the right hand and right lower leg were chosen, respectively. This decision was made because, prior to evaluation, it was not clear whether these two MA would produce significant effects on the right hip and they both heavily focus on distal movements. The right foot sensor was chosen for the Stomp initially because the MA is executed with the right foot. Because of especially bad performance of the foot sensors for all MAs, the reference was switched to the right lower leg as this sensor is securely attached to the participants’ tibialis and therefore is subject to minimal self-inflicted movement. Regarding the other sensors, the right side was chosen for uniformity, while the left-side sensors show mirrored results, so this decision will not impact the evaluation.

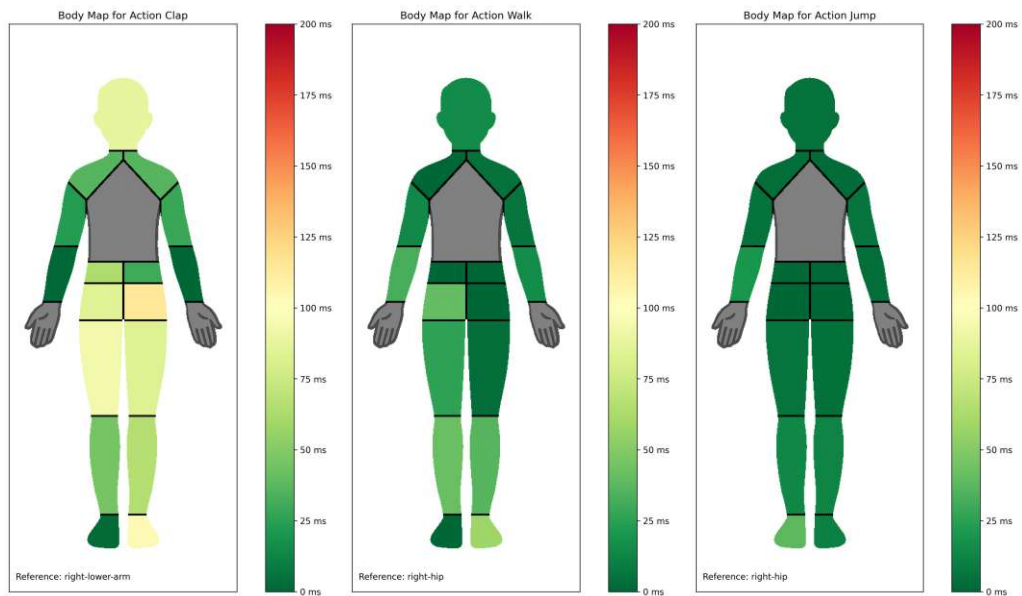
## 6.2 Results

This section presents the synchronization performance of each evaluated MA across all body positions. For each MA, the analysis focuses on two primary aspects. The accuracy is quantified by the mean lag between a reference position and all other sensors, as depicted in Figure 6.5, the precision is evaluated through the variance of the best calculated lag values and shown in Figure 6.6. Three MAs were chosen as representative examples for the body maps presented in this section. The MA clap acts as illustration of highly localized movements, where synchronization quality is dependent on the body position. To show the effects of asymmetric MAs, Walk was elected to showcase the difference between the right side and the left side of the body. The Jumping Jacks show how cyclic movements produce high accuracy on the full body but suffer from low precision. An in-depth discussion of all MAs will follow in Section 7, a comprehensive set of body maps, one for each MA and its respective reference position, can be found in Appendix A.3.

### 6.2.1 Detailed Analysis of Marker Actions

All MAs were analyzed relative to their respective reference positions. The following section provides a detailed overview of the resulting synchronization behavior. For each MA, acceleration time series from a representative repetition are shown for selected sensor positions in order to illustrate the characteristic kinematics underlying each movement.

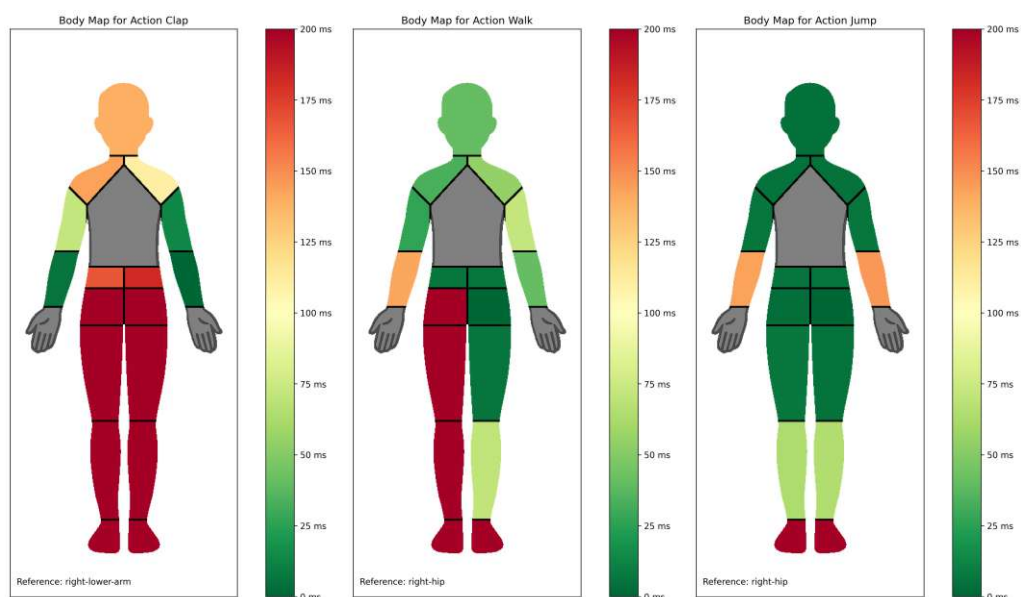
**Clap.** As assumed in Section 4.3.1, the Clap MA produced a distinct, high amplitude peak in the acceleration signals of sensors in close proximity to the lower arm. This pronounced spike served as a clear and temporally well-defined synchronization feature



(a) Average mean lag for MA Clap with reference Right Hip. (b) Average mean lag for MA Walk with reference Right Hip. (c) Average mean lag for MA Jump with reference Right Hip.

Figure 6.5: Body maps showing the average mean lag for the MAs Clap, Walk, and Jump in respect to their reference positions.

for this specific body region, as shown in Figure 6.7. In sensors close to the hands, such as the upper arms, the acceleration peak was still visible, but in sensors closer to the lower body, such as the hips, the event was not detectable any more. Due to the highly localized nature of the movement, its effectiveness as a full-body synchronization event was limited. While the mean lag values across all sensors were low, the synchronization stability varied considerably, with sensors positioned on the lower body exhibiting inconsistent temporal alignment. Using the right lower arm as a reference, the Clap MA produced a clear hierarchical pattern in synchronization accuracy across body segments. The most consistent synchronization was achieved for sensors on the upper limbs, particularly the left lower arm ( $M = +1.11$  ms,  $SD = 5.85$  ms) and right upper arm ( $M = -28.64$  ms,  $SD = 13.63$  ms). Other upper-body sensors exhibited slightly less stable results, including the left upper arm ( $M = -23.33$  ms,  $SD = 72.27$  ms), left shoulder ( $M = -36.33$  ms,  $SD = 143.66$  ms), and right shoulder ( $M = -36.39$  ms,  $SD = 110.16$  ms). The head and torso regions showed increased variability, with the head ( $M = -87.67$  ms,  $SD = 138.68$  ms), left lower back ( $M = -63.50$  ms,  $SD = 166.76$  ms), and right lower back ( $M = -30.33$  ms,  $SD = 182.11$  ms) displaying broader temporal spreads. Hip and upper leg sensors followed a similar trend, with mean lags of  $-84.71$  ms to  $93.39$  ms and standard deviations between  $229.05$  ms and  $262.61$  ms. The lower limbs showed the largest deviations, with the left and right legs ( $M = -45.56$  ms and  $-66.78$  ms,  $SD = 236.64$  ms and  $241.94$  ms) and the feet ( $M = +2.08$  ms and  $-103.86$  ms,  $SD = 417.96$  ms and  $439.38$  ms) exhibiting the



(a) Average SD for MA Clap with reference Right Hip. (b) Average SD for MA Walk with reference Right Hip. (c) Average SD for MA Jump with reference Right Hip.

Figure 6.6: Body maps showing the average standard deviation for the MAs Clap, Walk, and Jump in respect to their reference positions.

highest variability within the dataset. Across all target sensors, the per-pair mean lags was  $-9.04$  ms, the average per-pair standard deviation was  $10.47$  ms.

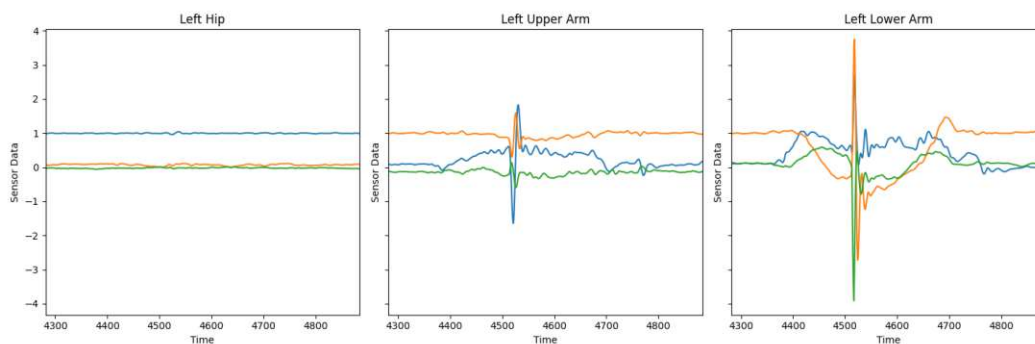


Figure 6.7: Visualization of the raw acceleration data produced by the Clap MA, showing that sensors close to the hands exhibit high acceleration while .

**Stomp.** Similar to the Clap MA, the Stomp produced a single, sharp peak in the acceleration signal corresponding to the movement of ground contact. Although categorized as a localized movement in Section 4.3.1, the resulting signals exhibited a measurable response even in upper-body sensors. Figure 6.8 shows that while the sensor on the right

lower leg shows the highest energy signal, a clear acceleration peak is still visible in the hip and the upper arm. Overall, it demonstrated good synchronization accuracy and moderate precision across the body. Using the right lower leg as a reference, the Stomp MA produced mean lag values ranging from  $-49.64$  ms to  $+43.14$  ms, with corresponding standard deviations between  $8.07$  ms and  $247.27$  ms. The smallest temporal deviations were observed in sensors located close to the reference and within the central body region, specifically the right upper leg ( $M = -16.83$  ms,  $SD = 8.07$  ms), right foot ( $M = 12.00$  ms,  $SD = 11.16$  ms), and right hip ( $M = 22.28$  ms,  $SD = 12.19$  ms). The lower back sensors also demonstrated moderate variability on the left ( $M = -30.44$  ms,  $SD = 45.28$  ms) and the right ( $M = -18.86$  ms,  $SD = 77.78$  ms). Upper-body sensors exhibited consistently negative mean lags accompanied by moderate to high dispersion. The shoulders ( $M = -27.61$  ms and  $-18.42$  ms,  $SD = 49.22$  ms and  $76.41$  ms), the upper arms ( $M = -41.31$  ms and  $-29.58$  ms,  $SD = 91.72$  ms and  $109.03$  ms), and the lower arms ( $M = -35.33$  ms and  $-41.72$  ms,  $SD = 142.58$  ms and  $91.23$  ms) all showed a similar pattern with rising standard deviations in more distal sensors. The head sensor ( $M = 9.58$  ms,  $SD = 119.69$  ms) displayed a small positive mean lag, falling within the range observed for the upper-body segments. In the lower body, asymmetries between left and right segments were evident, with the left lower leg ( $M = 5.94$  ms,  $SD = 181.09$  ms), left upper leg ( $M = -49.64$  ms,  $SD = 179$  ms), and left foot ( $M = 43.14$  ms,  $SD = 247.27$  ms) showing high dispersion. Across all target sensors, the per-pair mean lags was  $-9.04$  ms, the average per-pair standard deviation was  $10.47$  ms.

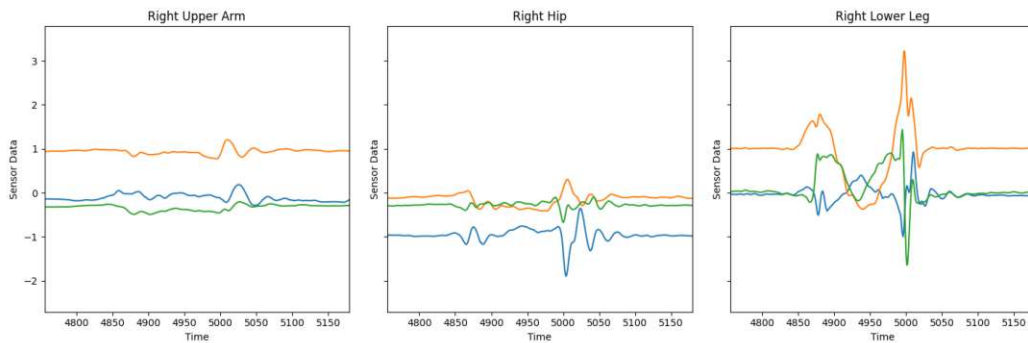


Figure 6.8: Visualization of the raw acceleration data produced by the Stomp MA, showing that sensors close to the hands exhibit high acceleration.

**Jump.** Jumping Jacks yielded precise and consistent synchronization results across almost all body positions. Because of its full-body movement, this movement generated pronounced and repetitive peaks in the acceleration data that are easily identifiable throughout the entire set of sensors, as shown in Figure 6.9. The periodic and symmetric nature of the jumping jacks motion led to minimal phase shifts between sensors, confirming a high degree of intra-body synchrony. Using the hip as a reference, the Jump MA produced mean lag values ranging from  $-10.28$  ms to  $+38.25$  ms with corresponding standard deviations between  $3.36$  ms and  $254.86$  ms. The most stable synchronization

was observed for sensors located near the center of the body, including the left hip ( $M = 0.32$  ms,  $SD = 3.36$  ms), right lower back ( $M = -0.86$  ms,  $SD = 5.49$  ms), and left lower back ( $M = -1.33$  ms,  $SD = 5.48$  ms). Similarly, sensors located on the head ( $M = 5.36$  ms,  $SD = 4.45$  ms), left upper leg ( $M = 5.80$  ms,  $SD = 7.07$  ms), and right upper leg ( $M = 4.33$  ms,  $SD = 4.80$  ms) exhibited low variability. Comparable consistency was also observed across the upper limbs, including the left shoulder ( $M = 3.39$  ms,  $SD = 5.17$  ms), right shoulder ( $M = 2.94$  ms,  $SD = 4.90$  ms), left upper arm ( $M = 5.36$  ms,  $SD = 6.62$  ms), and right upper arm ( $M = 5.67$  ms,  $SD = 6.86$  ms). In contrast, sensors positioned on the lower legs and forearms showed considerably higher variability, with the left lower leg ( $M = 13.89$  ms,  $SD = 63.91$  ms), right lower leg ( $M = 12.47$  ms,  $SD = 64.21$  ms), left lower arm ( $M = 20.22$  ms,  $SD = 143.18$  ms), and right lower arm ( $M = 3.44$  ms,  $SD = 146.31$  ms) displaying moderate to high temporal dispersion. The largest deviations were observed at the extremities, particularly for the feet ( $M = 38.25$  ms and  $-10.28$  ms,  $SD = 249.85$  ms and  $254.86$  ms). Across all targets, the mean of the per-pair mean lags was  $6.81$  ms, the average per-pair standard deviation was  $61.03$  ms.

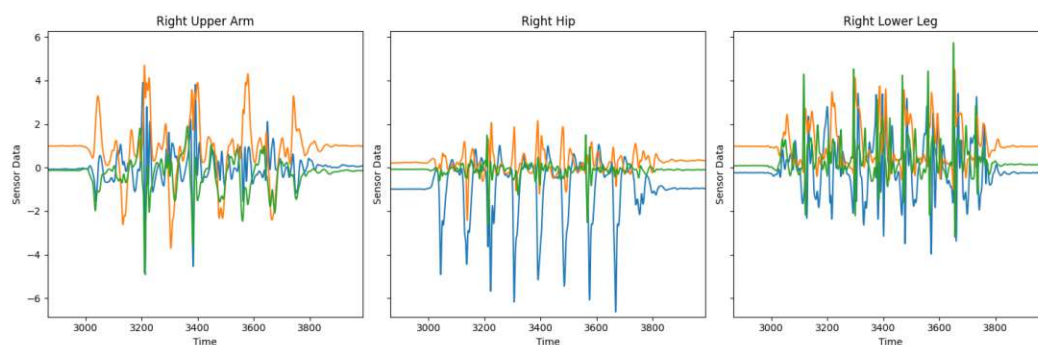


Figure 6.9: Visualization of the raw acceleration data produced by the Jump MA, showing that sensors close to the hands exhibit high acceleration.

**Fold.** In contrast to the other MA, the forward fold did not produce sharp amplitude peaks in the acceleration signals for any body position. Instead, it induced slow, gradual changes in acceleration accompanied by substantial orientation changes in the upper body, as shown in Figure 6.10. Particularly in the upper trunk sensors, such as the shoulders, the orientation change during the forward motion is clearly visible. On the contrary, in the feet, two acceleration peaks are visible where participants initiated the fold and went back up respectively. While mean synchronization across trials was acceptable, the temporal precision of the synchronization was relatively poor. Using the right hip as a reference, the Fold MA produced mean lag values ranging from  $-69.75$  ms to  $10.34$  ms, with corresponding standard deviations between  $87.20$  ms and  $476.04$  ms. The smallest temporal deviationist were observed for the right and left lower back ( $M = 9.05$  ms and  $10.34$  ms,  $SD = 87.20$  ms and  $105.19$  ms). Similarly, the left hip ( $M = 6.56$ ,  $SD = 116.07$ ) exhibited a small mean lag with high spread. In contrast, both upper legs ( $M = 16.42$  ms and  $-44.69$  ms,  $SD = -140.88$  ms and  $453.67$  ms). The left lower leg ( $M = -20.11$  ms,  $SD$

= 208.53 ms) and the right lower leg ( $M = -31.26$  ms,  $SD = 402.49$  ms) demonstrated even higher variability. The feet ( $M = -69.75$  ms and  $-27.49$  ms,  $SD = 447.95$  ms and  $476.04$  ms) displayed the largest dispersions within this MA. In the upper body, the sensors exhibited consistent negative mean lags accompanied by high standard deviations. The left shoulder ( $M = -45.50$ ,  $SD = 201.66$  ms), right shoulder ( $M = -40.67$  ms,  $SD = 195.56$  ms), left upper arm ( $M = -57.99$ ,  $SD = 242.07$  ms), and right upper arm ( $M = -48.18$  ms,  $SD = 213.43$  ms) showed better results than the more distal sensors on the left lower arm ( $M = -52.54$  ms,  $SD = 262.90$  ms) and the right lower arm ( $M = -50.67$  ms,  $SD = 240.43$  ms). The head ( $M = -53.35$ ,  $SD = 291.12$ ) sensor followed a similar trend, representing the most unstable among the upper body segments. Across all sensors, the overall mean of the per-pair mean lag was  $-33.29$  ms, while the average per-pair standard deviation was  $255.92$  ms. These values indicate substantial variability across body regions, with comparatively low temporal deviation around the torso and markedly higher dispersion in distal extremities.

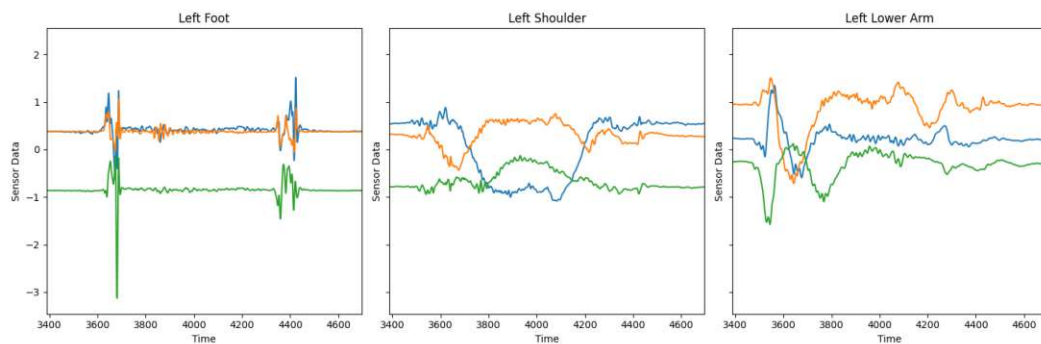


Figure 6.10: Visualization of the raw acceleration data produced by the Fold MA, showing that sensors close to the hands exhibit high acceleration.

**Walk.** As seen in Figure 6.14, the produced signals by ordinary walking are similar to those from the Jump MA, although amplitudes are not as high. However, the synchronization outcomes differed notably. Although the overall accuracy of the synchronization is comparable to that of the Jump MA, the precision is substantially worse for the lower body. This instability arises from the inherent phase asymmetry of walking. While one foot maintains ground contact, the other is in motion. Consequently, lower-body sensors on opposing sides produce very similar signal patterns that are temporally shifted. This observation is supported by the distribution of best-lag values illustrated in Figure 6.12, which reveals a consistent phase shift of approximately 100-150 ms between the left side and the right side. The bidirectional nature of this shift likely reflects inter-participant variation, as some participants initiated the walking motion with their right foot, while others began with their left. Using the right hip as a reference, the Walk MA produced mean lag values ranging from  $-40.57$  ms to  $58.31$  ms, with corresponding standard deviations between  $5.52$  ms to  $6002.78$  ms. The lowest temporal deviations were found for the lower back sensors ( $M = 0.22$  ms and  $0.72$  ms,  $SD = 6.34$  ms and  $6.50$  ms), indicating

close temporal alignment with the hip reference. The upper legs ( $M = 26.28$  ms and  $3.14$  ms,  $SD = 602.78$  ms and  $5.52$  ms) and lower legs ( $M = 41.50$  ms and  $36.42$  ms,  $SD = 524.87$  ms and  $70.80$  ms) showed clear differences in the standard deviations between the left and the right side of the body. The feet ( $M = 0.06$  ms and  $58.31$  ms,  $SD = 510.39$  ms and  $212.77$  ms) represented the most extreme case in terms of instability. The pattern stayed consistent for the shoulders ( $M = -0.58$  ms and  $4.89$  ms,  $SD = 32.82$  ms and  $55.36$  ms), upper arms ( $M = -14.58$  ms and  $5.53$  ms,  $SD = 26.89$  ms and  $72.31$  ms), and the lower arms ( $M = -32.64$  ms and  $-16.36$  ms,  $SD = 141.53$  ms and  $39.89$  ms). The head ( $M = 15.08$ ,  $SD = 40.60$ ) showed acceptable results. Across all targets, the mean of per-pair mean lags was  $4.77$  ms, and the average per-pair standard deviation was  $182.38$  ms, reflecting the instability induced by the synchronous nature of this MA.

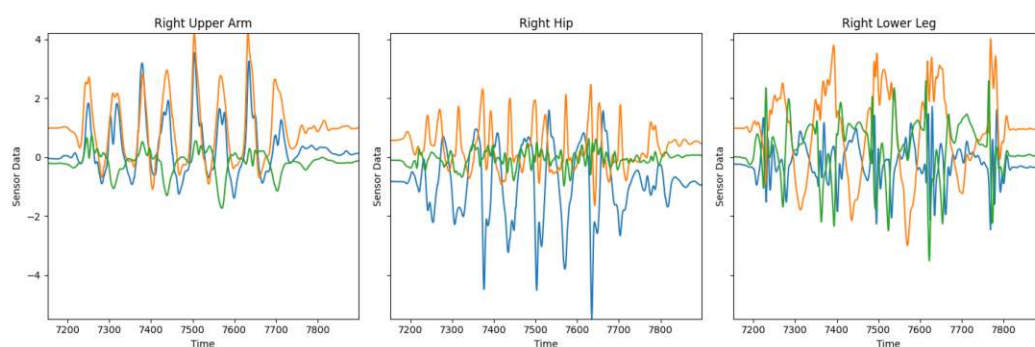
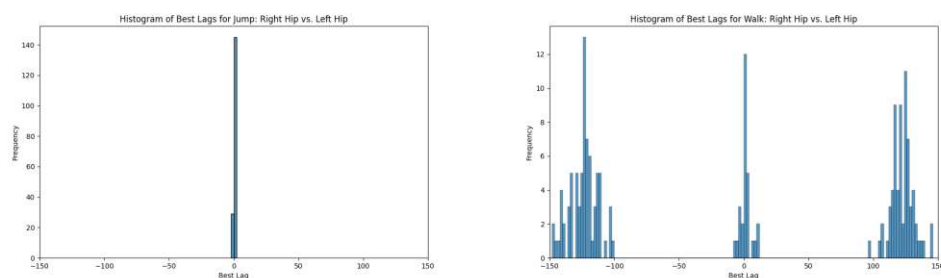


Figure 6.11: Visualization of the raw acceleration data produced by the Walk MA, showing that sensors close to the hands exhibit high acceleration.



(a) Distribution of best lags for MA Jump, (b) Distribution of best lags for MA Walk, comparing Right Hip and Left Hip.

Figure 6.12: Histograms showing the distribution of best lags computed by the windowed Pearson Correlation Coefficient.

**Heel.** The Heel MA is characterized by a brief, small-amplitude heel raise followed by a return to the ground while nonetheless triggering a clear, body-wide response in acceleration data, as seen in Figure 6.13. Notably, the foot sensor shows an orientation

change when participants raise their heels and, again, when they drop back down to the floor. Similar to the Stomp MA, the upward and subsequent downward motion affected all sensors consistently, despite the relatively low signal amplitude. The event could be detected reliably by the windowed PCC analysis and despite producing different signal characteristics across body segments, this MA demonstrated both high synchronization accuracy and temporal precision. Using the hip as a reference, the Heel MA produced mean lag values ranging from  $-21.29$  ms to  $+84.55$  ms, with corresponding standard deviations between  $5.02$  ms and  $344.43$  ms. The smallest temporal deviations were observed for the lower back sensors ( $M = -2.81$  ms and  $-1.07$  ms,  $SD = 9.78$  ms and  $8.92$  ms), followed closely by the head sensor ( $M = 7.72$  ms,  $SD = 10.50$  ms), indicating stable synchronization in the central body region. The left hip ( $M = -7.59$  ms,  $SD = 79.90$  ms) showed a small negative offset. The left upper leg ( $M = -0.11$  ms,  $SD = 79.43$  ms), right upper leg ( $M = 8.79$  ms,  $SD = 5.02$  ms), left lower leg ( $M = 5.76$  ms,  $SD = 78.91$  ms), and right lower leg ( $M = 17.05$  ms,  $SD = 6.39$  ms) showed minimal deviations and good to acceptable standard deviations. Upper-limb sensors, such as shoulders ( $M = -6.52$  ms and  $-3.43$  ms,  $SD = 8.04$  ms and  $7.83$  ms), displayed slightly larger temporal differences. The upper arms ( $M = -17.39$  ms and  $-15.76$  ms,  $SD = 8.66$  ms and  $8.54$  ms) and lower arms ( $M = -21.29$  ms and  $-17.47$  ms,  $SD = 8.59$  ms and  $8.46$  ms) followed the same trend while remaining within a consistent range. The feet ( $M = 84.55$  ms and  $71.94$  ms,  $SD = 344.43$  ms and  $210.33$  ms) exhibited the largest deviations, marking them yet again as the most temporally dispersed sensors in this motion. Across all targets, the mean of the per-pair lags was  $6.40$  ms, while the average per-pair standard deviation was  $55.23$  ms.

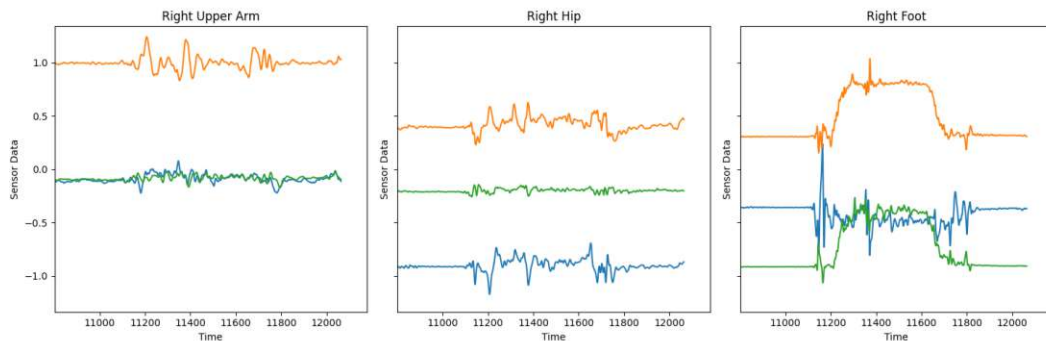


Figure 6.13: Visualization of the raw acceleration data produced by the Heel MA, showing that sensors close to the hands exhibit high acceleration.

**Run.** The Run MA exhibited patterns similar to those observed for Walk, as shown in Figure 6.14. Synchronization accuracy and precision were generally high of upper-body sensors but degraded in the lower body due to phase differences between the right and left limbs. These discrepancies reflect the natural alternation inherent to the running motion. Additionally, the data show that the acceleration spikes produced in the upper body are more pronounced than in the lower body, further aggravating precise synchronization.

Despite these limitations, the Run MA still produced coherent synchronization signals for segments not directly affected by alternating motion, indicating partial suitability for full-body synchronization when localized asymmetries are accounted for. Using the right hip as a reference, the Jump MA produced mean lag values ranging from  $-70.31$  ms to  $+26.69$  ms, with corresponding standard deviations between  $6.72$  ms and  $290.90$  ms. The lowest temporal deviations were observed for the lower back sensors ( $M = -0.58$  ms and  $1.03$  ms,  $SD = 32.01$  ms and  $6.72$  ms), indicating stable synchronization within the central body region. The head sensor ( $M = -2.03$ ,  $SD = 24.40$  ms) exhibited a similarly small deviation. The left hip ( $M = -18.48$  ms,  $SD = 164.08$  ms) showed a moderate offset, while the upper legs ( $M = -47.56$  ms and  $6.47$  ms,  $SD = 224.72$  ms and  $25.64$  ms) displayed asymmetric timing. The lower legs ( $M = -70.31$  ms and  $17.83$  ms,  $SD = 290.90$  ms and  $201.25$  ms) and feet ( $M = 22.17$  ms and  $24.03$  ms,  $SD = 201.97$  ms and  $225.40$  ms) showed the largest temporal deviations while following the trend asymmetric timing and high standard deviations. The upper limbs showed smaller and more consistent offsets in the shoulders ( $M = 4.06$  ms and  $3.81$  ms,  $SD = 8.29$  ms and  $8.14$  ms), upper arms ( $M = -2.78$  ms and  $10.19$  ms,  $SD = 56.74$  ms and  $41.67$  ms), and lower arms ( $M = 16.86$  ms and  $26.69$  ms,  $SD = 41.67$  ms and  $138.31$  ms). Across all targets, the mean of the per-pair mean lags was  $-3.31$  ms, while the average per-pair standard deviation was  $108.90$  ms.

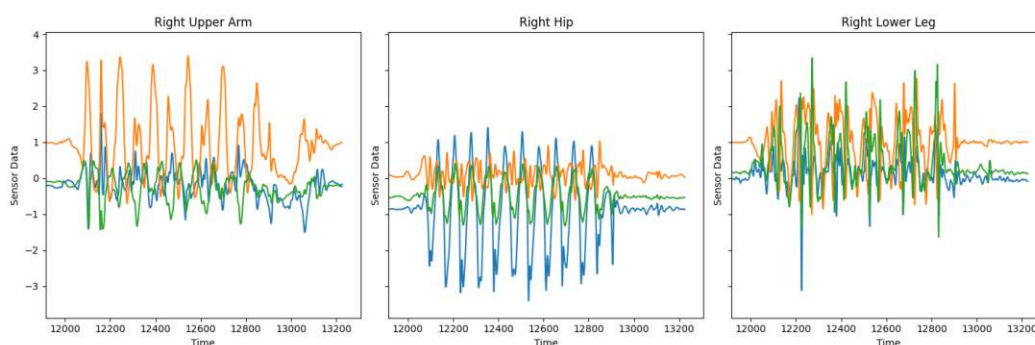


Figure 6.14: Visualization of the raw acceleration data produced by the Run MA, showing that sensors close to the hands exhibit high acceleration.

**Sit.** The Sit MA consists of a controlled lowering of the body into a seated position followed by a short static phase. Due to its slow and continuous nature, the action produces a less distinct global peak compared to impulsive movements but still generates measurable synchronization cues across body segments, particularly those near the hips and thighs. Looking at the time series in Figure 6.15, the signal characteristics on the right hip remind of those produced by the Heel MA, as both actions include a forward rotation of the upper body. Using the right hip as reference, the Sit MA produced mean lag values from  $-91.03$  ms to  $+90.75$  ms, with corresponding standard deviations between  $8.99$  ms and  $683.59$  ms. The smallest temporal deviations were observed in the lower back sensors ( $M = 3.58$  ms and  $-0.78$  ms,  $SD = 8.99$  ms and  $9.48$  ms) where both sides showed near-zero mean lags and low variability. Similarly, the left hip exhibited minimal

temporal offset ( $M = -0.06$  ms,  $SD = 28.49$  ms), indicating close alignment with the reference sensor. The upper legs ( $M = -15.64$  ms and  $-2.39$  ms,  $SD = 321.31$  ms and  $114.47$  ms) showed small to moderate temporal shifts with high variability. Even higher variability was found in the lower legs ( $M = -0.75$  ms and  $26.03$  ms,  $SD = 575.02$  ms and  $560.36$  ms). The left foot ( $M = 90.75$  ms,  $SD = 627.69$  ms) and the right foot ( $M = -91.03$  ms,  $SD = 683.59$  ms) reflect the most inconsistent synchronization across all body segments. In the upper body, the shoulders ( $M = -5.28$  ms and  $-7.31$  ms,  $SD = 21.85$  ms and  $18.81$  ms) remained comparatively stable. The upper arms ( $M = -17.78$  ms and  $-21.11$  ms,  $SD = 73.56$  ms and  $29.26$  ms) exhibited moderately higher variation, while the lower arms ( $M = -23.53$  ms and  $-29.17$  ms,  $SD = 154.86$  ms and  $156.45$  ms) presented even broader dispersion. The head ( $M = -2.81$  ms,  $SD = 94.10$  ms) also demonstrated noticeable spread. Across all targets, the mean of the per-pair mean lags was  $-9.33$  ms, while the average per-pair standard deviation was  $216.83$  ms.

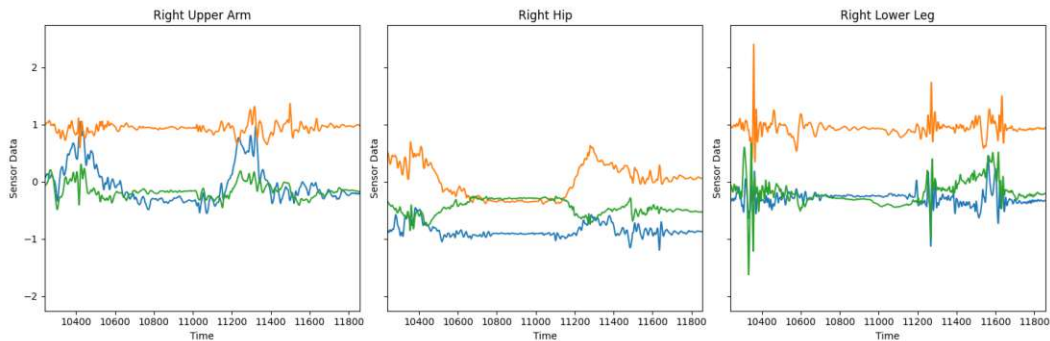


Figure 6.15: Visualization of the raw acceleration data produced by the Sit MA, showing that sensors close to the hands exhibit high acceleration.

Table 6.1 shows the mean and SD for accuracy and precision for every MA dependent on its reference position. For full-body coverage, all target positions are taken into account. For local coverage of the Clap MA, only sensors placed on the arms are used. Similarly, for MA Stomp, the sensors on the right leg and hip are used.

### 6.2.2 Questionnaire Data

Across all MAs, participants evaluated four identical questionnaire items, namely perceived physical demanding, embarrassment during performance, ease of understanding, and naturalness of motion. Mean ratings and standard deviations (SD) are reported per MA for each item.

Perceived physical demand was generally low across all MAs. The lowest mean ratings were observed for Clap ( $M = 1.0$ ,  $SD = 0.2$ ) and Sit ( $M = 1.1$ ,  $SD = 0.2$ ), followed closely by Stomp, Walk, and Heel (each  $M = 1.2$ ,  $SD = 0.5 / 0.4 / 0.4$ , respectively). Fold showed a slightly higher but still low perceived demand ( $M = 1.5$ ,  $SD = 0.7$ ). Higher physical demand ratings were reported for more dynamic movements. Run reached a

MA	Reference	Body Coverage	Accuracy	Precision
Clap	Right Lower Arm	Local (arms)	$-16.95 \text{ ms}$	$\pm 30.58 \text{ ms}$
Stomp	Right Lower Leg	Local (leg)	$-9.04 \text{ ms}$	$\pm 10.47 \text{ ms}$
Jump	Right Hip	Full-body	$+6.81 \text{ ms}$	$\pm 61.03 \text{ ms}$
Fold	Right Hip	Full-body	$-33.29 \text{ ms}$	$\pm 255.92 \text{ ms}$
Walk	Right Hip	Full-body	$+4.78 \text{ ms}$	$\pm 182.38 \text{ ms}$
Heel	Right Hip	Full-body	$+6.40 \text{ ms}$	$\pm 55.23 \text{ ms}$
Run	Right Hip	Full-body	$-3.31 \text{ ms}$	$\pm 109.00 \text{ ms}$
Sit	Right Hip	Full-body	$-9.33 \text{ ms}$	$\pm 216.83 \text{ ms}$

Table 6.1: Summary of synchronization accuracy and precision across all covered body positions for every MA in comparison to their reference positions.

MA	Physical Demand	Embarrassment	Understanding	Naturalness
Clap	$1.0 \pm 0.2$	$1.0 \pm 0.2$	$5.0 \pm 0.2$	$4.2 \pm 0.8$
Stomp	$1.2 \pm 0.5$	$1.1 \pm 0.3$	$4.9 \pm 0.2$	$2.5 \pm 1.0$
Jump	$2.3 \pm 1.0$	$1.3 \pm 0.6$	$4.9 \pm 0.2$	$2.2 \pm 1.1$
Fold	$1.5 \pm 0.7$	$1.1 \pm 0.3$	$4.9 \pm 0.2$	$3.7 \pm 0.8$
Walk	$1.2 \pm 0.4$	$1.1 \pm 0.2$	$4.9 \pm 0.2$	$5.0 \pm 0.2$
Heel	$1.2 \pm 0.4$	$1.1 \pm 0.3$	$5.0 \pm 0.0$	$4.0 \pm 1.0$
Run	$2.0 \pm 0.9$	$1.2 \pm 0.5$	$4.9 \pm 0.2$	$4.1 \pm 0.7$
Sit	$1.1 \pm 0.2$	$1.1 \pm 0.5$	$4.9 \pm 0.2$	$4.9 \pm 0.5$

Table 6.2: Descriptive statistics of questionnaire responses in matrix form. Values represent mean  $\pm$  standard deviation on a 5-point Likert scale (1 = strongly disagree, 5 = strongly agree).

mean of 2.0 (SD = 0.9), while Jump exhibited the highest perceived physical demand among all MAs (M = 2.3, SD = 1.0). Variability was also greatest for Jump, indicating more heterogeneous perceptions of physical effort for this gesture.

Ratings for embarrassment during performance were consistently low across all MAs. Clap received the lowest mean rating (M = 1.0, SD = 0.2). Stomp, Fold, Walk, Heel, and Sit all showed similarly low mean values (each M = 1.1), with standard deviations ranging from 0.2 to 0.5. Slightly higher mean ratings were observed for Run (M = 1.2, SD = 0.5) and Jump (M = 1.3, SD = 0.6). Despite these increases, all values remained close to the minimum of the scale, indicating that feelings of embarrassment were minimal across all evaluated gestures.

All MAs were rated positively in terms of ease of understanding. Mean ratings were consistently close to the maximum scale value. Clap and Heel achieved the highest possible mean scores (M = 5.0), with Heel showing no variability at all (SD = 0.0). Walk, Stomp, Jump, Fold, Run, and Sit each received a mean rating of 4.9 with low standard

deviations ( $SD = 0.2$ ). Overall, ease of understanding exhibited minimal variance across MAs, indicating strong agreement among participants that all gestures were clear and straightforward to perform.

Ratings for naturalness of motion varied more strongly between MAs than the other questionnaire items. The highest mean rating was observed for Walk ( $M = 5.0$ ,  $SD = 0.2$ ), followed closely by Sit ( $M = 4.9$ ,  $SD = 0.5$ ). Clap ( $M = 4.2$ ,  $SD = 0.8$ ), Run ( $M = 4.1$ ,  $SD = 0.7$ ), and Heel ( $M = 4.0$ ,  $SD = 1.0$ ) were also rated as largely natural, though with increased variability. Lower ratings were reported for Fold ( $M = 3.7$ ,  $SD = 0.8$ ). The lowest naturalness ratings were observed for Stomp ( $M = 2.5$ ,  $SD = 1.0$ ) and Jump ( $M = 2.2$ ,  $SD = 1.1$ ), both of which also exhibited comparatively high standard deviations, suggesting substantial inter-participant differences in how closely these gestures were associated with everyday movements.

## Results and Discussion

This section discusses the findings of the user study in relation to the three research questions formulated in Section 4. The focus lies on interpreting the underlying signal characteristics that contribute to robust synchronization (RQ1), examining how synchronization events can be reliably detected across different body positions (RQ2), and identifying with movement actions yield the most stable and accurate alignment across all body positions (RQ3). Through this interpretation, the mechanisms behind the observed synchronization quality can be clarified, and methodological implications for future multi-IMU synchronization procedures can be derived. The discussion, therefore, seeks to synthesize the experimental evidence into a coherent understanding of how movement characteristics, signal morphology, and spatial sensor configuration jointly influence synchronization quality within distributed inertial measurement setups.

Signal Feature	High Accuracy	High Precision	Example MA
High amplitude peak(s)	Strong	Partial	Clap, Jump, Run
Clear single event	Strong	Strong	Clap, Stomp
Periodic signal pattern	Strong	Limited	Jump, Walk
Symmetric movement	Strong	Strong	Jump, Heel
Asymmetric movement	Partial	Weak	Walk, Run
Smooth, low-variance signal	Limited	Weak	Fold

Table 7.1: Qualitative relationship between signal features and synchronization outcomes. The table summarizes how strong characteristics correlate with higher synchronization accuracy and precision across MA.

To enable the detection of the same synchronization event across all sensor locations, and therefore to answer **RQ2**, the 3-axis acceleration data was transformed into their Euclidean norm prior to analysis. This approach removes dependencies on sensor

orientation by reducing the three-dimensional acceleration vector to a single scalar magnitude that represents the overall acceleration intensity. The resulting magnitude signal retains the temporal information required for synchronization while discarding axis-specific directional components which are not relevant for identifying the timing of a distinct event. Consequently, orientation-induced inconsistencies are effectively mitigated, providing a uniform basis for event comparison among all sensor positions. For temporal alignment, pair-wise correlations between sensors were computed using the PCC and evaluated across potential temporal offsets. The PCC serves as a normalized measure of similarity that accounts for differences in signal amplitude and mean, focusing exclusively on the temporal alignment of the signal structure. This makes it particularly suitable for synchronizing acceleration signals from different body parts, where local motion amplitudes can differ substantially due to biomechanical factors. By determining the lag corresponding to the maximum correlation value, the relative delay between sensors can be estimated objectively and consistently. Overall, the analysis confirms that consistent event detection across sensors can be achieved when orientation-independent preprocessing and normalized correlation methods are applied, providing that the underlying movement generates a recognizable signal characteristic at all sensor locations. Full-body actions naturally fulfil this requirement and lead to stable synchronization across the entire sensor network. Conversely, localized movements require more cautious interpretation, as weaker or delayed transients at distant sensors may increase synchronization variability. These findings, as illustrated in Table 7.1, highlight that synchronization quality across body positions is not solely a function of the computational method but also inherently tied to the physical characteristics of the movement used as an action marker.

The signal characteristics produced by each MA allows answering **RQ1**. Actions that produce a sudden change in acceleration yield the most accurate and stable synchronization across the body. The underlying mechanism is that impulsive, high-jerk events generate a brief transient with a pronounced extremum in the acceleration magnitude, which in turn produces a sharp maximum in the correlation function used for lag estimation. Conversely, actions dominated by slow or smoothly varying movements exhibit the least stable synchronization. Gradual onsets and low jerk distribute the informative content over a longer interval, which flattens the correlation function around its maximum and increases the sensitivity to minor amplitude modulation and participant specific kinematics. The consequence is a broader peak with lower prominence and, therefore, greater uncertainty in the lag estimate.

Lastly, **RQ3** requires a more holistic look on the MAs and their synchronization performance. For highly localized MA, synchronization quality depends strongly on sensor proximity to the action's origin. Local mechanical energy and limited coupling across body positions yield clear and distinctive events only in nearby segments, whereas distant sensors may not reflect the MA in their signals. This proximity effect manifests as robust, low-variance lags for sensors close to the active limb and weaker, or no peaks at remote positions. Importantly, this pattern is specific to localized actions. When the MA engages the whole body (i.e., qualifies as a full-body MA), the transient propagates

---

through the whole body, and cross-body synchronization remains stable and accurate across positions. Cyclic actions warrant a more nuanced interpretation. Instability arises primarily when the cycle is generated by alternating, out-of-phase limbs (e.g., running or walking), where the left and right side never produce the event simultaneously. In such cases, the correlation function contains multiple plausible maxima separated by approximately half a cycle as shown in Figure 6.12. This pattern is most plausibly explained by start-foot asymmetry, i.e., some participants initiated the Walk MA with the left foot, while others began with the right, shifting the dominant sub-event to one or the other. The same rationale can be assumed for the Run MA. Therefore, the dispersion observed for these movements is driven by inter-limb phase structure and start-phase heterogeneity, not by a deficiency of the correlation method. This is further supported by the fact that, by contrast, the bilaterally synchronous cyclic MA Jump, in which both sides execute the movement at the same time, does not suffer from this phase shift.

Taken together, these observations indicate that movement class and inter-limb phase structure jointly determine synchronization quality. Brief and impulsive actions produce (globally) consistent and highly reliable alignment events because their acceleration transients are short and well-defined. Localized movements are only suitable for synchronizing sensors that are situated in close proximity to the active body part. Cyclic actions can achieve stable synchronization when both sides of the body perform the movement simultaneously, as seen in bilaterally synchronous MA. A central implication of the presented results emerges when they are considered in light of prior work reporting that machine-learning-based human activity recognition (HAR) performance can already degrade at inter-sensor misalignments on the order of 150 ms, with larger temporal offsets further amplifying this effect [WKT25]. Against this threshold, the observed synchronization behavior across MAs reveals clear differences in practical suitability for HAR applications. MAs characterized by short, impulsive, and body-wide acceleration responses frequently achieved mean lags and temporal variability that remained well below this critical range for large parts of the body, particularly in proximal segments and along the trunk. For these actions, even sensors not directly involved in motion generation often exhibited lag distributions whose standard deviations stayed below or close to the reported 150 ms tolerance. From an HAR perspective, this suggests that such MAs can provide synchronization quality sufficient to avoid substantial performance degradation, at least for models that rely on features aggregated over multiple body locations. For future synchronization protocols, it is therefore advisable to employ short, high-jerk actions when uniform cross-body synchronization is required, to restrict localized movements to local alignment scenarios, and to apply phase-aware analysis procedures when working with alternating cyclic movements.

For the computations mentioned in Section 5.2, tri-axial acceleration signals are transformed using the Euclidean norm in order to obtain an orientation-invariant representation. This preprocessing step reduces the three-dimensional sensor measurements to a scalar magnitude, thereby mitigating dependencies on the local sensor coordinate frame and on mounting orientation. As a consequence, the approach is less sensitive to practical

variations in attachment, such as small rotations introduced by strap placement, motion suit fit, or differences in how sensors align with anatomical axes. The trade-off is that direction-specific information is discarded. While the magnitude preserves the timing and overall intensity of motion transients, it eliminates orientation cues that could, in principle, help distinguish between movement directions or disambiguate complex multi-axis patterns. For the synchronization objective pursued here, this loss is acceptable because the key requirement is a consistent temporal signature rather than a physically interpretable direction. Importantly, Skog et al. [SH06] showed that norm-based methods can even improve detectability of synchronization markers and correlation-based alignment. Furthermore, the orientation-invariant representation increases the generality of the method for heterogeneous systems, where sensors may be mounted at different orientations or where device-specific coordinate conventions differ. By relying on magnitude rather than axis-aligned components, the synchronization pipeline becomes more transferable across sensor placements and hardware configurations, which is particularly relevant for multi-IMU deployments that cannot guarantee strict and reproducible alignment of sensor frames across body positions or devices.

The results presented in this thesis should also be interpreted in light of soft-tissue motion effects, which influence how body-mounted sensors move relative to the underlying skeleton. The SMPL body model [LMR<sup>+</sup>15] demonstrates that human motion is inherently non-rigid, with pose-dependent and dynamic surface deformations causing body surface points to deviate systematically from joint-level kinematics, particularly in regions with substantial soft tissue such as the torso and upper limbs. As IMUs were attached to the body surface, their measurements inevitably reflect a combination of skeletal motion and deformation-induced surface dynamics. Consequently, part of the variability observed in the recorded signals, and by extension in synchronization performance, may be attributed not only to sensor placement and movement execution, but also to soft-tissue deformation that alters the local motion characteristics at the sensor location.

A consideration that needs to be addressed is the fact that the present study was conducted under controlled, study-like conditions rather than in unconstrained real-world settings. This raises the question of whether participants' movements may have been influenced by being observed, thereby limiting ecological validity. However, existing evidence suggests that the gap between laboratory and field data may be smaller than commonly assumed. Hoelzemann et al. [HBVB<sup>+</sup>23] provide a data-based investigation of the Hawthorne effect, i.e., behavioral changes that can occur when participants are aware of being observed. In their study, participants performed five workout-based movements while wearing IMUs, and the authors analyzed whether observation altered the recorded motion patterns and the predictive performance of deep-learning classifiers. Their results indicate that observation only marginally influences the captured patterns and classification performance. While the Hawthorne effect cannot be ruled out in general, these findings challenge the assumption that laboratory-collected wearable sensor data is necessarily less representative than data collected in field tests. In the context of this thesis, this supports interpreting the observed synchronization patterns as meaningful

---

beyond the immediate laboratory setting, while still motivating future validation under more naturalistic conditions.

While the primary contributions of this work are derived from quantitative, signal-based synchronization analyses, the accompanying questionnaire responses provide complementary insight into how participants subjectively experienced the individual MAs. These subjective measures were not used to derive synchronization performance metrics or to formulate the final design guidelines. However, they offer valuable context for interpreting the observed differences between MAs. Across all MAs, participants consistently reported low levels of perceived physical demand and minimal embarrassment during performance. This uniformity suggests that none of the evaluated gestures introduced substantial discomfort or social inhibition that might have systematically altered movement execution. From a synchronization perspective, this is relevant insofar as it reduces the likelihood that poor alignment results can be attributed to participants hesitating, modifying, or abbreviating movements due to discomfort or self-consciousness. Ease of understanding was rated very highly for all MAs, with means close to the upper bound of the scale and negligible variance. This indicates that participants were able to reliably interpret and execute the instructed gestures without ambiguity. Consequently, differences in synchronization quality across MAs are unlikely to stem from misunderstandings of the task, but rather from inherent properties of the movements themselves and the resulting IMU signal characteristics. In contrast to the other questionnaire items, ratings for naturalness of motion showed substantial variation between MAs. Gestures such as walking and sitting were perceived as highly natural, while jumping and stomping were rated as less representative of everyday movements. Importantly, these subjective assessments did not map directly onto synchronization performance. MAs that were rated as highly natural did not necessarily yield the most reliable synchronization results, whereas several actions characterized by more abrupt, high-energy movements produced stronger and more distinctive synchronization cues despite lower naturalness ratings. This divergence reinforces a central finding of this thesis. Effective synchronization is primarily driven by signal properties such as temporal sharpness, high jerk, and pronounced acceleration changes, rather than by how natural or familiar a movement feels to participants. Subjectively natural movements often involve smoother, more continuous motion patterns, which may be advantageous for comfort and ecological validity but provide weaker temporal anchors for alignment across multiple IMUs. Overall, the questionnaire results support the interpretation that participant experience did not act as a confounding factor in the synchronization analysis. Instead, they highlight a tension between subjective naturalness and technical suitability for synchronization. By treating these subjective measures as contextual information rather than performance indicators, the results underscore that MAs optimized for synchronization need not align with those perceived as most natural, provided they remain easy to understand and do not impose undue physical or social burdens on participants.

## 7.1 Limitations

Sensors attached to the feet exhibited higher variability in the estimated lags across MAs using the Rokoko SmartSuit Pro II. This reduced precision is plausibly attributable to suit-specific factors, including attachment-related slippage. Such effects broaden the effective acceleration peak and increase estimator variance, thereby diminishing the suitability of the foot-mounted sensors in this particular setup as reference sites for synchronization. Importantly, this observation should not be interpreted as a general limitation of foot-mounted IMUs, but rather as a characteristic of the mounting and mechanical coupling provided by the employed suit. In practical deployments, this finding motivates either stricter fixation strategies or alternative attachment designs when using similar full-body suits, rather than discouraging foot-mounted sensing per se. An additional limitation concerns the set of sensor locations available for analysis. While the study covers multiple body positions, it does not include sensors mounted on the wrists or the sternum, both of which are relevant in practical wearable deployments [Rob03, YH10, TIH<sup>+</sup>07]. Wrist-mounted sensors can differ meaningfully from lower-arm placements, as the wrist is more susceptible to independent local motion [Zea17] (e.g., hand and wrist articulation) that is not necessarily representative of the motion of the forearm segment. These local kinematic contributions may alter signal morphology and potentially affect the detectability and stability of synchronization cues compared to lower-arm sensors [Zea17]. Likewise, a sternum-mounted sensor would have provided a valuable central reference location [Rob03, YH10] particularly since major commercial fitness devices, such as the Garmin HRM 200<sup>1</sup> or the Polar H10<sup>2</sup>, employ chest placements to estimate movement and derive running-related metrics. The absence of these locations limits the extent to which the present conclusions can be directly transferred to wearable configurations that rely on wrist- or chest-based sensing and constrains the evaluation of how centrally mounted reference signals might influence cross-body synchronization quality.

In general, the analysis assumes uniform sampling and stable clocks across devices. Even small discrepancies in effective sampling frequency, timestamping precision, or clock drift can accumulate and distort lag estimates when alignment relies on signal similarity rather than absolute time sources. Without independent verification of clock stability, residual timing errors cannot be excluded and should be considered when interpreting absolute lag magnitudes. Further, at 200 Hz, the sampling interval constrains theoretical timing resolution to 5 ms per sample. While this rate exceeds that used in much of the literature [SZ19, GDHW22, GLD<sup>+</sup>24, BAL09, SBM<sup>+</sup>22], it nonetheless sets a lower bound on detectable lag differences. Reported time discrepancies should therefore be understood within this limit.

Event alignment were based on the Euclidean norm of 3-axis acceleration. This choice enhances orientation robustness but discards directional and rotational information that could disambiguate complex or localized transients. In particular, exuding angular velocity

<sup>1</sup><https://www.garmin.com/de-AT/p/1530957/>, accessed 02.02.2026

<sup>2</sup><https://www.polar.com/at-de/sensors/h10-heart-rate-sensor>, accessed 02.02.2026

may limit detectability where rotational components carry salient timing cues, and it may contribute to higher uncertainty at distal or weakly coupled sensor positions. Similarly, data were recorded under scripted and controlled conditions, which reduced environmental noise and contained within-participant variability. While this improves internal validity for comparing different MA, it limits direct inference to naturalistic settings where unconstrained movement, or incidental disruptions may alter the characteristics and propagation of synchronization events within the signal. Within this experiment, all measurements were recorded with a single IMU model and shared acquisition settings. The resulting conclusions therefore do not directly generalize to heterogeneous sensor networks in which devices may differ in sensing range, on-sensor filtering, sampling strategies, or communication latencies. In such contexts, device-specific characteristics could introduce systematic lag offsets independent of biomechanics.

A further limitation concerns the composition of the participant sample. For this initial study, participants were recruited under the explicit criterion of being relatively fit, which resulted in a comparatively homogeneous group dominated by young, physically capable individuals. While this constraint helped reduce confounding variance due to limited mobility or fatigue and enabled a controlled first evaluation of MAs, it restricts the generalizability of the findings. Movement execution, impact intensity, and inter-limb coordination patterns can vary substantially across age groups and fitness levels, which may affect both the morphology of acceleration transients and the precision of correlation-based lag estimation. Consequently, the derived recommendations should be interpreted primarily as applicable to populations with similar physical characteristics, and future work should validate the results on more diverse cohorts with broader variation in age, fitness, and movement styles. Future work should extend the present investigation to participant groups whose movement characteristics are likely to violate the signal assumptions that emerged as critical in this thesis. In particular, the results indicate that synchronization is most stable when the MA produces a brief, high-jerk transient with a dominant peak, whereas actions with slower dynamics or less temporally distinct signatures yield less stable lag estimates. Older adults constitute a relevant group in this regard because age-related changes in neuromuscular control, strength, and joint mobility often lead to slower movement execution and lower peak accelerations [KS04]. Under such conditions, MAs that elicited sharp transients in the current cohort may instead produce more gradual onsets and reduced peak prominence, thereby approaching the signal regime that, in this study, was associated with increased lag variability. Evaluating older adults would therefore directly test whether the guidelines proposed in Section 7.2 remain applicable when high-jerk events cannot be generated consistently and when movement timing is more heterogeneous across repetitions. Further, more complex movements, such as standing up, are performed differently depending on the age of individuals [vdKSK<sup>+</sup>22]. A similar argument motivates investigating individuals with higher body mass. Increased soft-tissue motion and damping can attenuate and temporally smear acceleration transients, particularly in the lower body [FZB<sup>+</sup>15], and may introduce additional measurement variability through less rigid coupling between the sensor and the underlying segment [GPA<sup>+</sup>08]. Relative to the signal characteristics

that produced the best synchronization in this thesis, these effects plausibly reduce peak sharpness and increase noise-like components in the acceleration magnitude, thereby shifting the signal morphology toward conditions under which correlation maxima become broader and less stable. Finally, clinical populations with motor impairments offer an additional and complementary test case, as altered coordination, gait asymmetries, and irregular timing can affect both the temporal distinctiveness of synchronization cues and the phase structure of cyclic movements. Such deviations may increase trial-to-trial variability or introduce systematic offsets that are not present in healthy participants, thereby challenging assumptions of repeatable event morphology and consistent bilateral timing. Studying these groups would therefore strengthen external validity by assessing whether the derived guidelines generalize under biomechanical and motor conditions that are likely to produce the slower, noisier, and more heterogeneous signal patterns that, in the present results, were associated with reduced synchronization precision.

Taken together, these limitations indicate that synchronization quality reflects not only the chosen MA and analytical method but also sensor placement, device timing characteristics, measurement resolution, signal modality, participant homogeneity, and the recording context. Interpreting absolute lags and cross-site precision should therefore account for these factors, particularly when extrapolating to mixed-hardware deployments or field conditions.

### 7.2 Guidelines

Based on the empirical findings across RQ1–RQ3, several practical design guidelines for data-based offline synchronization of multi-IMU systems can be derived. These guidelines summarize the observed relationships between movement characteristics, signal representation, and alignment precision into applicable rules to improve both experimental protocol design and post-hoc data analysis.

First, synchronization markers should be chosen to exhibit a distinct and temporally unique signature. Actions that generate a single, high-jerk acceleration transient with a dominant peak consistently yield the most stable lag estimates. Such events concentrate discriminative temporal information within a narrow window, resulting in sharp and unambiguous maxima in correlation-based alignment. In contrast, repetitive or smoothly varying movements distribute informative content over longer intervals and increase the likelihood of competing correlation peaks, which degrades synchronization precision.

Second, full-body or bilaterally synchronous movements should be preferred when global cross-body synchronization is required. Movements in which both sides of the body act simultaneously produce unimodal lag distributions and consistent alignment across sensor locations. Alternating or bilaterally asynchronous actions, such as gait, introduce inherent phase offsets that manifest as multimodal lag distributions and increased variability unless explicitly accounted for. Localized movements can still serve as effective synchronization cues, but only for sensors situated in close proximity to the active segment and should therefore not be used as global markers.

Third, preprocessing should employ orientation-invariant signal representations. Converting tri-axial acceleration to its Euclidean norm effectively removes dependencies on sensor orientation and mounting variability, ensuring that equivalent events exhibit comparable signal morphology across body locations. This step is critical for multi-sensor setups where consistent orientation cannot be guaranteed and where synchronization depends on shared temporal structure rather than directional information.

Fourth, relative timing between sensors should be estimated using normalized, windowed correlation methods, such as the Pearson correlation coefficient. Normalization reduces sensitivity to amplitude scaling and baseline offsets, while windowing constrains the analysis to the relevant temporal neighborhood of the synchronization event. Lag searches should be limited to physically plausible ranges, and peak-selection criteria should be applied to avoid spurious alignments in the presence of residual periodicity or noise.

Finally, movement phase structure and sensor placement must be considered explicitly. Cyclic movements should be treated as phase-structured signals; when alternating cycles are unavoidable, synchronization should rely on limb-specific events, phase-aligned landmarks, or consensus strategies rather than raw correlation maxima. Additionally, sensor locations subject to strong impact or attachment instability, such as the feet, should not be used as primary synchronization references for whole-body alignment. More centrally located sensors typically provide more stable and reliable reference signals.

Together, these guidelines emphasize that robust offline synchronization is not solely a matter of selecting an appropriate alignment algorithm. Instead, it emerges from the deliberate coordination of movement design, signal preprocessing, sensor placement, and analysis strategy. By adhering to these principles, practitioners can substantially improve the accuracy and precision of data-based synchronization in multi-IMU systems.



Die approbierte gedruckte Originalversion dieser Diplomarbeit ist an der TU Wien Bibliothek verfügbar  
The approved original version of this thesis is available in print at TU Wien Bibliothek.

# Conclusion

The objective of this thesis was to investigate the suitability of predefined MAs for offline synchronization of multi-IMU motion data in scenarios without shared hardware clocks. The work focuses on identifying which types of movements enable reliable temporal alignment across different body positions and on characterizing the signal properties that support stable synchronization. While prior work demonstrated the feasibility of signal-based synchronization in HAR, there is limited empirical understanding of how MAs should be designed and how their effectiveness varies across sensor location. Consequently, this thesis deliberately focuses its scope to the event-driven, offline synchronization and evaluates a fixed set of MAs in a controlled user study. Rather than proposing a novel synchronization algorithm, the work aims to provide an empirical comparison and characterization of synchronization performance under controlled conditions.

To address these objectives, a systematic evaluation pipeline for event-driven offline synchronization was developed and applied. A controlled between-subject study design ensured that all participants performed the same MAs under identical recording conditions, allowing for direct comparison across actions and body positions. Multi-IMU acceleration data were processed using an orientation-independent representation to support cross-position alignment. Temporal offsets between sensors were estimated via windowed Pearson correlation, enabling the extraction of best-fit lag values as well as measures of variability across trials and sensor pairs. This facilitated a detailed, pairwise assessment of synchronization quality. In addition to numerical summary metrics, the methodology incorporates visual analyses, including lag distributions and body-map representations, to capture spatial patterns in synchronization performance.

This thesis demonstrates that the effectiveness of event-driven synchronization depends strongly on the temporal structure of the performed MA. Actions that produce short, temporally distinctive signal patterns enable more stable and less ambiguous lag estimation than actions characterized by smooth, repetitive or cyclic motion. Furthermore, it was shown that synchronization of the same event across different body positions is feasible

when using orientation-independent signal representations, but that synchronization quality varies substantially across the body. MAs that induce motions observable across multiple body segments result in more consistent alignment between sensors, while localized movements exhibit increased variability for sensors located on distant body parts. In addition, this thesis provides empirical evidence that MAs differ not only in their average synchronization accuracy but also in the robustness of their lag estimates across trials and participants. The analysis shows that low mean temporal offsets do not necessarily imply reliable synchronization if accompanied by high variability, especially in cyclic motions. Consequently, both accuracy and precision must be considered when assessing the suitability of synchronization events.

Based on these findings, this thesis illustrates that synchronization performance in multi-IMU systems can be substantially improved through the deliberate selection and evaluation of MAs. Rather than relying on convention and convenience, synchronization events should be chosen based on their empirical synchronization properties, particularly their temporal distinctiveness and cross-body observability.

### Future Work

The results of this thesis motivates future research in the area of event-driven synchronization for multi-IMU systems. A natural extension of the presented work concerns the scale and diversity of the experimental setup. Future studies should include a larger and more heterogenous participant pool, as well as a broader range of motion types. As slow movements produced worse results compared to high-energy movements, a (single-leg) hop jump or drop jump could be investigated as a more explosive extension of the heel raise. To provide more upper-body MAs beyond clapping, arm swings, or shoulder shrugs could be incorporated. Also, additional and sensor placements, especially on the sternum and the wrists could yield interesting data. This would allow the observed synchronization characteristics be validated across different movement styles, body proportions, and recording conditions, thereby improving generalizability. In addition, evaluating synchronization events in less constrained or semi-naturalistic settings would provide insights into their robustness under real-world conditions. Another important direction is the combination of multiple synchronization events. This thesis evaluates MAs in isolation. However, using multiple events within a recording could enable more robust alignment by reducing ambiguity and compensating for occasional misdetections. Investigating strategies for aggregating synchronization information from several events, potentially distributed over time, represents a promising avenue for improving alignment stability and tackling further challenges, such as clock drift.

From a methodological standpoint, future work could focus on automatic detection and segmentation of synchronization events. Extending the framework from this thesis to automatically identify suitable synchronization events within continuous motion data would increase its applicability, particularly for long recordings or in-the-wild datasets. Further extensions could also explore hybrid synchronization approaches, for example

---

combining event-driven alignment using signal correlation with additional techniques, such as drift correction of complementary alignment cues. Evaluating how event-driven synchronization interacts with other post-hoc alignment strategies remains an open research question. Finally, future work may investigate the integration of the presented evaluation framework into other applications, such as HAR or motion analysis pipelines. Explicitly quantifying how synchronization quality affects higher-level tasks would help establish practical thresholds for acceptable temporal misalignment and further motivate the systematic evaluation of synchronization events.



Die approbierte gedruckte Originalversion dieser Diplomarbeit ist an der TU Wien Bibliothek verfügbar  
The approved original version of this thesis is available in print at TU Wien Bibliothek.

# Overview of Generative AI Tools Used

## Google Gemini, OpenAI ChatGPT

Gemini<sup>1</sup> and ChatGPT<sup>2</sup> are chatbots created by Google and OpenAI, respectively. They were used in the evaluation phase of this thesis to create simple scripts for quick data validation and to help create automation scripts such as the annotation tool. Furthermore, they were used for the written work in terms of structural guidelines, grammatical improvements, and a more scientific writing style.

## Github Copilot

Copilot<sup>3</sup> is an AI coding assistant by Github that helps with auto-completion of code. It was used to autocomplete single lines of code during the development of the synchronization, evaluation, and visualization scripts.

Other than the aforementioned use cases, no help from generative AI tools was used.

---

<sup>1</sup><https://gemini.google.com>, accessed on 07.02.2026

<sup>2</sup><https://chatgpt.com>, accessed on 07.02.2026

<sup>3</sup><https://github.com/copilot>, accessed on 22.01.2026



Die approbierte gedruckte Originalversion dieser Diplomarbeit ist an der TU Wien Bibliothek verfügbar  
The approved original version of this thesis is available in print at TU Wien Bibliothek.

# List of Figures

2.1	Schematic illustration of an IMU based on three types of sensors and their sensing abilities. [AGKK13] . . . . .	6
2.2	Schematic illustration of message exchange and delay estimation using round-trip time between master and slave. The slave estimates the delay as $[(t_2 - t_1) + (t_4 - t_3)]/2$ , assuming a symmetric delay. [PDST20] . . . . .	9
2.3	Identification of synchronization points (SP) for Event-Driven Synchronization in acceleration data and force data time series. [BAL09] . . . . .	10
2.4	Illustration of the cross-correlation $r(d)$ between two signals $x(i)$ and $y(i)$ . [Bou96]	13
4.1	Illustration of the temporal order and relative positioning of user study procedure steps showing a briefing phase, a pre- and post-questionnaire phase, and the recording phase as a central element. . . . .	34
5.1	Schematic representation of the 17 body positions where IMU data were recorded during the user study. . . . .	39
5.2	Setup of the user study in the laboratory showing the execution area in the middle and the technical setup on the right. . . . .	40
6.1	Illustration of the data processing pipeline from raw sensor data to aggregated body maps showing estimated lags using PCC. . . . .	45
6.2	Annotation tool for MA segmentation of the recordings showing 3-axis acceleration data of three important body positions and the MA to annotate next. . . . .	47
6.3	Visualization of the correlation coefficient $r(\tau)$ plotted against the lag $\tau$ , and the corresponding base signal $x(t)$ and shifted signal $y(t + \tau_{best})$ below. . .	49
6.4	Body maps showing the MA Jump, once with the left hip as the reference, once as the right hip as the reference. . . . .	50
6.5	Body maps showing the average mean lag for the MAs Clap, Walk, and Jump in respect to their reference positions. . . . .	52
6.6	Body maps showing the average standard deviation for the MAs Clap, Walk, and Jump in respect to their reference positions. . . . .	53
6.7	Visualization of the raw acceleration data produced by the Clap MA, showing that sensors close to the hands exhibit high acceleration while . . . . .	53
		79

6.8	Visualization of the raw acceleration data produced by the Stomp MA, showing that sensors close to the hands exhibit high acceleration. . . . .	54
6.9	Visualization of the raw acceleration data produced by the Jump MA, showing that sensors close to the hands exhibit high acceleration. . . . .	55
6.10	Visualization of the raw acceleration data produced by the Fold MA, showing that sensors close to the hands exhibit high acceleration. . . . .	56
6.11	Visualization of the raw acceleration data produced by the Walk MA, showing that sensors close to the hands exhibit high acceleration. . . . .	57
6.12	Histograms showing the distribution of best lags computed by the windowed Pearson Correlation Coefficient. . . . .	57
6.13	Visualization of the raw acceleration data produced by the Heel MA, showing that sensors close to the hands exhibit high acceleration. . . . .	58
6.14	Visualization of the raw acceleration data produced by the Run MA, showing that sensors close to the hands exhibit high acceleration. . . . .	59
6.15	Visualization of the raw acceleration data produced by the Sit MA, showing that sensors close to the hands exhibit high acceleration. . . . .	60
A.1	Mean lag for the MA Clap, Stomp, Jump, Fold with their respective reference positions. . . . .	15
A.2	Mean lag for the MA Walk, Heel, Run, Sit with their respective reference positions. . . . .	16
A.3	Average SD for the MA Clap, Stomp, Jump, Fold with their respective reference positions. . . . .	17
A.4	Average SD for the MA Walk, Heel, Run, Sit with their respective reference positions. . . . .	18

# List of Tables

4.1	Qualitative relationship between signal features and synchronization outcomes. The table summarizes how strong characteristics correlate with higher synchronization accuracy and precision across MA. . . . .	30
4.2	Overview of the eight MAs performed by participants. The set includes both cyclic and non-cyclic gestures with varying intensity, motion patterns, and synchronization difficulty across body positions. . . . .	32
6.1	Summary of synchronization accuracy and precision across all covered body positions for every MA in comparison to their reference positions. . . . .	61
6.2	Descriptive statistics of questionnaire responses in matrix form. Values represent mean $\pm$ standard deviation on a 5-point Likert scale (1 = strongly disagree, 5 = strongly agree). . . . .	61
7.1	Qualitative relationship between signal features and synchronization outcomes. The table summarizes how strong characteristics correlate with higher synchronization accuracy and precision across MA. . . . .	63



Die approbierte gedruckte Originalversion dieser Diplomarbeit ist an der TU Wien Bibliothek verfügbar  
The approved original version of this thesis is available in print at TU Wien Bibliothek.

# Bibliography

- [AGKK13] Norhafizan Ahmad, Raja Ariffin Raja Ghazilla, Nazirah M. Khairi, and Vijayabaskar Kasi. Reviews on Various Inertial Measurement Unit (IMU) Sensor Applications. *International Journal of Signal Processing Systems*, pages 256–262, 2013.
- [Alt11] Uwe Altmann. Investigation of Movement Synchrony Using Windowed Cross-Lagged Regression. In Anna Esposito, Alessandro Vinciarelli, Klára Vicsi, Catherine Pelachaud, and Anton Nijholt, editors, *Analysis of Verbal and Nonverbal Communication and Enactment. The Processing Issues*, pages 335–345, Berlin, Heidelberg, 2011. Springer.
- [Arm19] Richard A Armstrong. Should Pearson’s correlation coefficient be avoided? *Ophthalmic and Physiological Optics*, 39(5):316–327, 2019. [\\_eprint: https://onlinelibrary.wiley.com/doi/pdf/10.1111/opo.12636](https://onlinelibrary.wiley.com/doi/pdf/10.1111/opo.12636).
- [ARS20] Vicente Amorim, Ricardo Rabelo, and Mauricio Silva. *Recent Trends in Wearable Computing Research: A Systematic Review*. November 2020.
- [BAL09] David Bannach, Oliver Amft, and Paul Lukowicz. Automatic Event-Based Synchronization of Multimodal Data Streams from Wearable and Ambient Sensors. In Payam Barnaghi, Klaus Moessner, Mirko Presser, and Stefan Meissner, editors, *Smart Sensing and Context*, pages 135–148, Berlin, Heidelberg, 2009. Springer.
- [BC] Donald J Berndt and James Clifford. Using Dynamic Time Warping to Find Patterns in Time Series.
- [BCHC09] Jacob Benesty, Jingdong Chen, Yiteng Huang, and Israel Cohen. Pearson Correlation Coefficient. In Israel Cohen, Yiteng Huang, Jingdong Chen, and Jacob Benesty, editors, *Noise Reduction in Speech Processing*, pages 1–4. Springer, Berlin, Heidelberg, 2009.
- [BGJ15a] Terrell R. Bennett, Nicholas Gans, and Roozbeh Jafari. A data-driven synchronization technique for cyber-physical systems. In *Proceedings*

- of the Second International Workshop on the Swarm at the Edge of the Cloud*, SWEC '15, pages 49–54, New York, NY, USA, April 2015. Association for Computing Machinery.
- [BGJ15b] Terrell R. Bennett, Nicholas Gans, and Roozbeh Jafari. Multi-sensor data-driven: synchronization using wearable sensors. In *Proceedings of the 2015 ACM International Symposium on Wearable Computers*, ISWC '15, pages 113–116, New York, NY, USA, September 2015. Association for Computing Machinery.
- [BGJ17] Terrell R. Bennett, Nicholas Gans, and Roozbeh Jafari. Data-Driven Synchronization for Internet-of-Things Systems. *ACM Trans. Embed. Comput. Syst.*, 16(3):69:1–69:24, April 2017.
- [BH01] Kai Briechle and Uwe D. Hanebeck. Template matching using fast normalized cross correlation. In *Optical Pattern Recognition XII*, volume 4387, pages 95–102. SPIE, March 2001.
- [BK59] R. Bellman and R. Kalaba. On adaptive control processes. *IRE Transactions on Automatic Control*, 4(2):1–9, November 1959.
- [BMBK20] F. Behrens, R. G. Moulder, S. M. Boker, and M. E. Kret. Quantifying Physiological Synchrony through Windowed Cross-Correlation Analysis: Statistical and Theoretical Considerations, August 2020. Pages: 2020.08.27.269746 Section: New Results.
- [Bou96] Paul Bourke. Cross Correlation. August 1996.
- [BRR13] Maxim Buevich, Niranjini Rajagopal, and Anthony Rowe. Hardware Assisted Clock Synchronization for Real-Time Sensor Networks. In *2013 IEEE 34th Real-Time Systems Symposium*, pages 268–277, December 2013. ISSN: 1052-8725.
- [CA20] Giuseppe Coviello and Gianfranco Avitabile. Multiple Synchronized Inertial Measurement Unit Sensor Boards Platform for Activity Monitoring. *IEEE Sensors Journal*, 20(15):8771–8777, August 2020.
- [CGDSVdP24] Jona Cappelle, Sarah Goossens, Lieven De Strycker, and Liesbet Van der Perre. Low-Power Synchronization for Multi-IMU WSNs. *IEEE Embed. Syst. Lett.*, 16(2):210–213, June 2024.
- [Cha24] Rajan Chattamvelli. Pearson’s Correlation. In Rajan Chattamvelli, editor, *Correlation in Engineering and the Applied Sciences: Applications in R*, pages 55–76. Springer Nature Switzerland, Cham, 2024.
- [CLX<sup>+</sup>23] Ci Chen, Frank L. Lewis, Kan Xie, Yi Lyu, and Shengli Xie. Distributed output data-driven optimal robust synchronization of heterogeneous multi-agent systems. *Automatica*, 153:111030, July 2023.

- [Cor01] A. Corradini. Dynamic time warping for off-line recognition of a small gesture vocabulary. In *Proceedings IEEE ICCV Workshop on Recognition, Analysis, and Tracking of Faces and Gestures in Real-Time Systems*, pages 82–89, July 2001. ISSN: 1530-1044.
- [CTVNVdB19] Jun Chen, Huan Tan, Katrien Van Nimmen, and Peter Van den Broeck. Data-Driven Synchronization Analysis of a Bouncing Crowd. *Shock and Vibration*, 2019(1):8528763, 2019. \_eprint: <https://onlinelibrary.wiley.com/doi/pdf/10.1155/2019/8528763>.
- [DRE<sup>+</sup>21] Tanja Dorst, Yannick Robin, Sascha Eichstädt, Andreas Schütze, and Tizian Schneider. Influence of synchronization within a sensor network on machine learning results. *Journal of Sensors and Sensor Systems*, 10(2):233–245, August 2021. Publisher: Copernicus GmbH.
- [EGE02] Jeremy Elson, Lewis Girod, and Deborah Estrin. Fine-Grained Network Time Synchronization using Reference Broadcasts. December 2002.
- [Eme15] Robert Wall Emerson. Causation and Pearson’s Correlation Coefficient. *Journal of Visual Impairment & Blindness*, 109(3):242–244, May 2015. Publisher: SAGE Publications Inc.
- [EOBW18] Aly El-Osery, Stephen Bruder, and Kevin Wedeward. Using multiple IMUs in a stacked filter configuration for calibration and fine alignment. In *Sensors and Systems for Space Applications XI*, volume 10641, pages 120–131. SPIE, May 2018.
- [FMPP13] Jordan Frank, Shie Mannor, Joelle Pineau, and Doina Precup. Time Series Analysis Using Geometric Template Matching. *IEEE Transactions on Pattern Analysis and Machine Intelligence*, 35(3):740–754, March 2013.
- [FWD<sup>+</sup>03] A. Fort, J.-W. Weijers, V. Derudder, W. Eberle, and A. Bourdoux. A performance and complexity comparison of auto-correlation and cross-correlation for OFDM burst synchronization. In *2003 IEEE International Conference on Acoustics, Speech, and Signal Processing, 2003. Proceedings. (ICASSP ’03).*, volume 2, pages II–341, April 2003. ISSN: 1520-6149.
- [FZB<sup>+</sup>15] Xiao-Yu Fu, Karl E. Zelik, Wayne J. Board, Raymond C. Browning, and Arthur D. Kuo. Soft Tissue Deformations Contribute to the Mechanics of Walking in Obese Adults. *Medicine and science in sports and exercise*, 47(7):1435–1443, July 2015.
- [FZF26] Mingfei Feng, Qiwei Zhang, and Hongbin Fang. A comprehensive IMU dataset for evaluating sensor layouts in human activity and

- intensity recognition. *Scientific Data*, January 2026. Publisher: Nature Publishing Group.
- [GDHW22] Thomas Gilbert, Sally Day, Antonia F De C Hamilton, and Jamie Ward. A Simple Method for Synchronising Multiple IMUs using the Magnetometer. In *Proceedings of the 2022 ACM International Symposium on Wearable Computers*, pages 100–102, Cambridge United Kingdom, September 2022. ACM.
- [GJ06] Jie Gu and Xiaomin Jin. A Simple Approximation for Dynamic Time Warping Search in Large Time Series Database. In David Hutchison, Takeo Kanade, Josef Kittler, Jon M. Kleinberg, Friedemann Mattern, John C. Mitchell, Moni Naor, Oscar Nierstrasz, C. Pandu Rangan, Bernhard Steffen, Madhu Sudan, Demetri Terzopoulos, Dough Tygar, Moshe Y. Vardi, Gerhard Weikum, Emilio Corchado, Hujun Yin, Vicente Botti, and Colin Fyfe, editors, *Intelligent Data Engineering and Automated Learning – IDEAL 2006*, volume 4224, pages 841–848. Springer Berlin Heidelberg, Berlin, Heidelberg, 2006. Series Title: Lecture Notes in Computer Science.
- [GKS03] Saurabh Ganeriwal, Ram Kumar, and Mani B Srivastava. Timing-sync Protocol for Sensor Networks. November 2003.
- [GLD<sup>+</sup>24] Thomas J. Gilbert, Zexiao Lin, Sally Day, Antonia F. de C. Hamilton, and Jamie A. Ward. A magnetometer-based method for in-situ syncing of wearable inertial measurement units. *Frontiers in Computer Science*, 6, April 2024. Publisher: Frontiers.
- [GPA<sup>+</sup>08] Marion Geerligs, Gerrit W.M. Peters, Paul A.J. Ackermans, Cees W.J. Oomens, and Frank P.T. Baaijens. Linear viscoelastic behavior of subcutaneous adipose tissue. *Biorheology*, 45(6):677–688, November 2008. Publisher: SAGE Publications.
- [HBVB<sup>+</sup>23] Alexander Hoelzemann, Marius Bock, Ericka Andrea Valadares Bastías, Salma El Ouazzani Touhami, Kenza Nassiri, and Kristof Van Laerhoven. A Data-Driven Study on the Hawthorne Effect in Sensor-Based Human Activity Recognition. In *Adjunct Proceedings of the 2023 ACM International Joint Conference on Pervasive and Ubiquitous Computing & the 2023 ACM International Symposium on Wearable Computing*, UbiComp/ISWC '23 Adjunct, pages 486–491, New York, NY, USA, October 2023. Association for Computing Machinery.
- [HKB<sup>+</sup>23] Oto Haffner, Erik Kučera, Lukáš Beňo, Rudolf Pribiš, Matin Pajpach, and Dominik Janecký. Gesture Recognition System Based on Motion

Capture Suit and LSTM Neural Network. In *2023 International Conference on Modeling, Simulation & Intelligent Computing (MoSICom)*, pages 71–76, December 2023.

- [HKB<sup>+</sup>25] Oto Haffner, Erik Kučera, Lukáš Beňo, Anna Melekhova, Martin Pajpach, and Dominik Janecký. Gesture Recognition for Mechatronic System Control Using Motion-Capture Suit Rokoko SmartSuit Pro II. In *2025 International Conference on Control, Automation and Diagnosis (ICCAD)*, pages 1–6, July 2025. ISSN: 2767-9896.
- [HYH12] Makoto Harashima, Hiroyuki Yasuda, and Mikio Hasegawa. Synchronization of Wireless Sensor Networks Using Natural Environmental Signals Based on Noise-Induced Phase Synchronization Phenomenon. In *2012 IEEE 75th Vehicular Technology Conference (VTC Spring)*, pages 1–5, May 2012. ISSN: 1550-2252.
- [KS04] Caroline J. Ketcham and George E. Stelmach. Movement Control in the Older Adult. In *Technology for Adaptive Aging*. National Academies Press (US), 2004.
- [LAK19] Ariel Larey, Eliel Akin, and Itzik Klein. Feasibility Study of Multi Inertial Measurement Unit. *Proceedings*, 42(1):74, 2019. Number: 1 Publisher: Multidisciplinary Digital Publishing Institute.
- [LC10] Sami M. Lasassmeh and James M. Conrad. Time synchronization in wireless sensor networks: A survey. In *Proceedings of the IEEE SoutheastCon 2010 (SoutheastCon)*, pages 242–245, March 2010. ISSN: 1558-058X.
- [LCC<sup>+</sup>09] Konrad Lorincz, Bor-rong Chen, Geoffrey Werner Challen, Atanu Roy Chowdhury, Shyamal Patel, Paolo Bonato, and Matt Welsh. Mercury: a wearable sensor network platform for high-fidelity motion analysis. In *Proceedings of the 7th ACM Conference on Embedded Networked Sensor Systems*, pages 183–196, Berkeley California, November 2009. ACM.
- [LD09] Loïc Lemoine and Didier Delignières. Detrended Windowed (lag one) Autocorrelation: A new Method for Distinguishing between Event-Based and Emergent Timing. *Quarterly Journal of Experimental Psychology*, 62(3):585–604, March 2009. Publisher: SAGE Publications.
- [LDCE09] Martin Lukac, Paul Davis, Robert Clayton, and Deborah Estrin. Recovering temporal integrity with Data Driven Time Synchronization. In *2009 International Conference on Information Processing in Sensor Networks*, pages 61–72, April 2009.

- [LHB04] Jonathan Lester, Blake Hannaford, and Gaetano Borriello. “Are You with Me?” – Using Accelerometers to Determine If Two Devices Are Carried by the Same Person. In Alois Ferscha and Friedemann Mattern, editors, *Pervasive Computing*, pages 33–50, Berlin, Heidelberg, 2004. Springer.
- [LHY<sup>+</sup>20] Yiqin Lu, Bingjian Huang, Chun Yu, Guahong Liu, and Yuanchun Shi. Designing and Evaluating Hand-to-Hand Gestures with Dual Commodity Wrist-Worn Devices. *Proc. ACM Interact. Mob. Wearable Ubiquitous Technol.*, 4(1):20:1–20:27, March 2020.
- [LJS<sup>+</sup>02] Paul Lukowicz, H. Junker, M. Stäger, T. von Büren, and G. Tröster. WearNET: A Distributed Multi-sensor System for Context Aware Wearables. In *Proceedings of the 4th international conference on Ubiquitous Computing, UbiComp '02*, pages 361–370, Berlin, Heidelberg, September 2002. Springer-Verlag.
- [LMR<sup>+</sup>15] Matthew Loper, Naureen Mahmood, Javier Romero, Gerard Pons-Moll, and Michael J. Black. SMPL: A skinned multi-person linear model. *ACM Trans. Graphics (Proc. SIGGRAPH Asia)*, 34(6):248:1–248:16, October 2015.
- [MRR80] C. Myers, L. Rabiner, and A. Rosenberg. Performance tradeoffs in dynamic time warping algorithms for isolated word recognition. *IEEE Transactions on Acoustics, Speech, and Signal Processing*, 28(6):623–635, December 1980.
- [NR07] Vit Niennattrakul and Chotirat Ann Ratanamahatana. On Clustering Multimedia Time Series Data Using K-Means and Dynamic Time Warping. In *2007 International Conference on Multimedia and Ubiquitous Engineering (MUE'07)*, pages 733–738, April 2007.
- [NSR12] Vit Niennattrakul, Dararat Srisai, and Chotirat Ann Ratanamahatana. Shape-based template matching for time series data. *Knowledge-Based Systems*, 26:1–8, February 2012.
- [Oka19] Manabu Okawa. Template Matching Using Time-Series Averaging and DTW With Dependent Warping for Online Signature Verification. *IEEE Access*, 7:81010–81019, 2019.
- [ON01] Julian D. Olden and Bryan D. Neff. Cross-correlation bias in lag analysis of aquatic time series. *Marine Biology*, 138(5):1063–1070, May 2001.
- [ONNK06] R. Ohmura, F. Naya, H. Noma, and K. Kogure. B-Pack: a Bluetooth-based wearable sensing device for nursing activity recognition. In *2006*

*1st International Symposium on Wireless Pervasive Computing*, pages 6 pp.–6, January 2006.

- [OSK<sup>+</sup>21] Aleksandr Ometov, Viktoriia Shubina, Lucie Klus, Justyna Skibińska, Salwa Saafi, Pavel Pascacio, Laura Fluoratoru, Darwin Quezada Gai-bor, Nadezhda Chukhno, Olga Chukhno, Asad Ali, Asma Channa, Ekaterina Svertoka, Waleed Bin Qaim, Raúl Casanova-Marqués, Sylvia Holcer, Joaquín Torres-Sospedra, Sven Casteleyn, Giuseppe Ruggeri, Giuseppe Araniti, Radim Burget, Jiri Hosek, and Elena Simona Lohan. A Survey on Wearable Technology: History, State-of-the-Art and Current Challenges. *Computer Networks*, 193:108074, July 2021.
- [PDST20] Henning Puttnies, Peter Danielis, Ali Rehan Sharif, and Dirk Timmermann. Estimators for Time Synchronization—Survey, Analysis, and Outlook. *IoT*, 1(2):398–435, December 2020. Publisher: Multidisciplinary Digital Publishing Institute.
- [PGH<sup>+</sup>09] B. Podobnik, I. Grosse, D. Horvatić, S. Ilic, P. Ch. Ivanov, and H. E. Stanley. Quantifying cross-correlations using local and global detrending approaches. *The European Physical Journal B*, 71(2):243–250, September 2009.
- [RCSANTPM25] Jhonathan L. Rivas-Caicedo, Laura Saldaña-Aristizabal, Kevin Niño-Tejada, and Juan F. Patarroyo-Montenegro. A Multi-Sensor Dataset for Human Activity Recognition Using Inertial and Orientation Data. *Data*, 10(8):129, August 2025. Publisher: Multidisciplinary Digital Publishing Institute.
- [RN10] Prakash Ranganathan and Kendall Nygard. Time Synchronization in Wireless Sensor Networks: A Survey. *International Journal of UbiComp*, 1(2):92–102, April 2010.
- [Rob03] Philippe Robert. Ambulatory system for human motion analysis using a kinematic sensor: monitoring of daily physical activity in the elderly. *Biomedical Engineering*, January 2003.
- [RZL25] Lala Shakti Swarup Ray, Bo Zhou, and Paul Lukowicz. W2W: A Simulated Exploration of IMU Placement Across the Human Body for Designing Smarter Wearable. In *Proceedings of the 2025 ACM International Symposium on Wearable Computers, ISWC '25*, pages 170–176, New York, NY, USA, October 2025. Association for Computing Machinery.
- [SA05] W. Su and I.F. Akyildiz. Time-diffusion synchronization protocol for wireless sensor networks. *IEEE/ACM Transactions on Networking*, 13(2):384–397, April 2005.

- [SBK05] Bharath Sundararaman, Ugo Buy, and Ajay D. Kshemkalyani. Clock synchronization for wireless sensor networks: a survey. *Ad Hoc Networks*, 3(3):281–323, May 2005.
- [SBM<sup>+</sup>22] Shaban Shabani, Alan K. Bourke, Amir Muaremi, Jens Praestgaard, Kate O’Keeffe, Rob Argent, Martin Brom, Celeste Scotti, Brian Caulfield, and Lorcan C. Walsh. An Automatic Foot and Shank IMU Synchronization Algorithm: Proof-of-concept. In *2022 44th Annual International Conference of the IEEE Engineering in Medicine & Biology Society (EMBC)*, pages 4210–4213, July 2022. ISSN: 2694-0604.
- [Sed12] Philip Sedgwick. Pearson’s correlation coefficient. *BMJ*, 345:e4483, July 2012. Publisher: British Medical Journal Publishing Group Section: Endgames.
- [Sen09] Pavel Senin. Dynamic Time Warping Algorithm Review. January 2009.
- [SH06] Isaac Skog and Peter Handel. CALIBRATION OF A MEMS INERTIAL MEASUREMENT UNIT. September 2006.
- [SM23] Andreas Spilz and Michael Munz. Synchronisation of wearable inertial measurement units based on magnetometer data. *Biomedizinische Technik. Biomedical Engineering*, 68(3):263–273, June 2023.
- [SPB09] J.N. Sarvaiya, Suprava Patnaik, and Salman Bombaywala. Image Registration by Template Matching Using Normalized Cross-Correlation. In *2009 International Conference on Advances in Computing, Control, and Telecommunication Technologies*, pages 819–822, December 2009.
- [SS16] Timo Sztyler and Heiner Stuckenschmidt. On-body localization of wearable devices: An investigation of position-aware activity recognition. In *2016 IEEE International Conference on Pervasive Computing and Communications (PerCom)*, pages 1–9, March 2016.
- [Sta18] Statista Research Department. The global wearables market is all about the wrist, 2018. accessed on 06.02.2026.
- [Sta25] Statista Research Department. Inertial measurement unit (imu) market overview, 2025. accessed on 06.02.2026.
- [SWR<sup>+</sup>09] Gerhard Schall, Daniel Wagner, Gerhard Reitmayr, Elise Taichmann, Manfred Wieser, Dieter Schmalstieg, and Bernhard Hofmann-Wellenhof. Global pose estimation using multi-sensor fusion for outdoor Augmented Reality. In *2009 8th IEEE International Symposium on Mixed and Augmented Reality*, pages 153–162, October 2009.

- [SY04] F. Sivrikaya and B. Yener. Time synchronization in sensor networks: a survey. *IEEE Network*, 18(4):45–50, July 2004. Conference Name: IEEE Network.
- [SZ19] Ala Shaabana and Rong Zheng. CRONOS: A Post-hoc Data Driven Multi-Sensor Synchronization Approach. *ACM Transactions on Sensor Networks*, 15(3):26:1–26:20, May 2019.
- [SZL<sup>+</sup>13] Salvatore Sessa, Massimiliano Zecca, Zhuohua Lin, Luca Bartolomeo, Hiroyuki Ishii, and Atsuo Takanishi. A Methodology for the Performance Evaluation of Inertial Measurement Units. *Journal of Intelligent & Robotic Systems*, 71(2):143–157, August 2013.
- [TIH<sup>+</sup>07] Emmanuel Munguia Tapia, Stephen S. Intille, William Haskell, Kent Larson, Julie Wright, Abby King, and Robert Friedman. Real-Time Recognition of Physical Activities and Their Intensities Using Wireless Accelerometers and a Heart Rate Monitor. In *2007 11th IEEE International Symposium on Wearable Computers*, pages 37–40, October 2007. ISSN: 2376-8541.
- [TKKN03] K. Tabata, Y. Kishi, S. Konishi, and S. Nomoto. A study on the autonomous network synchronization scheme for mesh wireless network. In *14th IEEE Proceedings on Personal, Indoor and Mobile Radio Communications, 2003. PIMRC 2003.*, volume 1, pages 829–833 Vol.1, September 2003.
- [vdKSK<sup>+</sup>22] Eline van der Kruk, Paul Strutton, Louis J. Koizia, Michael Fertleman, Peter Reilly, and Anthony M. J. Bull. Why do older adults stand-up differently to young adults?: investigation of compensatory movement strategies in sit-to-walk. *npj Aging*, 8(1):13, September 2022. Publisher: Nature Publishing Group.
- [VJH<sup>+</sup>25] Théo Velletaz, Stefan Janaqi, Sébastien Harispe, Julien Lagarde, and Patrice Guyot. A Review of Human Synchronization Datasets. *IEEE Access*, 13:67269–67285, 2025.
- [WKTM25] Florian Wolling, David Kostolani, Patrick Trollmann, and Florian Michahelles. Impact of Time Discrepancies on Machine Learning Performance for Multi-Wearable Human Activity Recognition. In *Proceedings of the 2025 ACM International Symposium on Wearable Computers, ISWC '25*, pages 98–105, New York, NY, USA, October 2025. Association for Computing Machinery.
- [WLF<sup>+</sup>24] Yueqi Wang, Tangyou Liu, Licheng Feng, Jinze Wang, Yang Yang, Jianjun Bao, Binghao Li, and Liao Wu. Hardware-Based Time Synchronization for a Multi-Sensor System. In *2024 IEEE/RSJ International*

*Conference on Intelligent Robots and Systems (IROS)*, pages 4600–4607, October 2024. ISSN: 2153-0866.

- [WSL<sup>+</sup>19] Chaofan Wang, Zhanna Sarsenbayeva, Chu Luo, Jorge Goncalves, and Vassilis Kostakos. Improving Wearable Sensor Data Quality Using Context Markers. September 2019.
- [XGM17] Tongtong Xu, Ao Guo, and Jianhua Ma. Analysis of Temporal Features in Data Streams from Multiple Wearable Devices. In *2017 3rd IEEE International Conference on Cybernetics (CYBCONF)*, pages 1–6, June 2017.
- [XGMW17] Tongtong Xu, Ao Guo, Jianhua Ma, and Kevin I-Kai Wang. Feature-Based Temporal Statistical Modeling of Data Streams from Multiple Wearable Devices. In *2017 IEEE 15th Intl Conf on Dependable, Autonomic and Secure Computing, 15th Intl Conf on Pervasive Intelligence and Computing, 3rd Intl Conf on Big Data Intelligence and Computing and Cyber Science and Technology Congress(DASC/PiCom/DataCom/CyberSciTech)*, pages 119–126, November 2017.
- [YH10] Che-Chang Yang and Yeh-Liang Hsu. A Review of Accelerometry-Based Wearable Motion Detectors for Physical Activity Monitoring. *Sensors*, 10(8):7772–7788, August 2010. Publisher: Molecular Diversity Preservation International.
- [YTLH19] Zhenyu Yan, Rui Tan, Yang Li, and Jun Huang. Wearables Clock Synchronization Using Skin Electric Potentials. *IEEE Transactions on Mobile Computing*, 18(12):2984–2998, December 2019.
- [Zea17] Clint Zeagler. Where to wear it: functional, technical, and social considerations in on-body location for wearable technology 20 years of designing for wearability. In *Proceedings of the 2017 ACM International Symposium on Wearable Computers, ISWC '17*, pages 150–157, New York, NY, USA, September 2017. Association for Computing Machinery.
- [ZLG22] Yuanqiang Zhou, Dewei Li, and Furong Gao. Data-Driven Optimal Synchronization Control for Leader-Follower Multiagent Systems, June 2022.
- [ZW12] He Zhao and Zheyao Wang. Motion Measurement Using Inertial Sensors, Ultrasonic Sensors, and Magnetometers With Extended Kalman Filter for Data Fusion. *IEEE Sensors Journal*, 12(5):943–953, May 2012.

[ZZ04]

Rong Zhu and Zhaoying Zhou. A real-time articulated human motion tracking using tri-axis inertial/magnetic sensors package. *IEEE Transactions on Neural Systems and Rehabilitation Engineering*, 12(2):295–302, June 2004.



Die approbierte gedruckte Originalversion dieser Diplomarbeit ist an der TU Wien Bibliothek verfügbar  
The approved original version of this thesis is available in print at TU Wien Bibliothek.

CHAPTER **A**

# Appendices

## A.1 User Study Forms

# Information Sheet

User Study of the project „Motion-Based Offline Synchronization of Wearable Devices“

Experiment leader: Christoff Kügler

Contact: [christoff.kuegler@tuwien.ac.at](mailto:christoff.kuegler@tuwien.ac.at)

Main supervisor: Univ.Prof. Florian Michahelles

Co-Supervisor: Florian Wolling

Dear study participant!

You are invited to take part in the user study taking place as part of my master's thesis. Please read the information on the study carefully to decide on your participation in the study.

## **Aim of the study:**

As part of my master's thesis, acceleration data and gyroscope data are recorded at various body positions. During the recording, the participants perform a series of distinct actions. These actions are then synchronized across body positions, only relying on the motion data. The aim of the study is to find out how accurately wearable devices at different body positions can be synchronized using this motion-based approach.

## **Voluntary participation:**

Your participation in the study is voluntary and can be withdrawn at any time without giving reasons.

## **Use of your data and privacy:**

- The measurement data from acceleration and gyroscope sensors will initially be used as part of the master's thesis. They will then be used to write scientific publications and pseudonymously publicized in the form of a publicly available data set for non-commercial, scientific use by third parties.
- The published data set contains the acceleration and gyroscope signals, the marker positions recorded by the infrared camera, and the personal data age, gender, height and weight.
- The published data is pseudonymized by assigning an ID.
- Recordings made with a video camera are only used to verify the correct execution of the performed actions, and to identify errors. These are deleted immediately after completion of the master's thesis.

### **Procedure of the study:**

During your participation you will be asked to perform a series of physical activities, such as clapping, jumping, and simple stretches. Multiple repetitions are performed for each of these activities. The execution of each activity will be explained verbally in advance. Before the experiment, you will be asked to put on sports clothing and a motion capturing suit. You are expected to bring your own sports clothing and sports shoes. You will be provided with a separate changing room.

The motion capturing suit, the infrared cameras, and the video camera will record data continuously during the experiment, even in periods of rest between the activities. Acceleration data and gyroscope data is recorded by the motion capturing suit at 17 different body positions (2x foot, 2x lower leg, 2x upper leg, sternum, pelvis, 2x hand, 2x forearm, 2x upper arm, 2x shoulder, forehead). The infrared camera tracks your full-body movement with a precision of 0.5 millimeters. All measurement data is stored pseudonymously by assigning an ID.

The recording made by the video camera is for subsequent analysis only; it is used exclusively to verify the correct execution of activities and to identify the influence of errors. It will not be published and will be deleted immediately after completion of the project.

We look forward to your participation! Please do not hesitate to contact us if you would like further information to help you decide whether to participate.

# Consent Form

User Study of the project „Motion-Based Offline Synchronization of Wearable Devices“

Experiment leader: Christoff Kügler

Contact: [e11807868@student.tuwien.ac.at](mailto:e11807868@student.tuwien.ac.at)

Main supervisor: Univ.Prof. Florian Michahelles

Co-supervisor: Florian Wolling

- I hereby confirm that I have carefully read and understood the information sheet and that I have been given the opportunity to ask questions.
- I am aware that my participation is voluntary and that I can withdraw my consent at any time without giving reasons and cancel the experiment.
- I am aware of the purposes for and the way my data is processed and stored.
- I agree that my measurement data recorded during the experiment may be stored and processed anonymously for scientific purposes.
- I am aware that my measurement data is recorded continuously during the experiment, and I can ask for the recording to be interrupted or stopped at any time.
- I agree that my recorded data is used and published pseudonymously in the Master's thesis and publications based on it. Also, a public dataset for scientific purposes.
- I agree that a video of me will be recorded during the study, which will not be published and will only be used to analyze the measurement data and identify error influences. The video recording can be stopped and deleted at any time on request. No video will be recorded without consent.
- I am aware of the task and feel able to carry it out.
- I have no physical limitations (e.g. muscle/bone diseases, scoliosis, ...) that contribute to an increased risk of injury.
- I agree to participate in the study.

\_\_\_\_\_  
Name of the participant

\_\_\_\_\_  
Date

\_\_\_\_\_  
Signature

\_\_\_\_\_  
Name of the experiment leader

\_\_\_\_\_  
Date

\_\_\_\_\_  
Signature

## A.2 User Study Questionnaires

## Pre-Questionnaire: Motion-Based Offline Synchronization of Wearable Devices NEW



Please answer these questions before the interactive part of the user study. This questionnaire is part of the user study and not optional.

\* Erforderlich

### Demographic Information

Participant ID \*

Age (years) \*

Der Wert muss eine Zahl sein.

Body Weight (kg) \*

Der Wert muss eine Zahl sein.

Body Height (cm) \*

Der Wert muss eine Zahl sein.

Gender \*

- Female
- Male
- Non-binary

How were you recruited for this study? \*

- lecture "Wissenschaftliches Arbeiten"
- personally by the researcher
- Sonstiges

What is your level of education? \*

- Less than High School
- High School (e.g. Matura/Abitur)
- Bachelor's Degree
- Master's Degree
- Doctoral Degree
- Sonstiges

What is your employment status? \*

- (self-) employed
- student
- retired
- unemployed

What is your field of work or study? \*

## General Questions

Please answer these questions about the study.

How often do you engage in physical activities? \*

- every day
- more than 3 times a week
- at least once a week
- at least once a month
- less than once a month
- never

How often do you play video games? \*

- every day
- more than 3 times a week
- at least once a week
- at least once a month
- less than once a month
- never

Have you ever interacted with a VR/AR environment? \*

- Yes
- No

Have you ever interacted with a motion tracking controller from a video console (Kinect, Wii Sports, ...)? \*

- Yes
- No

Have you ever worked with a motion tracking system apart from video consoles (i.e. no Kinect, ...) before this study? \*

- Yes
- No

Which motion tracking systems have you worked with and in what context? Please be sure that this response cannot be tracked back to you. \*

Have you ever worn a motion tracking suit before this study? \*

Yes

No

Which motion tracking suits have you worn before? \*

---

Dieser Inhalt wurde von Microsoft weder erstellt noch gebilligt. Die von Ihnen übermittelten Daten werden an den Formulareigentümer gesendet.

 Microsoft Forms

# Post-Questionnaire: Motion-Based Offline Synchronization of Wearable Devices

Please answer these questions immediately after completing the interactive part of the user study. This questionnaire is part of the user study and not optional.

\* Erforderlich

Participant ID \*

General \*

	Strongly agree	Agree	Neutral	Disagree	Strongly disagree
I consider myself as physically active.	<input type="radio"/>	<input type="radio"/>	<input type="radio"/>	<input type="radio"/>	<input type="radio"/>
The motion tracking suit felt comfortable to wear.	<input type="radio"/>	<input type="radio"/>	<input type="radio"/>	<input type="radio"/>	<input type="radio"/>
My movement was impaired by the motion tracking suit.	<input type="radio"/>	<input type="radio"/>	<input type="radio"/>	<input type="radio"/>	<input type="radio"/>

Was your comfort level affected by the study setting? \*

- Yes
- No

How was your comfort level affected by the study setting? \*

## Gesture Rating

Please answer the questions for every gesture you performed today.

Stomp on the Ground \*

	Strongly agree	Agree	Neutral	Disagree	Strongly disagree
The gesture was physically demanding.	<input type="radio"/>	<input type="radio"/>	<input type="radio"/>	<input type="radio"/>	<input type="radio"/>
I felt self-conscious or embarrassed performing this gesture.	<input type="radio"/>	<input type="radio"/>	<input type="radio"/>	<input type="radio"/>	<input type="radio"/>
The gesture was easy to understand and follow.	<input type="radio"/>	<input type="radio"/>	<input type="radio"/>	<input type="radio"/>	<input type="radio"/>
The gesture resembles a motion I perform in my everyday life.	<input type="radio"/>	<input type="radio"/>	<input type="radio"/>	<input type="radio"/>	<input type="radio"/>

Jumping Jacks \*

	Strongly agree	Agree	Neutral	Disagree	Strongly disagree
The gesture was physically demanding.	<input type="radio"/>	<input type="radio"/>	<input type="radio"/>	<input type="radio"/>	<input type="radio"/>
I felt self-conscious or embarrassed performing this gesture.	<input type="radio"/>	<input type="radio"/>	<input type="radio"/>	<input type="radio"/>	<input type="radio"/>
The gesture was easy to understand and follow.	<input type="radio"/>	<input type="radio"/>	<input type="radio"/>	<input type="radio"/>	<input type="radio"/>
The gesture resembles a motion I perform in my everyday life.	<input type="radio"/>	<input type="radio"/>	<input type="radio"/>	<input type="radio"/>	<input type="radio"/>

Clapping \*

	Strongly agree	Agree	Neutral	Disagree	Strongly disagree
The gesture was physically demanding.	<input type="radio"/>	<input type="radio"/>	<input type="radio"/>	<input type="radio"/>	<input type="radio"/>
I felt self-conscious or embarrassed performing this gesture.	<input type="radio"/>	<input type="radio"/>	<input type="radio"/>	<input type="radio"/>	<input type="radio"/>
The gesture was easy to understand and follow.	<input type="radio"/>	<input type="radio"/>	<input type="radio"/>	<input type="radio"/>	<input type="radio"/>
The gesture resembles a motion I perform in my everyday life.	<input type="radio"/>	<input type="radio"/>	<input type="radio"/>	<input type="radio"/>	<input type="radio"/>

Run in Place \*

	Strongly agree	Agree	Neutral	Disagree	Strongly disagree
The gesture was physically demanding.	<input type="radio"/>	<input type="radio"/>	<input type="radio"/>	<input type="radio"/>	<input type="radio"/>
I felt self-conscious or embarrassed performing this gesture.	<input type="radio"/>	<input type="radio"/>	<input type="radio"/>	<input type="radio"/>	<input type="radio"/>
The gesture was easy to understand and follow.	<input type="radio"/>	<input type="radio"/>	<input type="radio"/>	<input type="radio"/>	<input type="radio"/>
The gesture resembles a motion I perform in my everyday life.	<input type="radio"/>	<input type="radio"/>	<input type="radio"/>	<input type="radio"/>	<input type="radio"/>

Walk Around \*

	Strongly agree	Agree	Neutral	Disagree	Strongly disagree
The gesture was physically demanding.	<input type="radio"/>	<input type="radio"/>	<input type="radio"/>	<input type="radio"/>	<input type="radio"/>
I felt self-conscious or embarrassed performing this gesture.	<input type="radio"/>	<input type="radio"/>	<input type="radio"/>	<input type="radio"/>	<input type="radio"/>
The gesture was easy to understand and follow.	<input type="radio"/>	<input type="radio"/>	<input type="radio"/>	<input type="radio"/>	<input type="radio"/>
The gesture resembles a motion I perform in my everyday life.	<input type="radio"/>	<input type="radio"/>	<input type="radio"/>	<input type="radio"/>	<input type="radio"/>

Forward Fold (Stretch) \*

	Strongly agree	Agree	Neutral	Disagree	Strongly disagree
The gesture was physically demanding.	<input type="radio"/>	<input type="radio"/>	<input type="radio"/>	<input type="radio"/>	<input type="radio"/>
I felt self-conscious or embarrassed performing this gesture.	<input type="radio"/>	<input type="radio"/>	<input type="radio"/>	<input type="radio"/>	<input type="radio"/>
The gesture was easy to understand and follow.	<input type="radio"/>	<input type="radio"/>	<input type="radio"/>	<input type="radio"/>	<input type="radio"/>
The gesture resembles a motion I perform in my everyday life.	<input type="radio"/>	<input type="radio"/>	<input type="radio"/>	<input type="radio"/>	<input type="radio"/>

Heel Raise \*

	Strongly agree	Agree	Neutral	Disagree	Strongly disagree
The gesture was physically demanding.	<input type="radio"/>	<input type="radio"/>	<input type="radio"/>	<input type="radio"/>	<input type="radio"/>
I felt self-conscious or embarrassed performing this gesture.	<input type="radio"/>	<input type="radio"/>	<input type="radio"/>	<input type="radio"/>	<input type="radio"/>
The gesture was easy to understand and follow.	<input type="radio"/>	<input type="radio"/>	<input type="radio"/>	<input type="radio"/>	<input type="radio"/>
The gesture resembles a motion I perform in my everyday life.	<input type="radio"/>	<input type="radio"/>	<input type="radio"/>	<input type="radio"/>	<input type="radio"/>

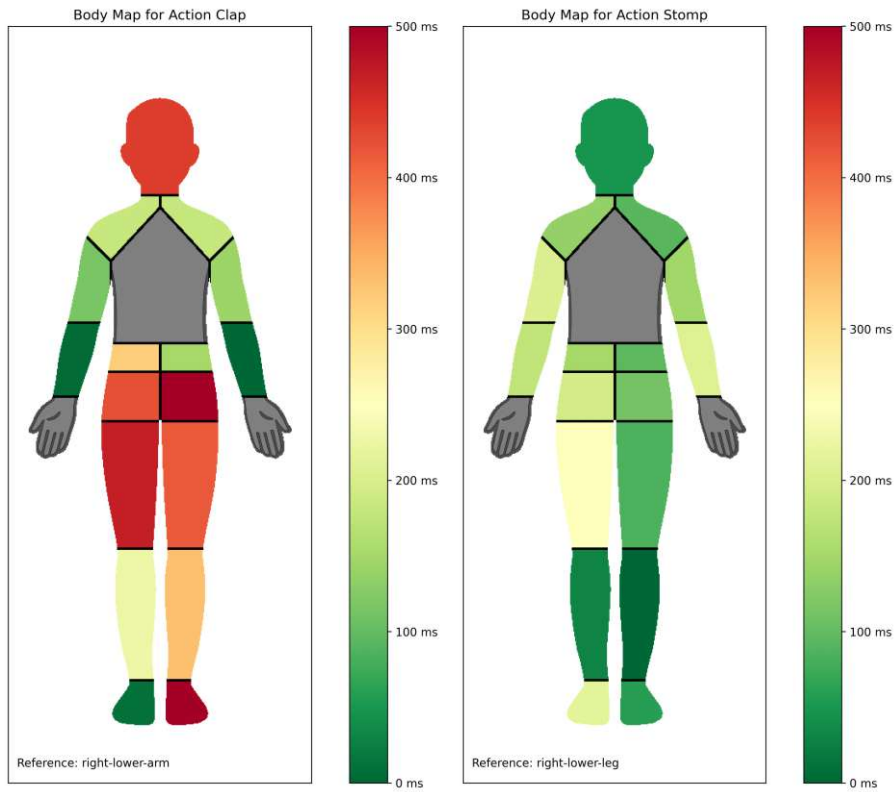
Sit Down / Stand Up \*

	Strongly agree	Agree	Neutral	Disagree	Strongly disagree
The gesture was physically demanding.	<input type="radio"/>	<input type="radio"/>	<input type="radio"/>	<input type="radio"/>	<input type="radio"/>
I felt self-conscious or embarrassed performing this gesture.	<input type="radio"/>	<input type="radio"/>	<input type="radio"/>	<input type="radio"/>	<input type="radio"/>
The gesture was easy to understand and follow.	<input type="radio"/>	<input type="radio"/>	<input type="radio"/>	<input type="radio"/>	<input type="radio"/>
The gesture resembles a motion I perform in my everyday life.	<input type="radio"/>	<input type="radio"/>	<input type="radio"/>	<input type="radio"/>	<input type="radio"/>

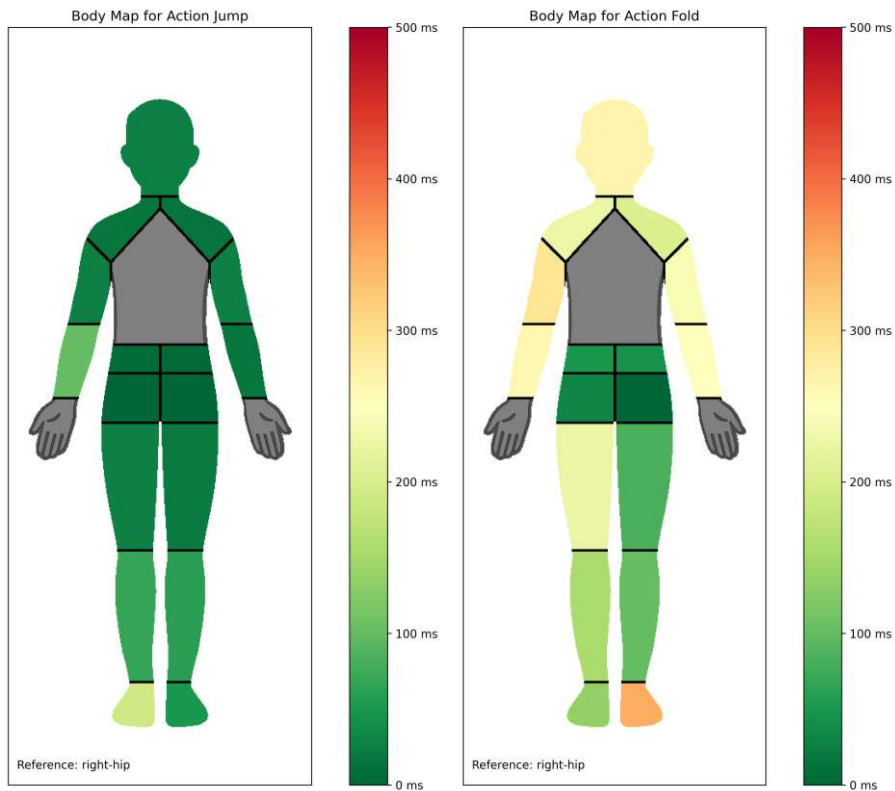
Dieser Inhalt wurde von Microsoft weder erstellt noch gebilligt. Die von Ihnen übermittelten Daten werden an den Formulareigentümer gesendet.



## A.3 Body Maps

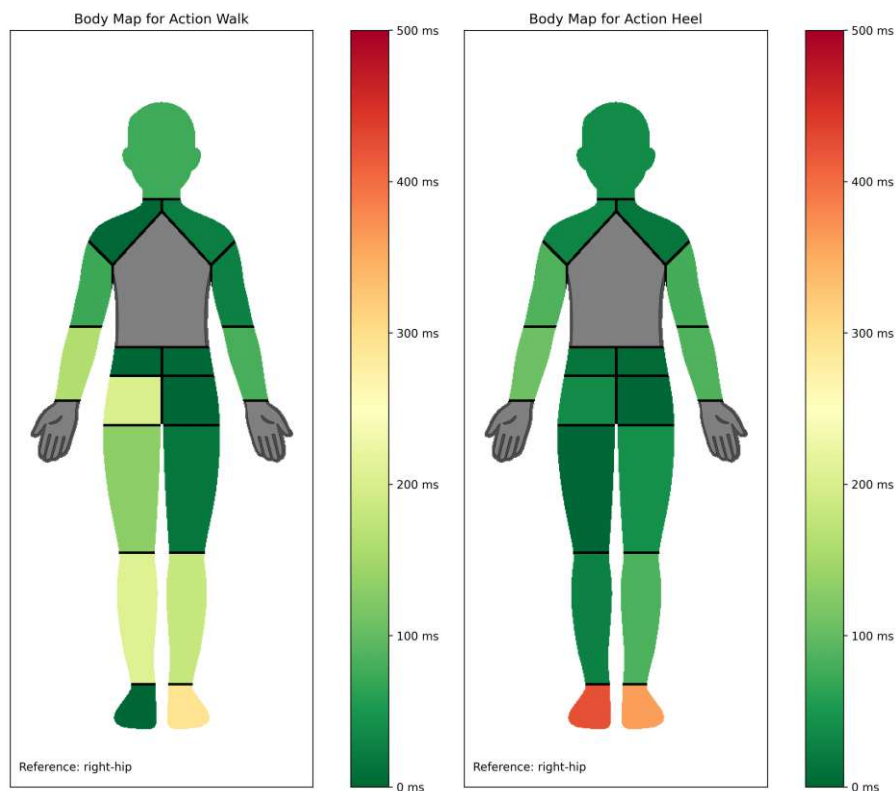


(a) Mean lag for MA Clap with reference Right Lower Arm. (b) Mean lag for MA Stomp with reference Right Foot.

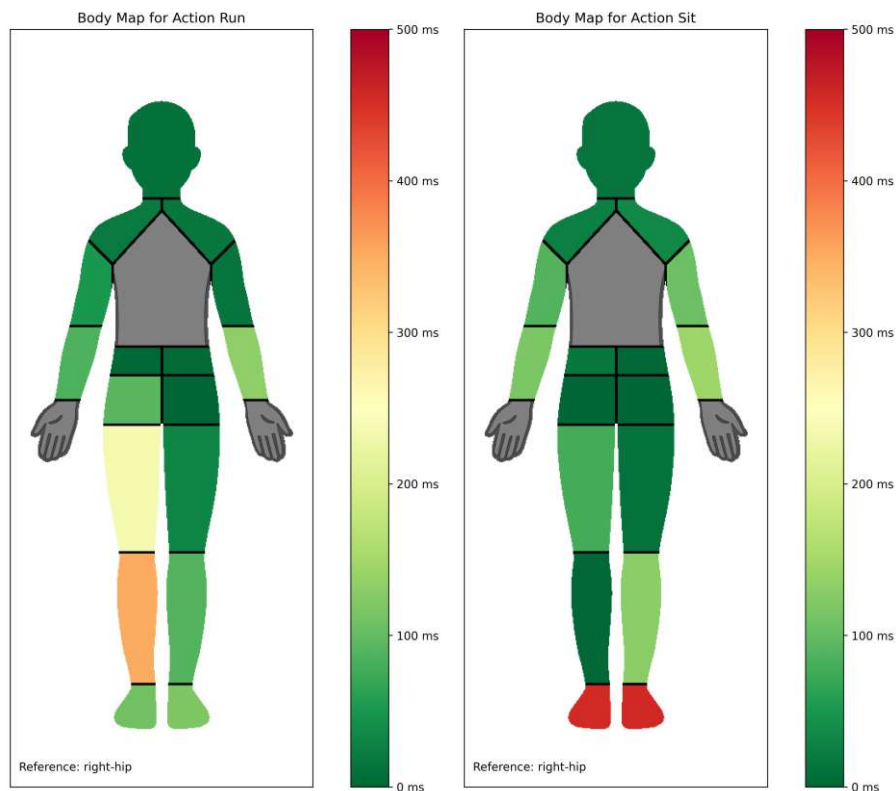


(c) Mean lag for MA Jump with reference Right Hip. (d) Mean lag for MA Fold with reference Right Hip.

Figure A.1: Mean lag for the MA Clap, Stomp, Jump, Fold with their respective reference positions.

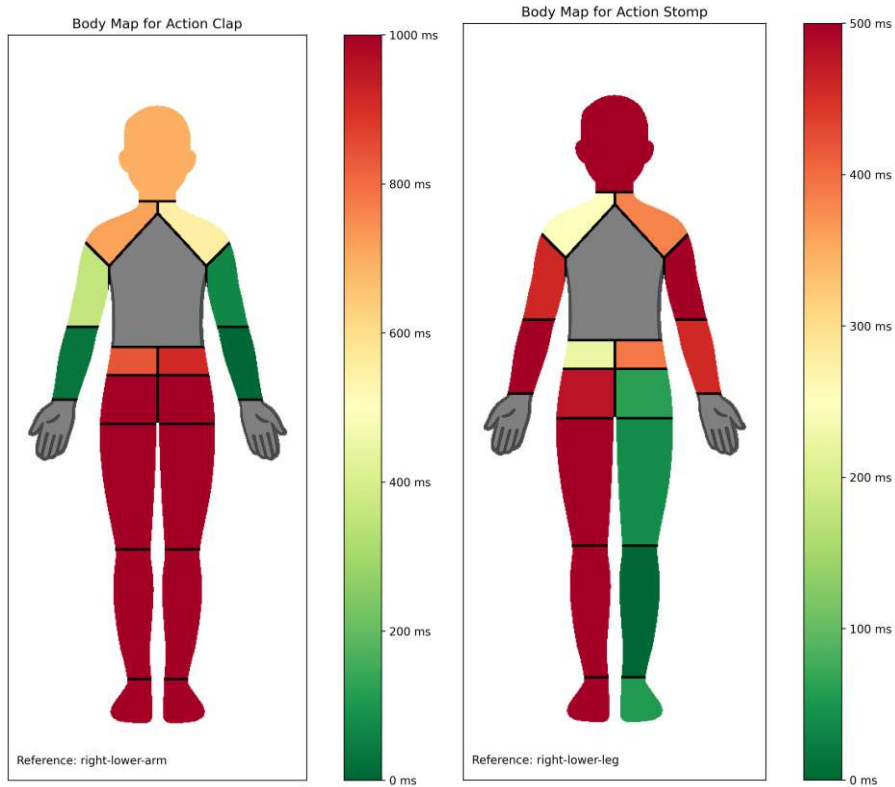


(a) Mean lag for MA Walk with reference Right Hip. (b) Mean lag for MA Heel with reference Right Hip.

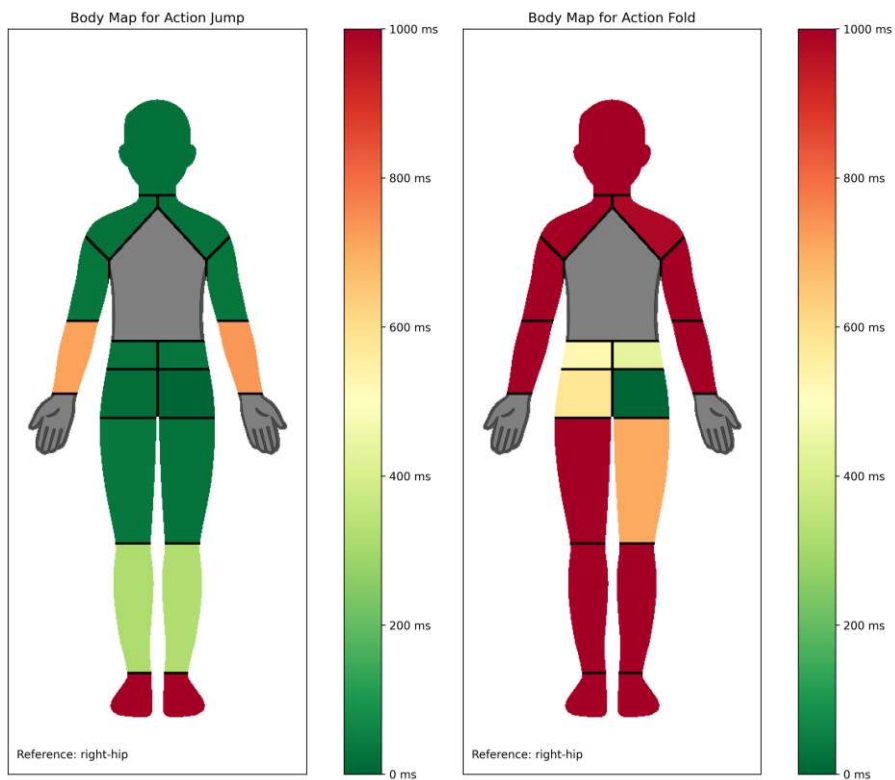


(c) Mean lag for MA Run with reference Right Hip. (d) Mean lag for MA Sit with reference Right Hip.

Figure A.2: Mean lag for the MA Walk, Heel, Run, Sit with their respective reference positions.

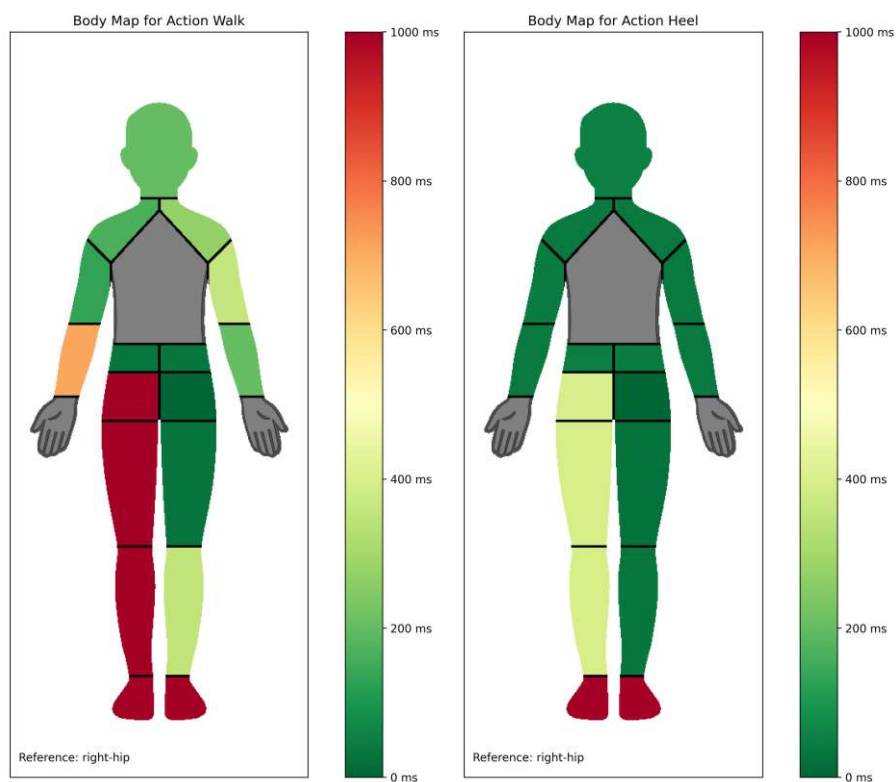


(a) Average SD for MA Clap with reference Right Lower Arm. (b) Average SD for MA Stomp with reference Right Foot.

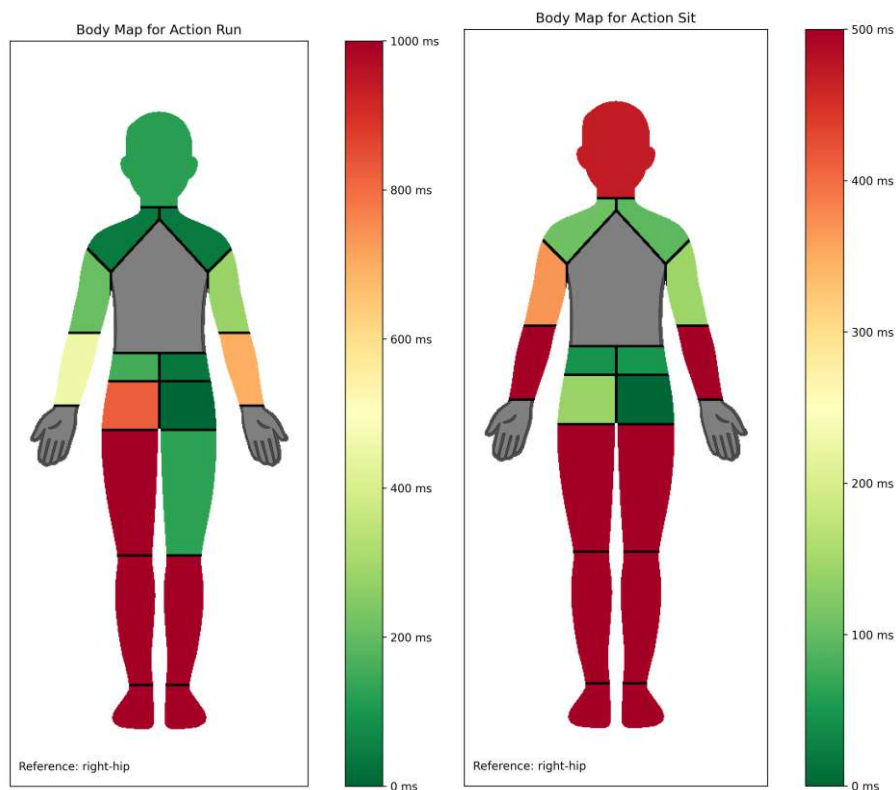


(c) Average SD for MA Jump with reference Right Hip. (d) Average SD for MA Fold with reference Right Hip.

Figure A.3: Average SD for the MA Clap, Stomp, Jump, Fold with their respective reference positions.



(a) Average SD for MA Walk with reference Right Hip. (b) Average SD for MA Heel with reference Right Hip.



(c) Average SD for MA Run with reference Right Hip. (d) Average SD for MA Sit with reference Right Hip.

Figure A.4: Average SD for the MA Walk, Heel, Run, Sit with their respective reference positions.